Title

Design and Evaluation of Multi-modal Receptors and Cellular Enhancements for Cancer Therapy

Author

Garcia, Julie

Publication Date

2023

Peer reviewed|Thesis/dissertation

Design and Evaluation of Multi-modal Receptors and Cellular Enhancements for Cancer Therapy

by

Julie Garcia

DISSERTATION

Submitted in partial satisfaction of the requirements for degree of

DOCTOR OF PHILOSOPHY

in

Biomedical Sciences

in the

GRADUATE DIVISION

of the

UNIVERSITY OF CALIFORNIA, SAN FRANCISCO

Approved:

DocuSigned by:

Matthew Spitzer

4793AE6232BE479...

Matthew Spitzer

Chair

DocuSigned by:

Justin Eyquem

Justin Eyquem

DocuSigned by:

Kole Roybal

Kole Roybal

DocuSigned by:

Thea Tlsty

8D636B0311E5409...

Thea Tlsty

Committee Members

In dedication to my parents,

Rob and Sharon Cole.

And to my husband, Noel Garcia.

Acknowledgements

To my mentor, Dr. Kole Roybal – thank you for your thoughtful guidance, both in science and in life. You have provided me with the best mentorship, training, opportunities, and professional growth I could have asked for, and I am very grateful to have learned so much from you. Thank you for teaching me how to effectively speak about our science and ideas, thank you for advocating for me throughout graduate school and beyond, and thank you for helping me become the scientist I am today.

To my committee – Drs. Matthew Spitzer, Justin Eyquem, and Thea Tlsty. Thank you for your feedback, enthusiasm, and constant encouragement.

To Camillia Azimi & Casey Burnett, thank you for helping me navigate graduate school and for creating a community of women supporting each other in science. I am so grateful to call you both lifelong colleagues and friends.

To the Roybal Lab – thank you for providing an environment of incredible motivation, creativity, and joy. Thank you for pushing me to learn and lead.

To my closest friends Daphne Superville & Saumya Bollam – thank you for your willingness to always have a glass of wine with me. I am so grateful for your steadfast friendship and love, and for the ability to be myself with both of you.

To my parents Rob and Sharon Cole – thank you for raising me, I would not be who I am today without the two of you.

Dad – you always taught me to advocate for myself, and that the worst someone could say is no. From you I have learned to speak confidently and to ask for what I deserve.

Mom – you gave me my enthusiasm for medicine and science, and you have shown me an example of gracious love. You are the reason I became a scientist.

To my siblings – Danielle & Evan – though we are siblings, in adulthood I consider both of you close friends, and I am so blessed to have you in my life. I am so proud of you both.

Danielle – I am thankful for our Grand Valley years and conversations at your dinner table (thank you for feeding me); you will always be my big sister and I appreciate the many hours on the phone together. You have cheered me on and helped me through.

Evan – I am grateful for the last years of high school, in band camp and drama club (we were nerds). I have loved seeing you soar in your career, and I love the way we can discuss science, medicine and life together.

To my bonus family – Noel, Diana, and Jeremy Garcia - thank you for supporting Noel and I, not just in our marriage, but also in all the challenges we have taken on. I am grateful to have married into a family that loves me as their own.

To my husband, Noel – thank you for your supportive partnership, incredible patience, and unwavering love. Thank you for saying “yes and…” to this life with me, you are my favorite comedian and my closest friend. Without you, this would not be. I love you.

Contributions

This dissertation was completed under the direct mentorship of Dr. Kole Roybal, PhD, with additional guidance provided by thesis committee members, Dr. Matthew Spitzer, PhD, Dr. Thea Tlsty, PhD, and Dr. Justin Eyquem, PhD.

Chapter 1 is review accepted at Immunological Reviews:

Garcia, J.*, Burnett, C.*, Roybal, K. T. Towards the clinical development of synthetic immunity to cancer. *Immunological Reviews.* (2023) In press.

*These authors contributed equally to this work.

Chapter 2 is a manuscript in review at Nature:

Garcia, J.*, Daniels, J.*, Lee, Y., Zhu, I., Cheng, K., Liu, Q., Goodman, D., Burnett, C., Law, C., Thienpont, C., Alavi, J., Azimi, C., Montgomery, G., Roybal, K. T.†, Choi, J†. Naturally occurring mutations in human T cell lymphomas enhance engineered T cell therapies. *Nature*. (2023). In Review.

*These authors contributed equally to this work.

†Corresponding authors.

Conceptualization: J.G., J.D., K.T.R., J.C.; experimental methodology: J.G., J.D., I.Z., D.G., K.T.R., J.C; investigation: all authors; writing: J.G., J.D., K.T.R., J.C.; funding acquisition: K.T.R. and J.C.; and supervision: K.T.R. and J.C.

Chapter 3 is a manuscript in preparation:

Burnett, C.*, Garcia J.*, Alavi, J., Guldberg S., Thienpont, C., Tamaka, S., Spitzer, M., Roybal, K. T. The immunological impact of CARD11-PIK3R3 CAR T cell anti-tumor responses in immunotherapy refractory solid tumors. (2023). Manuscript in Preparation.

*These authors contributed equally to this work.

Conceptualization: C.B, J.G., M.S., and K.T.R.; experimental methodology: C.B, J.G., M.S., and K.T.R.; computational methodology: C.B., S.G., and M.S.; investigation: all authors; writing: C.B, J.G., M.S., and K.T.R.; funding acquisition: M.S., and K.T.R.; and supervision: M.S., and K.T.R.

Chapter 4 is a manuscript in preparation:

Garcia J.*, Foisey M.*, Hyrenius-Wittsten A., Liu R., Zhu I., Roybal K. T. Engineering modular multi-modal receptors for enhanced cancer cell therapies. (2023). Manuscript in Preparation.

*These authors contributed equally to this work.

Conceptualization: J.G., M.F., A.H.-W., and K.T.R.; experimental methodology: J.G., M.F., A.H.-W., R.L., and K.T.R.; investigation: all authors; writing: J.G., M.F., and K.T.R.; funding acquisition: K.T.R.; and supervision: K.T.R.

Abstract

Design and Evaluation of Multi-modal Receptors and Cellular Enhancements for Cancer Therapy

Julie M. Garcia

Adoptive T cell therapies have produced exceptional responses in a subset of cancer patients. However, therapeutic efficacy can be hindered by poor T cell persistence and function. In human T cell cancers, evolution of the disease positively selects for mutations that improve fitness of T cells in challenging situations analogous to those faced by therapeutic T cells. Therefore, we hypothesized that many of these mutations could be co-opted to improve T cell therapies. Through systematic screening we identify a gene fusion, CARD11-PIK3R3, found in a CD4+ cutaneous T cell lymphoma that augments CARD11-BCL10-MALT1 complex signaling to increase anti-tumor efficacy of therapeutic T cells in multiple xenograft models. Inclusion of CARD11-PIK3R3 also dramatically improves CAR therapy in immunologically cold syngeneic models, without the requirement for pre-conditioning. Furthermore, CARD11-PIK3R3 CAR therapy induces significant changes within the periphery and tumor microenvironment (TME), shifting cold tumors towards a state of greater inflammation and recruiting infiltration of the endogenous immune system.

In parallel to the discovery of CARD11-PIK3R3, we developed a new class of synthetic receptors called SNIPR CARs. These receptors induce short timescale signaling and long term custom transcriptional responses in a single receptor architecture, providing researchers with

the ability to redirect patient T cells against cancerous cells while simultaneously delivering payloads to counteract challenges encountered in cancers. We have paired these receptors with payloads such as CARD11-PIK3R3, and found they induce sufficient CAR activity and antigen restricted payload expression, resulting in improved anti-tumor efficacy with a hypothesized more favorable safety profile.

Altogether, these results indicate that exploiting naturally occurring mutations represents a promising approach for improving T cell therapies, particularly in cold solid tumor microenvironments where few therapies have made impact. Additionally, we suggest that engineering solutions, such as SNIPR CARs, can allow us to tune or control potent but oncogenic sourced or systemically toxic modifiers, to create highly safe and efficacious cell therapies.

Table of Contents

List of Figures

List of Abbreviations

AA – Amino Acids

ACT – Adoptive Cell Therapy

ALPPL2 – Alkaline phosphatase, placental-like 2

ANOVA – Analysis of Variance

AP-1– Activator Protein 1

APC – Antigen Presenting Cell

BCMA – B Cell Maturation Antigen

BFP – Blue Fluorescent Protein

BiTE – Bi-Specific T-cell Engager

CAR – Chimeric Antigen Receptors

CARD11 - Caspase Recruitment Domain-Containing Protein 11

CBM – CARD11-BCL10-MALT1 Complex

CD – Cluster of Differentiation

CRISPR – Clustered Regularly Interspaced Short Palindromic Repeats

CRS – Cytokine Release Syndrome

CTFR – Cell Trace Far Red

CyTOF – Cytometry by Time of Flight

ELISA - Enzyme-Linked Immunoassay

FACS – Fluorescence Activated Cell Sorting

FBS – Fetal Bovine Serum

FLT3-L – FMS-like Tyrosine Kinase 3 Ligand

GEM – Genetically Engineered Mouse

GFP – Green Fluorescent Protein

Grb2 – Growth Factor Receptor-bound Protein 2

GS Linker – Glysine Serine Linker

GVHD – Graft-versus-host Disease

H&E – Hematoxylin and Eosin

HIF1α – Hypoxia-inducible Factor 1α

ICANS – Emmune Effector Cell-associated Neurotoxicity Syndrome

IFN-γ – Interferon Gamma

IL – Interleukin

ITAM – Immunoreceptor Tyrosine-based Activation Motif

KIR- Killer Immunoglobulin-like Receptors

Lck – Lymphocyte-specific Protein Tyrosine Kinase

LN - Lymph Node

Luc - Luciferase

MCAM – Melanoma Cell Adhesion Molecule

MFI – Mean Fluorescence Intensity

MHC – Major Histocompatibility Complex

MIBI – Multiplexed Ion Beam Imaging

NFkB – Nuclear Factor Kappa B

NFAT – Nuclear Factor of Activated T Cells

NHP – Non-human Primates

NK – Natural Killer Cell

NSG – NOD.Cg-Prkdc^{scid} Il2rg^{tm1Wjl}/SzJ

OVA – Ovalbumin

PBMC – Peripheral Blood Mononuclear Cell

PBS – Phosphate Buffered Saline

PCA – Principal Component Analysis

PD-1 – Programmed Cell Death 1

PD-L1 – Programmed Cell Death 1 Ligand

PDAC – Pancreatic Ductal Adenocarcinoma

PDX – Patient Derived Xenografts

PDZbm – Post-synaptic Density-95, Discs Large and Zona Occuldens 1 Binding Moieties

PI3K – Phosphoinositide-3-kinase

PIK3R3 – Phosphoinositide-3-kinase Regulatory Subunit 3

PLCy – Phospholipase C Gamma 1

ProCAR – probiotic-guided CAR-T cell

RE – Response Element

scFv – Single Chain Variable Fragment

scRNA-seq – Single-cell RNA Sequencing

SNIPR – Synthetic Intramembrane Proteolysis Receptor

synNotch – Synthetic Notch Receptor

TAM – Tumor Associated Macrophages

TCR – T Cell Receptor

TF – Transcription Factor

TGF-b – Transforming Growth Factor b

TIL – Tumor Infiltrating Lymphocyte

TMD – Transmembrane Domain

TME – Tumor Microenvironment

TNF – Tumor Necrosis Factor

TNFRSF – Tumor Necrosis Factor Receptor Super Family

tNGFR – Truncated Nerve Growth Factor Receptor

TRAC – T Cell Receptor Alpha Constant

TRAF – Tumor Necrosis Receptor-associated Factor

Treg – Regulatory T cells

Chapter 1

Towards the Clinical Development of Synthetic Immunity to Cancer

Material for this chapter comes from the following work:

Garcia, J.*, Burnett, C.*, Roybal, K. T. Towards the clinical development of synthetic immunity to cancer. *Immunological Reviews.* (2023) In press.

*These authors contributed equally to this work.

1.1. Summary

Synthetic biology (synbio) tools, such as chimeric antigen receptors (CARs), have been designed to target, activate, and improve immune cell responses to tumors. These therapies have demonstrated an ability to cure patients with blood cancers. However, there are significant challenges to designing, testing, and efficiently translating these complex cell therapies for patients who do not respond or have immune refractory solid tumors. The rapid progress of synbio tools for cell therapy, particularly for cancer immunotherapy, is encouraging but our development process should be tailored to increase translational success. Particularly, next-generation cell therapies should be rooted in basic immunology, tested in more predictive preclinical models, engineered for potency with the right balance of safety, educated by clinical findings, and multi-faceted to combat a range of suppressive mechanisms. Here we lay out five principles for engineering future cell therapies to increase the probability of clinical impact, and in the context of these principles we provide an overview of the current state of synbio cell therapy design for cancer. Although these principles are anchored in engineering immune cells for cancer therapy, we posit that they can help guide translational synbio research for broad impact in other disease indications with high unmet need.

1.2. Introduction

Immunosurveillance is a quiet constant, finding and destroying dysregulated cells and preventing the progression of mutated clones to malignant tissue. Though our immune system is potent and curative in many contexts, malignant cells can escape surveillance and evade our immune system to survive[1]. While we have dramatically expanded our understanding of both

the protective role and the ultimate failures of immune protection in cancer, we have been limited in our ability to harness the broad capacity of natural immune mechanisms. To date, first line therapies for most malignancies rely on broad, non-specific approaches to kill or remove tumor cells such as radiation, chemotherapy, and surgery.

In contrast to previous cancer treatments, immunotherapies seek to engage and stimulate specific antitumor mechanisms of immunosurveillance and immune clearance. Clinical demonstration of exogenous delivery of cytokines or treatment with tumor infiltrating lymphocytes (TILs) has validated the hypothesis that stimulating the immune system is a viable strategy for treating tumors. In parallel, CTLA-4 and PD-1 checkpoint blockade has changed the way we treat cancer patients, providing durable tumor clearance in a subset of patients where long-term responses were previously impossible[2]. Synthetic biology is a field that incorporates novel capabilities into biological systems to customize and manipulate the activity of cells or networks of cells. Over the last decades, synthetic immunologists have started to leverage this approach to build tools for specific, discrete, and tunable control of immune cells providing a valuable platform for therapeutic intervention[3]. In this new era of synthetic immunity, we have an opportunity for broad impact in treatment-refractory cancers that require more sophisticated avenues of therapeutic attack and adaptive intervention.

Although there are far ranging therapeutic opportunities for synthetic immunology, here we focus on tools built to enhance cell therapies for cancer. While multiple CAR T cell therapies have gained FDA approval[4–9], many promising preclinical therapies for solid tumor models have not made significant impact in patients due to factors such as unexpected toxicity, antigen escape, or lack of persistence[10–15]. Tackling these issues, particularly in solid tumors, is the clinical frontier for synthetic immunology[16], and the lessons learned in this arena can pave the way for applications in other disease contexts. Some success of phase 1 trials of CAR T cells in

solid tumors have been reported[17–19], providing hope that engineered cell therapy can be effective in solid tumors, but currently these results are the exception. Our review seeks to identify obstacles learned from both preclinical experiments and clinical trials, describe the major remaining hurdles and current synthetic immunology approaches to overcome them, and propose a set of guidelines for successful translation of synthetic immunology from bench to bedside. Understanding the complex biological underpinnings of cancer, accurately modeling these challenges pre-clinically, and developing a cell engineering toolkit informed by clinical iteration is paramount for future clinical impact.

1.3. Clinical hurdles in cell therapy

To build an optimal toolkit, we must first consider the current challenges facing cell therapies for cancer treatment. The main obstacles can be broken down into three major categories: building an optimal cell graft, overcoming the suppressive tumor microenvironment, and developing relevant preclinical models for rapid iteration on novel solutions (Figure 1.1).

The graft, most commonly autologous products derived from each patient's peripheral blood, must be collected, engineered, and transfused back into the patient which can be expensive, technically cumbersome, and time consuming[20]. Retrospective analyses have described how graft composition[21], Treg abundance in the graft[22], cell state[23], receptor expression[24–26], and product manufacturing impact the capabilities and functions of CAR T cell therapies. Significant strides are being made to solve for issues of graft persistence, potency, and antigen specificity with novel synbio tools. Further investigation of the fundamental mechanisms of both successful and failed therapies will inform how to design an optimal cell

therapy product. This work will continue to be paramount to accelerating effective antitumor treatment and developing best practices moving forward.

As synbio therapies move beyond treating hematological malignancies, the importance and difficulty of understanding and tackling the tumor microenvironment has come into focus. This is particularly important as 90% of cancers are solid tumors and there currently are no FDA approved cell therapy products for any solid tumor indications[16]. Due to their intrinsic biology, solid tumors present unique challenges for engineered cell therapies including antigen heterogeneity, lack of tumor specific targets, and immune inhibitory cellular compositions[27,28]. The tumor microenvironment (TME) itself can be hostile; tumor cells secrete growth factors to co-opt surrounding stroma and endothelial cells and build pro-tumorigenic extracellular matrices and vasculature to support continuous growth. This environment contributes to poor CAR T cell infiltration, durability, and persistence[29,30]. Solid tumors can also be hypoxic and secrete immunosuppressive metabolites such as lactic acid or cytokines that inhibit immune recognition and activation[31]. Additionally, cancer cells can downregulate MHC-I, evolve mutations to dysregulate the IFN responsive pathway, and upregulate inhibitory ligands like PD-L1 to escape direct targeting and induce exhaustion of the adaptive immune response[32,33]. These mechanisms of immune evasion or escape act as brakes on engineered cell therapy products and need to be considered and overcome for effective tumor eradication.

Lastly, a key remaining roadblock to rapid cell engineering solutions is the biological discordance between the preclinical models used for exploratory investigation and the clinical diseases we are hoping to treat. *In vitro* testing, *in vivo* xenograft and syngeneic models, and non-human primate studies all pose unique advantages and limitations. Despite their ubiquitous use in preclinical investigation and tool validation, many commonly used murine models are often poor predictors for clinical success. To the best of our ability, choosing a clinically or

biologically relevant preclinical model to each specific scientific inquiry is essential to understand fundamental cell therapy mechanisms of action.

1.4. Principles of generating new synbio tools for clinical impact:

In this review we seek to define clear principles for generating new synbio tools for optimal clinical impact (Figure 2). Synthetic tools can and should be used broadly for biological discovery, however we believe there are foundational principles that can guide the use of synthetic immunology in building novel therapeutic approaches. We believe that successful translational synbio tools must 1) be rooted in the current understanding of immunology and cancer. Defining a specific need within a biological system with clear mechanistic understanding of the immunology and tumor microenvironment should be central to the tool building process. 2) Synbio tools need to be investigated and validated in relevant models. To iteratively design synbio tools that make clinical impact, investigators need to work in preclinical models that recapitulate the pathology and heterogeneity of human cancers and the immune system. 3) Synbio approaches should engineer for dominant rather than incremental effects with the appropriate evaluation of safety. Preclinical tool building should focus on synthetic enhancements that are robust across mouse and human tumor models, ideally against a broad range of suppressive mechanisms. Tools can be more easily tuned down or toxicity profiles modified, whereas it is often harder to amplify features we would like. 4) Synthetic tools should be developed with human compatible designs with insight from the clinic. Synthetic immunology can rapidly develop and translate novel solutions from bench to bedside. Building with human compatible tools for issues identified from clinical learnings could expedite this translational intersection. 5) As we layer synbio tools beyond monotherapies, our approaches should activate

complementary mechanisms, and future therapies should make best efforts to propagate multi-nodal solutions. Current and future synbio tools provide platforms to modulate multiple axes of the immune system. Engaging a multi-nodal, polyfunctional approach that mirrors natural immunology will likely be necessary for complete responses. A productive scientific discovery pipeline would incorporate these guiding principles in an efficient cyclical exchange, allowing clinical advances to fuel laboratory development and vice versa (Figure 1.2).

1.5. Principle 1: Rooting Synthetic Immunology in Current Understandings and Failures

Successful synbio tools are educated by natural immune signaling, function, and systems and future tools should build on these biologically informed advances. Designing and translating synthetic biology tools for immunology-based therapies requires expertise in both synthetic molecular technologies and the immunological and clinical problems to be solved. For cancer, sequencing and proteomic analysis continues to expand our understanding of therapeutic targets, tumor microenvironments, clonal evolution and the biological limitations of engineered immune cells34–37. All of these analytical tools should be implemented to better understand the current failures to catalyze better solutions (Figure 1.3).

Using Natural Receptor Signaling to Educate Synthetic Design

The design of a CAR was founded in learnings from natural T cell receptor (TCR) binding and signaling. Second generation CARs employ CD3z from the TCR complex for “signal 1” combined with domains such as 4-1BB or CD28, which mimic the natural “signal 2” that cells

receive through costimulatory receptors. Our group has employed screens to assess 40 alternative costimulatory domains in CARs, and determined that inclusion of BAFF-R, a costimulatory receptor expressed in B cells, improves CAR T cell signaling and *in vivo* efficacy[38]. Daniels and colleagues similarly sought to improve CAR T cell signaling, assessing hundreds of combinations of signaling motifs, and determined that non-natural combinations of signaling from PLCg and TRAF binding domains within a CAR improves overall cytotoxicity and cell state[39]. Comprehensive costimulatory evaluation is far from exhaustive to date, and it is possible that different disease contexts for cell therapies could benefit from an application specific "signal two" based upon the therapeutic requirement for graft expansion vs. persistence vs. activation.

The classical extracellular domain of a CAR is based on an antibody single chain variable fragment (scFv) and is significantly different to a natural TCR in antigen sensitivity, signaling strength, serial killing kinetics and overall functional phenotype[40–44]. To improve antigen sensitivity and persistence of engineered cellular therapies, many groups have sought to imitate TCR signaling by fusing scFvs to CD3 chains of the TCR (TRuCs) and found these receptors organized an effective TCR signaling complex in response to the scFv targeted antigen[45]. Similarly, some groups have fused heavy and light scFv chains to the constant regions of a TCR alpha and beta chain, creating HLA independent T cell receptors known as “HIT” receptors[46] . Beyond the ECD, others have included post-synaptic density-95, discs large and zona occuldens 1 binding moieties (PDZbm) domains in CAR intracellular domains - organizing the CAR synapse to mimic the TCR synapse more closely – and have demonstrated that these designs result in greater signaling outputs[47]. In a recent preprint, Finn and colleagues sought to mimic the “horizontal” signaling of TCR complexes and developed valency-controlled receptors, using small molecules to increase the clustering of CARs[48]. New receptor designs have sought to employ other natural multi-chain immunoreceptors, hypothesizing that multi-chain receptors

would allow for greater signaling diversity, and improved signaling. Wang and colleagues co-opted the c, which complexes with DAP12, for use as an engineered receptor by fusing an scFv to the ECD of a KIR (KIR-CARs). The authors found that KIR-CAR T cells, which depend on immunoreceptor tyrosine-based activation motif (ITAM) signaling from DAP-12 association with the KIR-CAR, had improved *in vivo* efficacy and persistence compared to canonical CD28 or BBz CAR T cells[49].

Overall, these approaches to engineering a CAR demonstrates that the quality of the CAR signaling, receptor avidity and affinity, and synapse duration, are critical for therapeutic outcome. By understanding effective T cell signaling, synbio approaches can be developed to mimic or co-opt these natural processes for better engineered therapies.

Understanding T Cell Exhaustion for the Design of Persistent Grafts

Basic T cell biology gives us the roadmap of T cell function and reveals mechanisms of failure that synbio tools can address. Upon effective encounter with cognate antigen, T cells rapidly proliferate and differentiate from naïve to effector and memory states, resulting in a pool of cytotoxic killer cells and a reservoir of long-lived antigen specific T cells. In the context of persistent antigen exposure, such as chronic infection or cancer, T cells can take on a dysfunctional exhausted state defined by upregulation of inhibitory receptors such as PD-1[50], Lag-3[51], and Tim-3[52], limited polyfunctionality of cytotoxic and inflammatory cytokines, and reduced proliferative and killing capacity[53]. The characteristics and mechanisms of T cell exhaustion have been reviewed elsewhere[54,55], and it is well understood that exhaustion limits the function of both endogenous and CAR T cells[56]. By understanding the mechanisms of T cell exhaustion, synbio approaches have been employed to prevent or avoid exhaustion. Recent

advances in the efficiency and ease of gene editing and sequencing have provided the opportunity to investigate the benefits of genetic insertions and/or deletions in combination with synthetic receptors.

Beyond the natural drivers of T cell exhaustion, recent pre-clinical and clinical studies have demonstrated that constitutive expression of CARs can also lead to a greater state of dysfunction due in part to tonic signaling of the receptors[26,57]. To address this issue, many groups have sought to regulate the surface expression of CARs, using T cell receptor alpha constant (TRAC) locus integration[24], synthetic circuits[25], or drug inducible or protease on/off systems[58,59]. Further investigation into the mechanisms of T cell exhaustion, both natural and induced by synthetic receptor expression, as well as understanding of optimal T cell signaling, cell state and differentiation will remain central to engineering a successful graft.

1.6. Principle 2: Iterative Design in Predictive Preclinical Models

Understanding the basic biology of the graft and clinical indication is the first step in developing useful tools. Next, we need models to test and validate new synbio solutions rapidly and accurately. Working *in vitro* is optimal for rapid, high throughput discovery, but does not recapitulate the cellular composition, metabolic constraints, and organizational complexities of tumors, particularly solid tumors. In contrast, mouse models are useful to test biologically relevant effect sizes but don't fully replicate human tumors, disease indications, or toxicity profiles. A more expansive exploration of the limitations of murine models have been reviewed nicely by Dranoff and colleagues[60]. As a result of these limitations, many of the flaws of cell therapy have only been revealed through clinical trial failures, where preclinical models were

insufficient to accurately predict toxicity or efficacy. To the best of our ability, preclinical evaluation should be grounded in the biology and specific immunology of each application, and where possible, use models that accurately reflect the clinical challenges (Figure 1.4).

Benefits and Considerations in Current Preclinical Modeling

Xenograft models use genetically immunodeficient mice that allow engraftment of human cells[61]. Xenograft models using human cancer cell lines that express clinical antigens are currently the gold standard for cell therapies seeking IND approval, however, these models lack the complexity of tumor heterogeneity and do not have an intact immune system. Typifying the limits of these models was the clinical discovery of cytokine release syndrome (CRS), a common toxicity seen in CAR T cell therapy, which can only be demonstrated in mouse models with a functional macrophage compartment[62,63]. Beyond their failure to recapitulate toxicity, xenograft models are also limited in their ability to demonstrate how cellular therapies would interact with and engage the endogenous immune system[60]. Further iterations of these models, such as patient derived xenografts (PDX) which replicate tumor heterogeneity or humanized mice which mimic an intact immune system, can be used to better reflect clinical hurdles. However, those approaches are expensive and time consuming, making it difficult to iterate on early high-risk, high-reward ideas.

Syngeneic models are a cheaper and more technically accessible way to model engineered cell therapies in a fully immunocompetent system. Typically, mouse cancer cell lines are implanted, and mice are treated with engineered mouse immune cells. This approach allows investigation of CAR T cell behavior in an immune competent tumor microenvironment and fully developed immune organs that more closely mimics what might happen in a patient. Syngeneic

mouse models also have the benefit of genetic tools and transgenic models that can be leveraged to probe cell intrinsic or endogenous immune accelerators or inhibitors that may be impacting the cell therapy. However, these models can be limited in their ability to accurately reflect human tumors[64]. To develop more physiologically relevant models, many have turned to genetically engineered mouse (GEM) systems that rely on cancer driving mutations to cause spontaneous tumor growth, which more accurately reflect human tumor progression[65]. CRISPR/Cas9 technology has increased the pace at which unique mouse models can be created, sidestepping the need for embryonic cell manipulation and years of crossing to create new lines[66]. The breadth of syngeneic tools makes these valuable models, however the discrepancies between mouse and human systems remain a hurdle.

Because of their genetic similarity, non-human primates (NHP) most closely replicate human biology, and studies performed in these models most accurately predict engineered cell therapy outcomes in patients[67–69]. However, target antigen biology and expression (as is the case for CD19) can be different between NHP and human cellular compartments, thus necessitating surrogate, non-clinical grade therapies for studies[69]. While NHP studies are occasionally performed to test aspects of safety and efficacy of engineered cell therapies[70], these studies are expensive and difficult to carry out and will never be the first line model for discovery and iterative testing[71].

Best in Class Preclinical Modeling

Patient tumors are broadly classified by tumor site, histologic type, grade and stage; however, biological features such as mutational burden, antigen expression, and immune infiltrate are starting to be evaluated as key predictors of response[72]. Just as synbio tool design

needs to be rooted in immunology, so too do the models we develop need to be rooted in pathobiology. Many research groups have begun to tackle this problem by defining critical features of the tumor immune landscape in human and mouse tumors, particularly in response to immunotherapy.

Recently, a pan-cancer deep immune phenotyping atlas was developed and published by the Krummel lab. The authors describe 12 immune archetypes common across an array of tumors, that they discovered by assessing and clustering transcriptomic data of over 300 patient tumors across 12 tumor types. Notably, they describe how these archetypes superseded the tumor site and can be used to predict tumor growth and patient survival, supporting ongoing sentiments that tumor immune composition is an essential component of understanding the tumor pathology[73]. This data set, and others that are similar[74], establishes an immune landscape of patient tumors and should be a resource to contextualize tumor immune compositions of murine models, particularly as synbio tools are developed to influence the tumor microenvironment. Further resolution into the spatial orientation of the tumor-immune compartment with multiplexed immunohistochemistry[75], Multiplexed Ion Beam Imaging (MIBI)[76,77] , CODEX imaging[78], or RNAscope[79] provide new modalities and insight into understanding the TME and requirements for tool building in difficult to treat human tumors. Understanding the complex cellular networks that form in tumors and support resistance to therapy or help drive immunity is critical to determining how living therapies can be engineered within these networks. Li and colleagues[80] developed an immune spectrum of mouse pancreatic ductal adenocarcinoma (PDAC) models to study intratumoral heterogeneity and mechanisms of therapy resistance. They isolated clones from a PDAC KPCY mouse cell line and identified a single clonal subtype that utilized CXCL1 as a driver of an immunotherapy resistant tumor microenvironment. In the process, the authors developed many useful PDAC cell lines that span

the spectrum of immune “hot” to “cold”, providing new opportunities to study immunotherapy across discrete TMEs and immune archetypes. In a similar mechanistic study, Park et al recently demonstrated that Ang-2 dependent spatial vascular destabilization promotes T cell exclusion in a melanoma mouse mode[81]. These types of discoveries allow us to gain deeper insight into mechanisms of resistance, identify parallels to a human TME, and investigate opportunities to utilize synbio tools.

In an excellent example of matching human tumor discoveries to murine models for further discovery, Mariathasan and colleagues[82] found that metastatic urothelial cancer patients who did not respond well to checkpoint therapy commonly had immune-excluded tumors and high TGFβ signatures. The authors then sought out syngeneic murine tumor models with a similar phenotype and found that co-administration of TGFβ antibodies improved responses to checkpoint therapy in these previously refractory tumors. As we develop synbio tools that can influence the immune phenotype of the TME, we need to thoroughly characterize and utilize tumor models to determine if our tools accurately combat the clinical challenge we are hoping to resolve.

Modeling Clinically Observed Toxicities

One major limitation of mouse models is the failure to accurately recapitulate toxicities observed clinically. The use of human model antigens in a murine system prevents the observations of on-target off-tumor toxicity since healthy mouse tissue won't be a target. Good off-target toxicity modeling can be done by targeting naturally occurring mouse proteins. For example, Riddell and colleagues[83] demonstrated lethal bone marrow toxicity when using a constitutively expressed murine ROR1 targeted CAR, however when expression was controlled

by “AND” gated SynNotch receptor, CAR activation was limited to the tumor and no bone marrow toxicity was detected. As mentioned earlier, CRS is another major adverse clinical event in CAR T cell therapy but was not reported in mouse models prior to the clinical presentation observed in early CAR T cell patients. Two mouse models have now been developed to recapitulate human CRS, from both a molecular and symptom perspective. These models have helped to elucidate key molecular drivers of CRS like T cell driven IL-1 and myeloid produced IL-6 that are essential to the pathology[62,63]. Mouse modeling of CRS allowed both groups to develop mechanistic insight into why CRS occurs and test interventions that can be applied to the clinical manifestation in humans. This feedback from clinical observations to accurate mouse modeling is essential to rapidly progress safe and effective therapies for patients.

Animal models are inherently limited in recapitulating the biology of human tumors and the human immune system. However, as our understanding of the human and mouse tumor biology, immunology, and spatial organization of tumors progress we can more accurately test new synbio approaches in mechanistically relevant models. This will allow us to develop synbio solutions for clinically observed problems and evaluate their efficacy and safety in *in vivo* systems that mirror them.

1.7. Principle 3: Engineering Solutions with Dominant Effects

While engineered cell therapies dramatically expanded the field of immuno-oncology for hematological malignancies, they have made far less clinical impact in solid tumors. This slow pace of forward movement is not for lack of research effort and dollars. Cancer immunology has been defined by numerous foundational shifts and step changes in therapy capabilities and

patient outcomes. Bone marrow transplant and TIL therapies pioneered the capabilities of adoptive cell therapy, checkpoint blockade demonstrated the capacity for immune mediated tumor clearance in previously incurable patients, and CAR and TCR therapies have paved the way to genetically retarget a patient's immune system altogether. Each step forward has come with incredible patient results, but has intermediate periods defined by smaller, iterative design changes. We are now in need of another step change if we hope to tackle solid tumors.

Approaches to Novel T Cell Enhancements

While modifications to CAR or TCR design, cell manufacturing, and combination therapies can improve engineered cell therapy performance, we believe T cell enhancements have to push further (Figure 1.5). Engineering for dominant rather than marginal improvement is particularly important for the patient populations who will first receive these therapies, as cell therapies are typically the last resort for a refractory tumor. Furthermore, cell therapy development is expensive and can hamper iteration at the clinical stage[84]. Real change in patient outcomes will not only continue to drive scientific discovery but promote continued investment for clinical stage programs.

Recent approaches to enhance T cell persistence and prevent exhaustion have included the permanent deletion of tumor suppressor genes, inhibitory receptors or negative regulators of T cell signaling[85–90]. Through a genome wide CRISPR deletion screen, Prinzing and colleagues have discovered that deletion of the DNA methylation enzyme DNMT3A improves CAR T cell persistence and prevents exhaustion related epigenetic changes that are thought to reinforce dysregulated CAR T cell states[91]. Genome wide *in vivo* and *in vitro* CRISPR screens have elucidated a number of other negative regulators such as RASA2, Regnase-1,

and Roquin-1 that when eliminated unleash long term survival and potency of CAR T cells[87,92,93]. In some cases, beneficial gene deletions were discovered serendipitously by evaluating strongly responding patients. In one patient, a single T cell clone was discovered to have expanded and be the primary anti-tumor responder as a result of the CAR randomly inserting into the TET2 locus, rendering the tumor suppressor gene non-functional[85]. While recent work has demonstrated safety risks of TET2 deletions[94], this fortuitous deletion has demonstrated the curable power of high-risk step changes that can be achieved through purposeful gene deletions in cell therapies.

Tunability and Synthetic Control of Dominant Immune Regulators

Disabling the brakes of the immune system or boosting phenotypes of proliferation and activity through potent cytokine activity are inherently risky approaches with mixed safety and efficacy results historically. However, we should be engineering for potency while simultaneously developing synthetic tools to tune these responses to function within acceptable safety profiles.

Synthetic circuits, which control expression of toxic or dangerous off-tumor payloads, provide a method for temporal and spatial control. On-target, off-tumor toxicity is a common problem, particularly in solid tumors where tumor specific antigens are rare and we rely on targeting tumor associated antigens, which may also be present in healthy tissue. In our lab, synthetic notch receptors such as synNotch and next generation SNIPR are designed to target tumor specific antigens, that then drive the expression of CARs targeting tumor associated antigens. Using combinatorial circuits such as these takes advantage of “AND” gating, only allowing for CAR expression within the relevant tumor microenvironment and preventing harm to healthy tissues[25,95,96]. Other groups have used the hypoxic nature of solid tumors for control of

CAR expression, fusing a hypoxia-inducible factor 1α (HIF1α) to the C-terminus of a CAR to induce CAR degradation at normal O2 concentrations, while at low O2 concentrations HIF1α stabilization allows for sustained surface expression and activity of the CAR[97]. Additionally, creative use of proximal signaling domains within CAR architectures has led to the development of “LINK” CARs, which signal only in the presence of both “AND” gate antigens[98]. Vincent et al. published a preprint reporting a probiotic-guided CAR-T cells (ProCARs), in which T cells are engineered to sense synthetic antigens that are produced and released by tumor-colonizing probiotic bacteria[99]. These types of synthetic circuits place normally toxic, or off-target CARs, under temporal and spatial control making previously untenable solutions safe.

Cytokines are potent immune mediators but are often pleiotropic and have unintended off-target effects. Synthetic cytokines (synthekines) such as engineered IL-2, have been designed with higher affinity for cytotoxic CD8 T cells than regulatory T cells (Tregs), and multiple groups have demonstrated that synthetic IL-2 drives expansion of the CD8+ compartment[96,100]. This provides the dominant desired effect of IL-2 while eliminating the negative side effects, maintaining a potent and targeted solution. Delivering synthetic-IL2 in combination with CAR T cells or under circuit control with synNotch receptors[101] is an effective way to promote antitumor immunity while mitigating the regulatory checks and balances of the endogenous immune response. Others have used T cells redirected for antigen-unrestricted cytokine-initiated killing (TRUCKs), also known as 4th generation CARs, that employ Similar approaches have been applied to engineering the potency of IL-18 to have lower affinity binding to the decoy receptor IL-18BP and therefore increase efficacy in potentiating anti-tumor response in solid tumors[102]. For systemically toxic cytokines that have yet to be engineered for greater safety, synthetic circuits can be employed for delivery, bringing a suite of potent anti-tumor but previously toxic cytokines back into play.

By combining synthetic regulation with engineered enhancements, we can take potent, dominant functionalities and tune them for efficacy and safety. This approach has the potential to drive step function change in therapeutic translation and clinical outcomes.

1.8. Principle 4: Human Compatible Designs from Clinically Derived Hypothesis

Human trials are expensive, high risk to patients, and limited in patient size and data collection. Because of the limited number and scope of these trials, results and mechanistic learnings from clinical trials are invaluable for the field to progress. Thus, clinical data from trials should be collected, analyzed, and shared widely with the broader scientific community to allow for more rapid solution development and preclinical innovation. One of the best implementations of rapid data sharing from clinic to lab is exemplified by the Immunotherapy Platform of MD Anderson Moon Shots program. Their work shortens the gap between clinical patient data and preclinical innovation, using clinical findings to drive basic research and elucidate mechanistically complex problems on a patient specific scale. Through comparison of checkpoint blockade responsive and resistant tumors, Blando and colleagues determined the immune checkpoint receptor, VISTA, is highly expressed in therapy resistant tumors[103]. This discovery has led to the development of clinical therapies targeting VISTA, which are currently being assessed for efficacy in deadly tumor types such as pancreatic cancer[104]. This clinic-to-research feedback loop provides a blueprint for cell therapy innovation that is highly iterative, rapid, and patient focused. For rapid translation, our preclinical investigation should be focused on human compatibility with clinically minded solutions so that once validated in the lab these solutions can be more easily translated to the clinic (Figure 1.6*)*. A parallel example is happening at UCSF with the Immunoprofiler Initiative, who are collecting a large repository of

scRNA sequencing, flow cytometry, and clinical data from patients with a broad range of disease indications from cancer to autoimmunity. Combes and colleagues[73] leveraged this data to elucidate fundamental cancer immune archetypes, previously described in Principle 2, which is catalyzing parallel studies and therapeutic development in mouse models. This type of clinical insight is key to driving better preclinical model development and a tight feedback loop for innovative solutions to reach clinical relevance.

Clinical Insight to Drive Novel Tool Development

One early insight from patients with failed CAR T cell treatment was the development of antigen negative or antigen low tumor relapse. Some patients, who initially responded to a CD19 CAR therapy and relapsed with antigen negative or low cancer, have been dosed with a second CAR therapy targeting an alternative antigen CD22[105]. While this strategy resulted in a 50% complete response rate, creating and dosing patients with two separate therapies is costly and risky. For this reason, single therapies that are dual targeted have been developed. With dual targeting comes the opportunity for designing Boolean logic gates. Bi-specific or tandem CARs employ “OR” gates where scFvs targeting CD19 and CD20 are placed in series[106], allowing CAR T cells to kill targets with either CD19, CD20 or both antigens expressed. Similar designs targeting CD19 and CD22 have also been developed. Phase I clinical trials assessing these approaches found success, though treatment failed in one patient determined to have CD19 and CD20 negative disease[107]. Relapse in one CD19/22 dual targeted clinical trial was attributed to lack of therapy persistence[108], while relapses in another trial were thought to be caused by a lower activity of the bi-specific CAR product against CD22, allowing for greater chance of relapse when CD19 antigen expression was lost[109]. Mechanisms of failure in these

trials demonstrate the evasive power of cancer, the limits of multi-antigen targeting, and the ongoing need for more persistent therapies. However, dual targeting approaches have multiplied, with CD19/CD123 dual targeting for B-ALL[110], HER2/IL13Ra2 targeted for glioblastoma[111], BCMA/CD38 or BCMA/CS1 targeted for multiple myeloma[112,113], and Mesothelin/Folate Receptor 1 designed for ovarian cancer[114].

While “OR” gate CARs have found some success, not all antigen combinations are candidates for this gating strategy as some tumor associated antigens like HER2 or CAIX can be expressed on healthy tissues and have demonstrated a risk for on-target off tumor toxicity[13,115]. As discussed in principle 3, SNIPR ‘prime-and-kill’ combinatorial circuits have been developed to take advantage of “AND” gating, only allowing for CAR expression within the relevant tumor microenvironment, avoiding on-target off-tumor toxicity[25,95,96]. First in-human trials have recently been initiated in ovarian cancer with ‘prime-and-kill’ ALPPL2/MSLN circuits (NCT05617755).

Human Compatible Designs

Many synthetic biology tools are developed and optimized in model organisms that are easily handled and manipulated, such as yeast and bacteria. Non-human proteins or non-native protein configurations can be recognized and eliminated by the immune system, making even the best non-human synthetic tools incompatible with clinical translation. CARs can even be recognized and rejected by the patient’s immune system and anti-CAR antibodies have been observed and can suppress the overall efficacy of the cell therapy or can induce anaphylaxis[10,116]. Humanization of scFvs[117,118], or other domains such as the transcription factors in SNIPRs[96], is an important step to reduce the likelihood of an anti-drug immune response. As

we think about translating genetic manipulations with CRISPR knock-out, knock-in, CRISPRa and CRISPRi, we also need to evaluate the compatibility and feasibility of introducing these systems in patients given their potential immunogenicity[119]. One approach to get around long-term expression CRISPR systems is to utilize Cas9-based chromatin modifiers[120], which can be used for multiplexed manipulation of gene expression that can last for months to potentially years after transient exposure of the targeted engineered chromatin modifier *ex-vivo*. Synthetic tool building in a laboratory can provide mechanistic insight or proof of concept validation but it is important for translational work to continue to be anchored in human compatible systems.

1.9. Principle 5: Designing Multi-Nodal Approaches for Tumor Eradication

While this review has focused on engineered T cells for anti-tumor activity, the complexity of solid tumors and accumulating clinical trial failures suggests monotherapies or even dual targeting cell therapies may not be sufficient to elicit complete tumor eradication Rather, we believe designing a synergistic multi-nodal therapy, either equipping the graft with multiple complementary anti-tumor weapons or simultaneously activating graft and endogenous immune response, will be required for full tumor clearance (Figure 1.7).

Engineering Complementary Mechanisms into T Cells

One challenge facing engineered cell therapies is trafficking to and infiltrating into a solid tumor. Unlike leukemia and lymphomas where cancer is more readily accessed by cell therapies

in the blood and lymphatics, solid tumors can develop complex and dense systems of fibroblasts, epithelial or endothelial cells, and extracellular matrix which effectively reduce the ability of T cells to infiltrate. While localized delivery (intratumoral, intrapleural, etc.) strategies have been used to overcome this, a better approach may be to engineer therapies for greater infiltration to the solid tumor. One approach is to express non-natural chemokine receptors on the cell therapy that respond to chemokines commonly expressed in solid tumor settings, such as CCR2, CCR4, CCR7 and others[121–127]. Fully synthetic approaches to improve trafficking to a user defined site have also been developed, where Park and colleagues[128] demonstrated that engineered G protein coupled receptors could be expressed in mammalian cells to respond to and traffic to sites of high expression of the orthogonal molecule clozapine-N-oxide. Beyond the axis of chemotaxis, some groups have begun engineering T cells to secrete enzymes to break down tough stroma, or even target and kill FAP+ fibroblasts within the tumor microenvironment, demonstrating that loosening or debulking tumor stroma can improve T cell penetration[129,130]. These approaches, coupled with the canonical targeting and activation through receptor design, are key examples of understanding the immunological hurdles of CAR T cell penetrance and using synthetic solutions to solve them. Not all tumors will require multiple synergistic tools, some immunologically “hot” tumors may already be permissive to CAR T cell infiltration whereas immunologically “cold” tumors may require combined approaches to overcoming TME exclusion.

Beyond the challenge of infiltration, the TME has a multitude of inhibitory mechanisms to resist cell therapy, such as growth factors like GM-CSF[131], VEGF[132], EGFR, PDGF and FGF, as well as immunosuppressive or Th2 skewed cytokines like, IL-4, IL-5, IL-10 and IL-13[133]. Additionally, TMEs often express inhibitory ligands that dampen CAR T cell response such as PD-L1 and require new solutions to overcome these suppressive arms. One approach is to

engineer CAR T cells to express switch receptors, fusing an inhibitory extracellular domain to a stimulatory intracellular domain. In short, these receptors convert a naturally inhibitory signal to a stimulatory one within the engineered cells. One example of this is the PD-1/CD28 switch receptor, which fuses the PD-1 receptor extracellular region to a CD28 costimulatory receptor intracellular domain. These receptors bind to PD-L1, which is highly expressed in suppressive tumor microenvironments, and boost activating T cell signaling rather than dampen it[134,135]. Switch receptors are modular with their inputs and outputs and multiple designs have been developed targeting other ligands such as Fas, fusing FasR to 4-1BB intracellular signaling domains[136], or targeting immunosuppressive cytokines such as the GM-CSF/IL-18 switch receptors[137], or even a TGFβ/IL-7[138]. In cases where these enhancements can conform to the cargo capacity of cell therapies, they equip the graft with additional capabilities to overcome multiple suppressive mechanisms. However, not all tumors engage the same immunosuppressive mechanisms so we must design the graft with the correct tools to overcome the TME we are hoping to treat.

Directly Targeting the Axes of Immunosuppression

While endowing the cell graft with cell intrinsic suppression-resistant tools is important, some groups have developed strategies to directly tackle and reverse the inhibitory mechanisms of solid tumors.

Tumor associated macrophages (TAMS) are relevant to all immunotherapy approaches since they compose a significant portion of intratumoral immune infiltrates and can play either a pro- or anti-tumor role in therapy efficacy[139–141] (reviewed elsewhere[142]). Although it's an oversimplification of their function, TAMS are broadly seen as immunosuppressive and CARs

targeting the macrophage marker F4/80 have been developed to debulk solid tumors of these immunosuppressive mediators. Preclinical data demonstrates that anti-F4/80 CAR T cells, when delivered systemically, traffic to the sites of tumors, reduce macrophage populations, and delay tumor progression. Additionally, researchers found that treatment with F4/80 CARs promoted the expansion of endogenous tumor antigen specific T cell populations and immune editing, indicating that TAM debulking via CAR T cell treatment has a ripple effect beyond the direct target killing and can successfully reinvigorate an endogenous anti-tumor immune response[143].

TGFβ is a parallel suppressive TME mechanism (reviewed in depth elsewhere[144]) and is often secreted at high levels in solid tumors. TGFβ, and its concomitant signaling pathway, are therefore targets of synbio development, with the goal of disrupting the suppressive TGFβ feed forward loop to promote a shift towards an anti-tumor immune response. Tang and colleagues sought to make engineered cells resistant to TGFβ signaling by deleting the TGFβRII and demonstrated improved solid tumor control in xenograft mouse models[145]. TGFβ dominant negative receptors have also been employed, these receptors have intracellular truncations that prevent signaling when TGFβ is bound extracellularly. Strong preclinical data has led to a phase I clinical trial to assess safety and efficacy of CAR T cells with this dominant negative receptor in prostate cancer[146]. Other groups have aimed to leverage the high abundance of TGFβ in the TME and target CAR receptors against the active form of TGFβ, demonstrating CAR T cell activation in response to a soluble tumor associated ligand and promoting endogenous cytotoxic CD8+ T cell activation[147].

Activating the endogenous immune response

Although PD-1 and CTLA-4 checkpoint blockade is designed to target and reinvigorate T cells, recent studies have demonstrated that these therapies induce significant changes across innate and adaptive cell types both locally and in the draining lymph node[131,148–151]. These discoveries suggest that cell therapies should also be designed to broadly restructure the endogenous immune system to elicit a greater anti-tumor efficacy.

Antigen heterogeneity and loss is a significant challenge of single targeted cell therapies, often resulting in initial promising tumor regression that relapses with antigen downregulation or outgrowth of antigen negative clones. Many groups seek to resolve this by activating the endogenous immune system to respond to naturally occurring tumor antigens, a phenomenon known as epitope spread. The goal is to design cell therapies against a tumor specific antigen while simultaneously promoting a broader polyclonal anti-tumor T cell response. While this phenomenon is less commonly observed with engineered cellular therapies, in one clinical study mesothelin targeted CAR T cells induced endogenous T cell responses in patients[152], providing proof of concept that the action of an engineered cell therapy can induce an endogenous immune response. Another effective approach demonstrated that an EGFRvIII- CAR T cell secreting an EGFR bi-specific T cell engager (BiTEs) could directly kill tumor targets and recruit and redirect bystander T cells to participate in tumor clearance. This resulted in elimination of a heterogenous antigen tumor model of glioblastoma[153]. Other synbio approaches have focused on recruiting and maturing antigen presenting cells within the tumor microenvironment. Some approaches make use of “armored” CARs to secrete factors such as IL-7, IL-12, IL-18, CCL19, or FLT3 to activate endogenous APCs[154–157], while constitutive expression of CD40L by CAR T cells has also been demonstrated to induce epitope spread[158]. It is key to evaluate these

potential solutions to epitope spread in syngeneic models where there is a competent immune system to engage.

Engineering alternative cell types for multilineage therapy

Engineered cell therapies have primarily focused on T cells to date, however the field has expanded to include engineering unconventional T cells, NK cells and macrophages for immunotherapy applications. NK cells are innate immune cells that target and kill infected cells and tumor cells in an HLA independent manner. Furthermore, NK cells recognize and activate in response to targets through a balance of positive and negative receptor signaling rather than through a single TCR receptor/ligand interaction. This killing mechanism may allow for CAR-NK killing of heterogeneous tumor settings without the need of dual antigen targeting.

These features make them an appealing platform for engineering, and unlike T cells, allows engineered CAR-NKs to be an off-the-shelf therapy, with current clinical products being engineered from the cell line NK92 as well as allogeneic engineered cells (Clinical Trial NCT05020678 and NCT04623944). Early CAR-NK studies focused on targeting blood cancers, engineering cells to express CD19, CD20 or CD22 targeting receptors, with some promising efficacy and low instances of CRS or immune effector cell-associated neurotoxicity syndrome (ICANS)[159]. More recent studies focusing on solid tumors have demonstrated preclinically efficacy[160], and there are now multiple phase I clinical trials assessing CAR-NK cells in solid tumors, however these have yet to report efficacy results. Despite their promise for off-the-shelf therapy, there remain significant hurdles to implementing CAR-NK cells including technical challenges of efficient manufacturing, in-patient expansion and persistence, and optimizing their potency for maximum impact[161].

Because of their abundance in solid tumors and ability to infiltrate the TME, macrophages are another innate immune cell type highly sought after for engineering applications. Although broadly considered immunosuppressive in the TME context, macrophages can have potent anti-tumor capabilities and can be repolarized or activated *in vivo* with anti-CD47 or CD40 agonist for anti-tumor functions[142,162,163]. Some groups have recently taken advantage of bone marrow derived monocytes' ability to be recruited from circulation and infiltrate into the TME, transducing them to express cytokines or even CARs. In preclinical data, myeloid cells engineered to constitutively express IL-12 differentiate into engineered monocytes and macrophages, successfully traffic to tumor sites and release cytokines to modulate the tumor microenvironment and delay tumor progression and metastasis[164]. Other groups have identified genetic modules upregulated in TAMs and engineered a tumor homing subset of Tie-2+ macrophages to secrete IFNα, which demonstrated slowed tumor progression[165]. Significant progress has also been made to develop CAR receptors in macrophages with costimulatory domains such as Fcg, Megf10, and MerTK to activate and leverage their phagocytosis capabilities against tumor antigens[166]. *In vitro* studies show CAR macrophages can uptake antigen specific targets via phagocytosis, while in preclinical mouse models, CAR macrophages have been demonstrated to traffic to the tumor and delay tumor growth[167]. While preliminary data from a phase I clinical trial using HER2 targeted CAR macrophages solid tumors showed good safety profiles and diverse immune cell activation, the best response reported was stable disease, indicating the need for greater potency in these therapies[168]. Monocytes and macrophages have unique natural capabilities to readily infiltrate tumors, set a homeostatic inflammatory setpoint, and phagocytose and present tumor antigens, all qualities that can be therapeutically leveraged if engineered correctly. However, the clinical potential has yet to be fully realized and will require further investigation, optimization, and potential collaboration or synergies with other immune activating therapies.

1.10. Conclusion

In the case of synthetic immune cells such as CAR T cells, the field has engineered a targeted and potent T cell to carry out tumor elimination, but there is more to understand about the checks and balances, both cell intrinsic and extrinsic, that may limit a complete response for many patients. Stromal, endothelial, and immunological components contribute the immune-refractory TME and these complexities cannot be understated. Generating preclinical mouse models that recapitulate challenges seen in the clinic is essential to efficiently design, develop, and iterate on solutions to overcome these hurdles. Given the unique capabilities of each cell type in the natural immune response, the field should leverage, redirect, and understand these unique functions to build an optimal engineered graft to tackle diverse tumor settings. Engineering multiple axes of the response, either through multilineage engineering or payload driven activation of endogenous immune cells will likely be essential to counteracting the many immunosuppressive checkpoints of natural immunity and tumor evolution. Expanding our perspective from T cell-specific modulations, which is one essential node of antitumor response, to a multi-nodal perspective will allow us to implement the most effective and collaborative tools to leverage the full power of the immune system.

As the field progresses it is essential that we utilize clinical data to understand patient disease, evaluate deficiencies of their antitumor response, and engineer solutions to initiate broad multi-nodal antitumor activation. If the scientific pipeline and clinical feedback loop can be efficiently linked together, ideally on patient specific scale, then we can design single or multilineage grafts with the correct repertoire of weapons to tackle each specific tumor. Even if the graft fails, with the appropriate translational assays in place, insight will be gained from the clinical trial to immediately inform development of more effective and safer synthetic immunology tools. An optimized ‘Cycle of Translation’ will be critical to realizing the vision of cell

therapy as a next pillar of medicine that is curative for a broad set of cancers relevant to other intractable diseases (Figure 2).

Acknowledgment and Funding

K.T.R was supported by the Parker Institute for Cancer Immunotherapy, the NIH-NCI Cancer Moonshot Immuno-Oncology Translational Network Center Grant (U54 CA244438), the UCSF Helen Diller Family Comprehensive Cancer Center, the NIH Director's New Innovator Award (DP2 CA239143), and the CRI Star Award.

Disclosures

K.T.R. is a cofounder, consultant, SAB member, and stockholder of Arsenal Biosciences, Dispatch Therapeutics, and Moonlight Bio. He was a founding scientist/consultant stockholder in Cell Design Labs, now a Gilead Company. K.T.R. holds stock in Gilead. K.T.R. is on the SAB of Alaunos Oncology and an exclusive Advisor to Venrock. J.M.G. is a founding scientist/consultant and stockholder of Moonlight Bio.

1.11. Figures

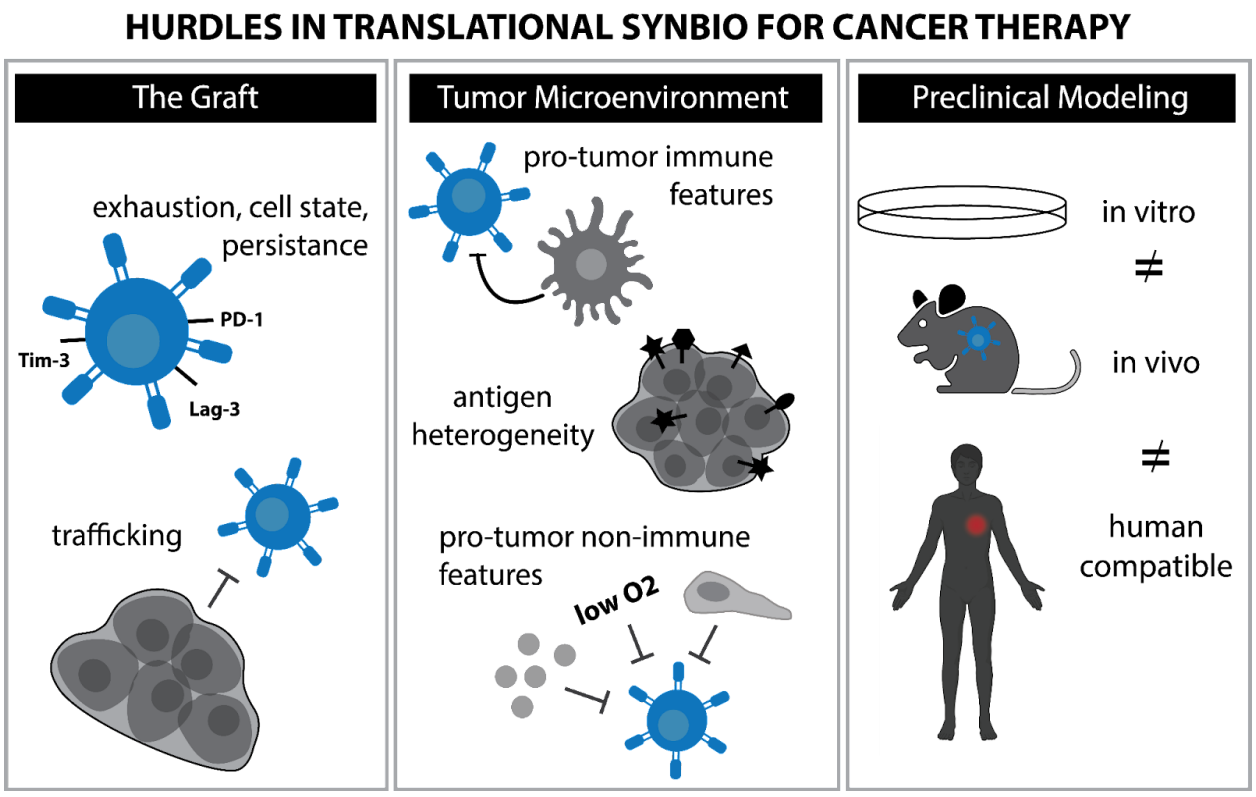

Figure 1.1 The Landscape of Clinical Hurdles in Cell Therapy.

There remain significant hurdles to successful translation of synbio tools for effective cancer immunotherapy that should be considered when generating new synthetic tools. Solid tumors contain a complex microenvironment and both immune and non-immune cell composition can support and sustain a pro tumor microenvironment. Additionally, antigen heterogeneity and antigen loss remain a significant hurdle. Manufacturing an optimal cell graft is essential and successful therapies need to persist, traffic, and maintain long term potency against tumor targets. Currently, preclinical *in vitro* and *in vivo* modeling and tool development fail to accurately represent human disease or be human compatible making predictive modeling of successful therapies difficult.

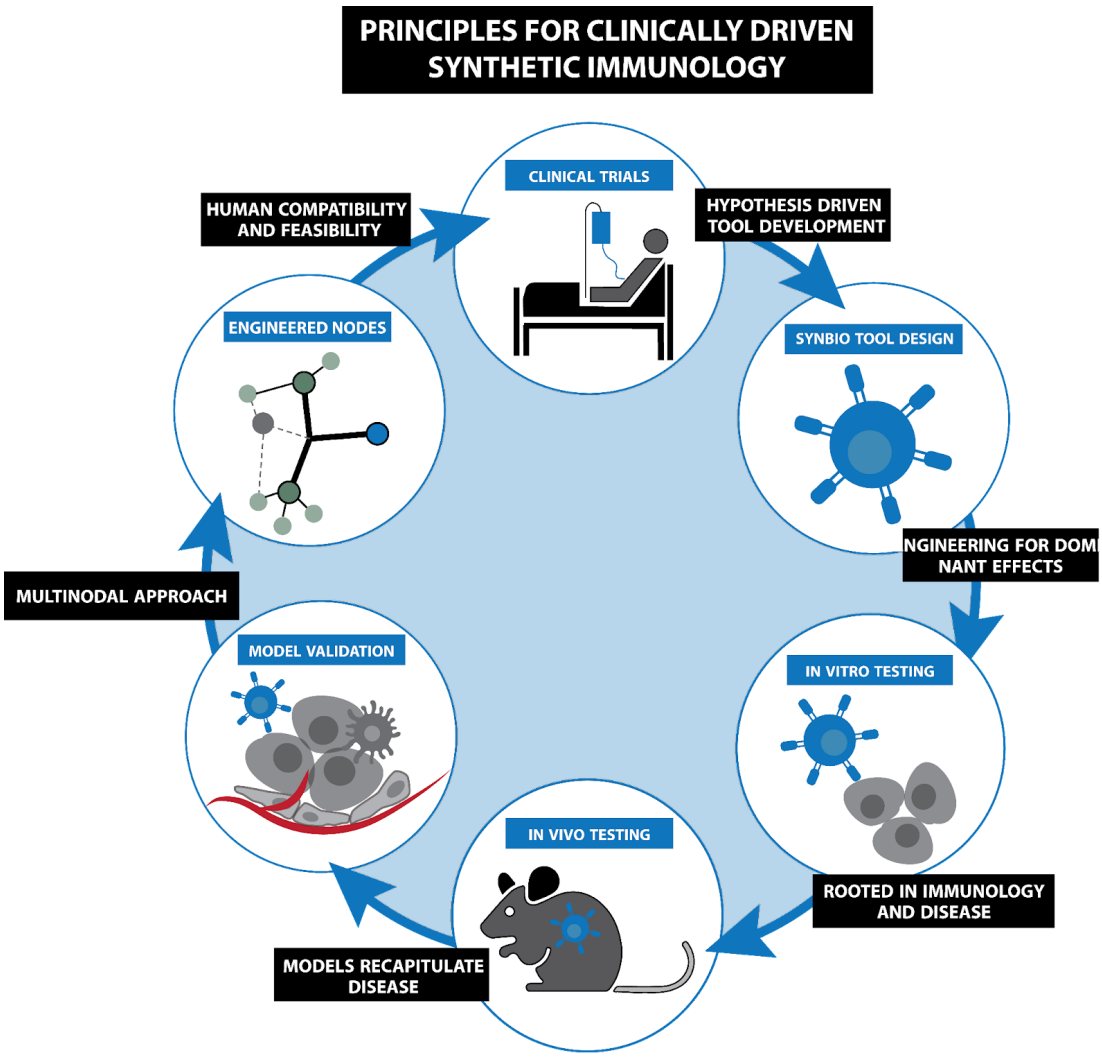

Figure 1.2 Principles of Generating New Synbio Tools for Clinical Impact.

The current discovery pipeline develops new therapeutic modalities for engineered immune cells, tests the intervention *in vitro* and *in vivo*, hopefully elucidates a mechanistic insight to the tumor microenvironment, therapy, or broader impact to the multimodal system, and if successful in the preclinical endeavors tests the new therapy in patients. We believe anchoring these steps in 5 guiding principles can increase efficiency, crosstalk, and maximal impact of this pipeline for optimal synbio tool development to translation.

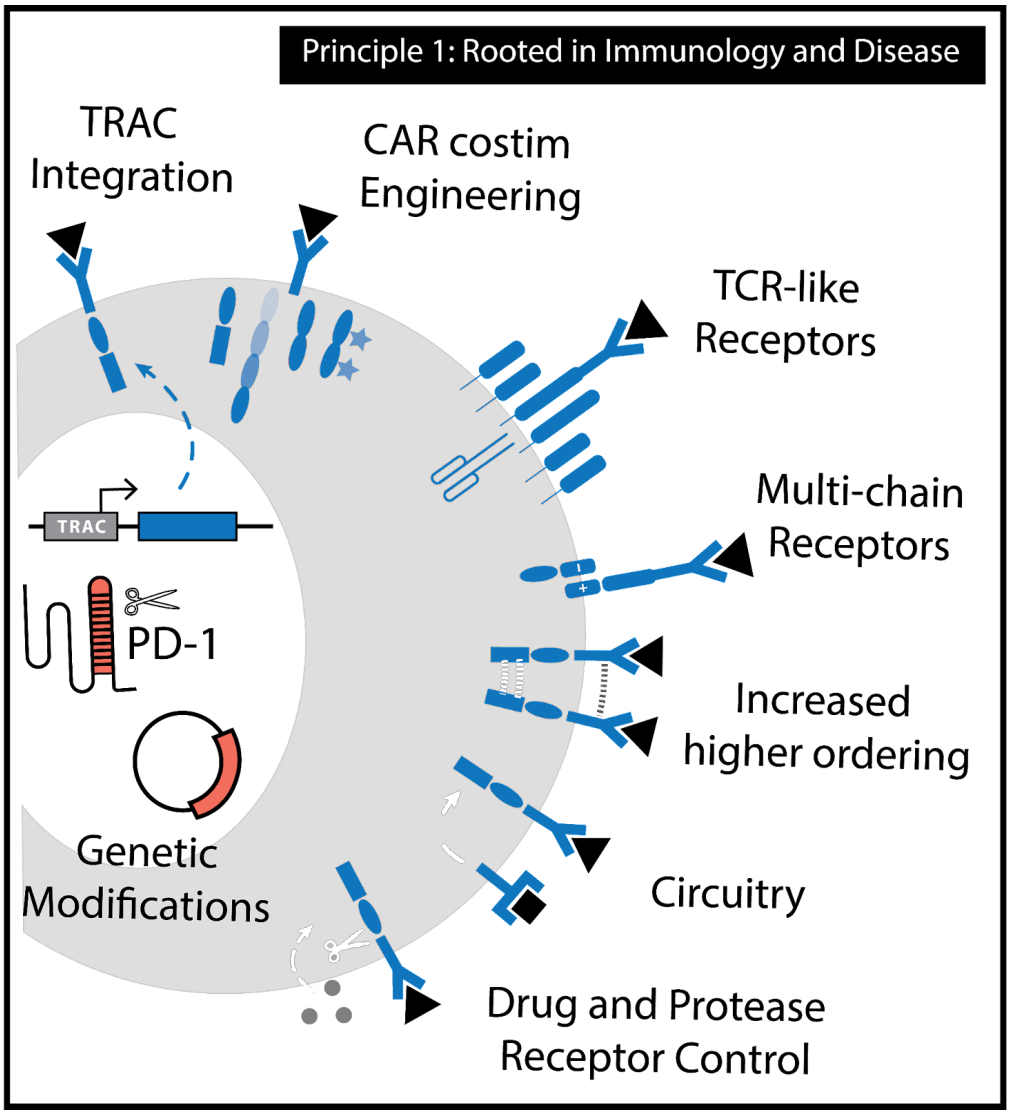

Figure 1.3 Rooting Synthetic Approaches in Basic Immunology and Disease Understandings and Failures.

New therapeutic approaches must be anchored in the basic mechanistic insight of the immunology that will be modified and the desired outcome or targets for the tumor microenvironment. T cell modifications to more closely mimic nature TCR signaling or modify specific aspects of T cell biology are key steps in developing more potent and persistent cell products. Simultaneously, further investigation into the breaks, accelerators, and tumor targets is essential to designing and matching the right tools to tumors.

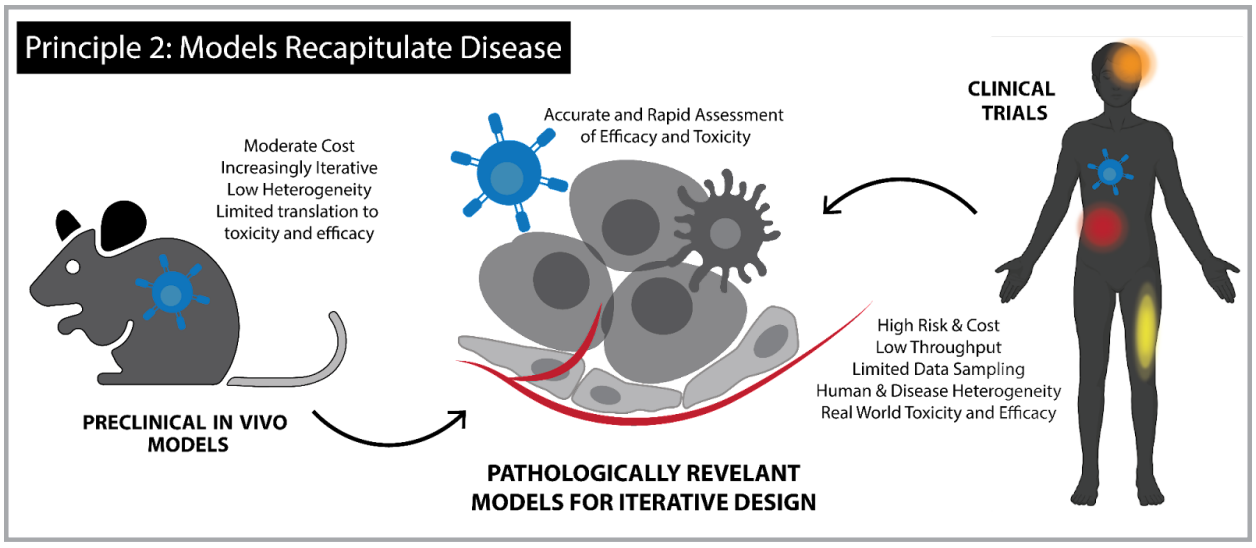

Figure 1.4 Preclinical Models that Recapitulate Disease State.

One major hurdle that remains in the field is the testing and validation of new synbio tools in relevant preclinical models. Each *in vivo* model, as it moves towards more clinically relevant features, has specific benefits and limitations, and should be carefully considered when evaluating preclinical synbio tools. To the best of our ability, tools should be built with humanized components and validated in mechanistically relevant settings that recapitulate human disease for rapid translation from preclinical to clinical testing.

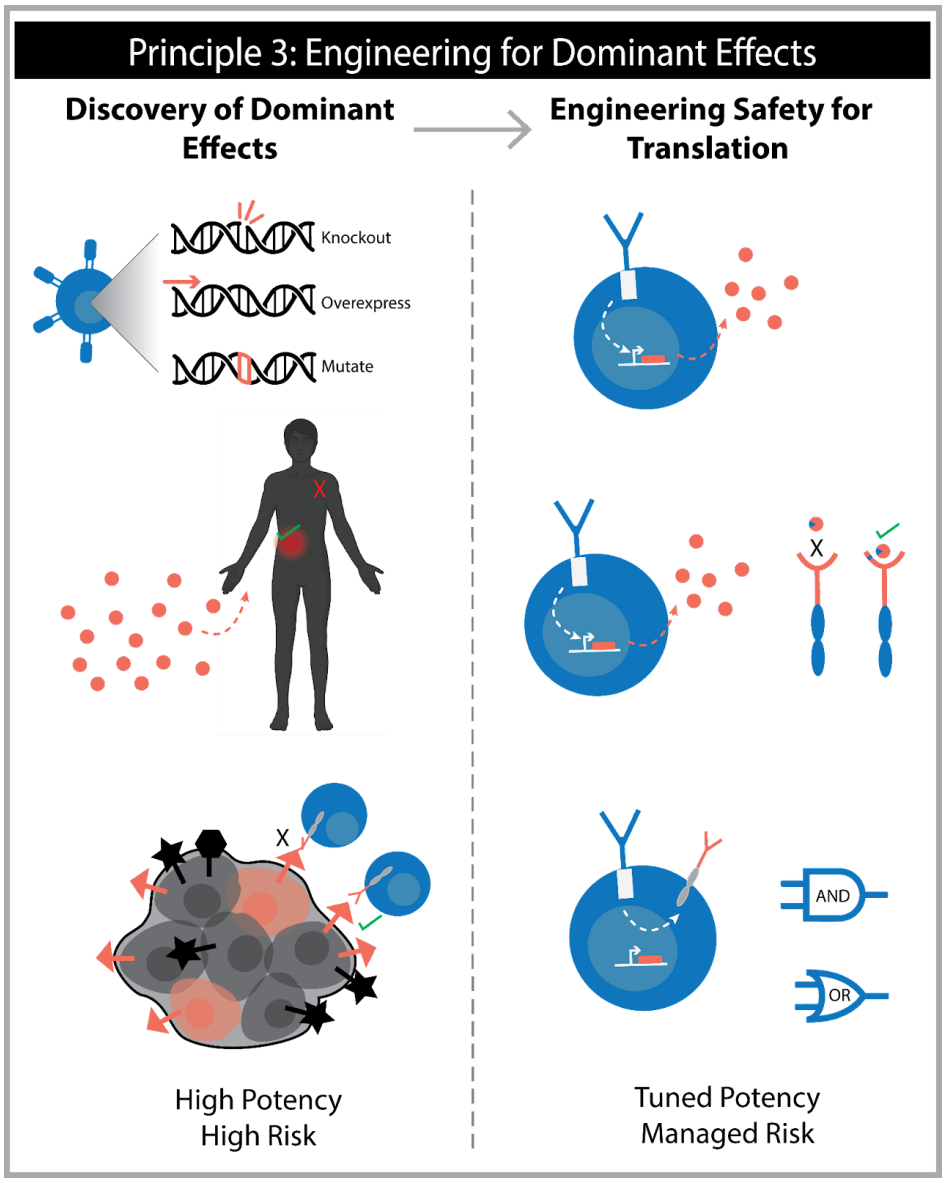

Figure 1.5 Engineering Solutions with Dominant Effects.

Tools should be developed to have dominant capabilities that induce significant effects as a monotherapy (e.g. genetic knockouts of key immune regulators or enhancements to drive dominant T cell clones). Synbio tools have, and continue to build, regulatory mechanisms to tune back, control the spatial and temporal activation, and direct specificity and we believe this approach of finding and fine-tuning dominant effects will drive the most significant clinical impact.

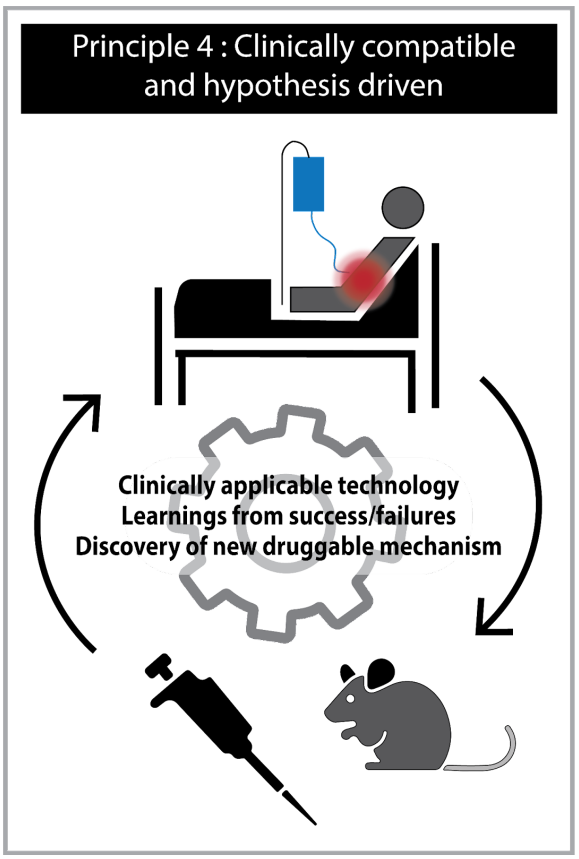

Figure 1.6 Clinically Driven and Human Compatible Approaches.

Clinical insight, from patient focused human compatible tool development to deep characterization of tumor suppressive mechanisms need to be central to the design and development of novel synbio tools. These insights should catalyze and guide which models to choose for preclinical evaluation and how we approach new tool development from target identification, enhancement of current therapies, and safety of current and future therapies. Only with a tight feedback loop between clinical and laboratory investigation can we rapidly iterate to drive innovative synbio solutions for patients in the near term.

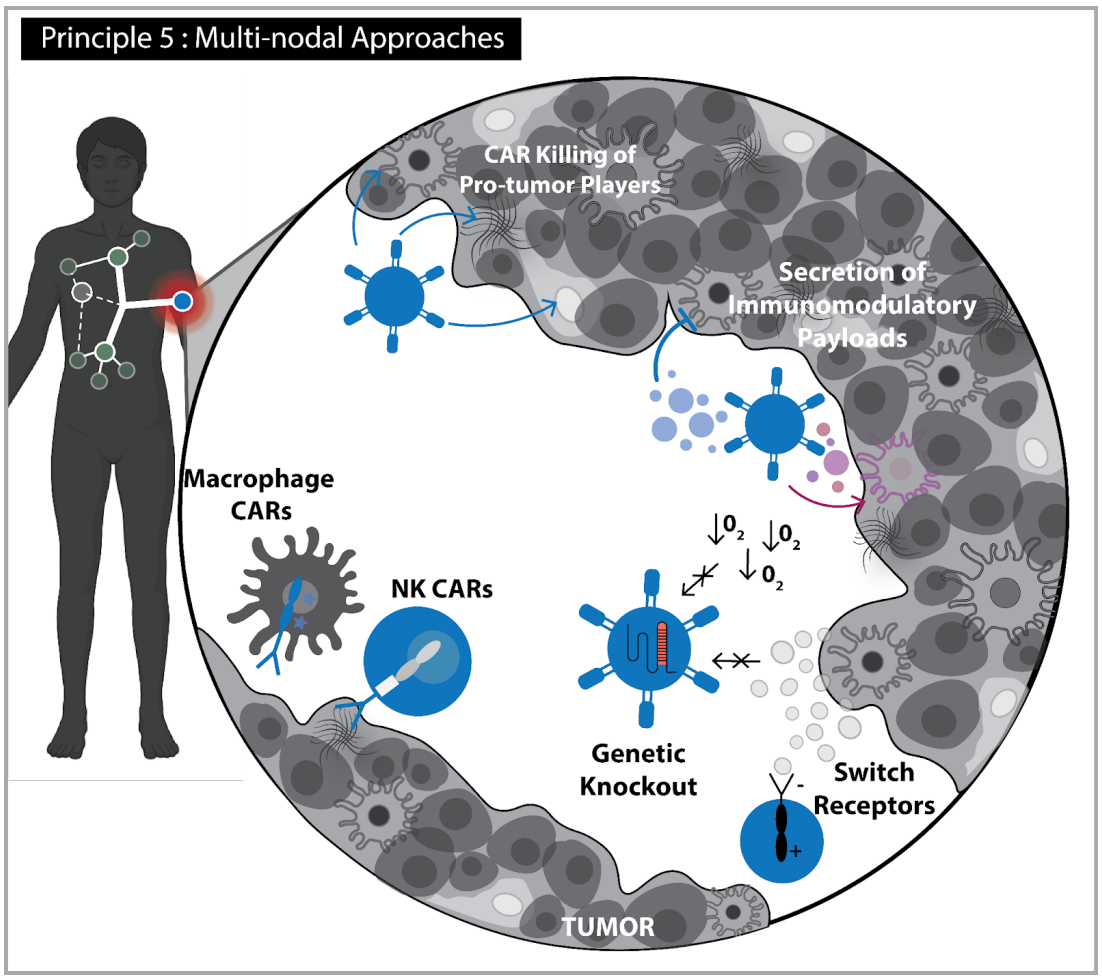

Figure 1.7 Designing Multi-Nodal Approaches for Tumor Eradication.

The immune system and mechanisms of T cell action are multi-nodal and have many axes of immunosuppression and activation. Successful tools will be designed to manipulate non-redundant mechanisms of immune activation, both within T cell intrinsic capabilities such as removing or redirecting inhibitory signals, and more broadly by driving endogenous immune activation with modulatory payloads. A new frontier of immune engineering is to co-opt functions on alternative immune cells for additional and complementary antitumor functions. Successful and complete tumor eradication will likely come from initiating a multi-nodal systemic response.

1.12. References

1. Dunn, G. P., Bruce, A. T., Ikeda, H., Old, L. J. & Schreiber, R. D. Cancer immunoediting: from immunosurveillance to tumor escape. *Nat. Immunol.* 3, 991–998 (2002).
2. Chen, D. S. & Mellman, I. Oncology meets immunology: the cancer-immunity cycle. *Immunity* 39, 1–10 (2013).
3. Roybal, K. T. & Lim, W. A. Synthetic Immunology: Hacking Immune Cells to Expand Their Therapeutic Capabilities. *Annu. Rev. Immunol.* 35, 229–253 (2017).
4. Patel, U. *et al.* CAR T cell therapy in solid tumors: A review of current clinical trials. *EJHaem* 3, 24–31 (2022).
5. Maude, S. L. *et al.* Tisagenlecleucel in Children and Young Adults with B-Cell Lymphoblastic Leukemia. *N. Engl. J. Med.* 378, 439–448 (2018).
6. Neelapu, S. S. *et al.* Axicabtagene Ciloleucel CAR T-Cell Therapy in Refractory Large B-Cell Lymphoma. *N. Engl. J. Med.* 377, 2531–2544 (2017).
7. Wang, M. *et al.* KTE-X19 CAR T-Cell Therapy in Relapsed or Refractory Mantle-Cell Lymphoma. *N. Engl. J. Med.* 382, 1331–1342 (2020).
8. Kamdar, M. *et al.* Lisocabtagene maraleucel versus standard of care with salvage chemotherapy followed by autologous stem cell transplantation as second-line treatment in patients with relapsed or refractory large B-cell lymphoma (TRANSFORM): results from an interim analysis of an open-label, randomised, phase 3 trial. *Lancet* 399, 2294–2308 (2022).
9. Munshi, N. C. *et al.* Idecabtagene Vicleucel in Relapsed and Refractory Multiple Myeloma. *N. Engl. J. Med.* 384, 705–716 (2021).
10. Berdeja, J. G. *et al.* Ciltacabtagene autoleucel, a B-cell maturation antigen-directed chimeric antigen receptor T-cell therapy in patients with relapsed or refractory multiple

myeloma (CARTITUDE-1): a phase 1b/2 open-label study. *Lancet* 398, 314–324 (2021).

11. Maus, M. V. *et al.* T cells expressing chimeric antigen receptors can cause anaphylaxis in humans. *Cancer Immunol Res* 1, 26–31 (2013).
12. Marofi, F. *et al.* CAR T cells in solid tumors: challenges and opportunities. *Stem Cell Res. Ther.* 12, 81 (2021).
13. Haas, A. R. *et al.* Phase I Study of Lentiviral-Transduced Chimeric Antigen Receptor-Modified T Cells Recognizing Mesothelin in Advanced Solid Cancers. *Mol. Ther.* 27, 1919–1929 (2019).
14. Morgan, R. A. *et al.* Case report of a serious adverse event following the administration of T cells transduced with a chimeric antigen receptor recognizing ERBB2. *Mol. Ther.* 18, 843–851 (2010).
15. Richman, S. A. *et al.* High-Affinity GD2-Specific CAR T Cells Induce Fatal Encephalitis in a Preclinical Neuroblastoma Model. *Cancer Immunol Res* 6, 36–46 (2018).
16. Majzner, R. G. & Mackall, C. L. Tumor Antigen Escape from CAR T-cell Therapy. *Cancer Discov.* 8, 1219–1226 (2018).
17. Brown, C. E. *et al.* Regression of Glioblastoma after Chimeric Antigen Receptor T-Cell Therapy. *N. Engl. J. Med.* 375, 2561–2569 (2016).
18. Geethakumari, P. R., Ramasamy, D. P., Dholaria, B., Berdeja, J. & Kansagra, A. Balancing Quality, Cost, and Access During Delivery of Newer Cellular and Immunotherapy Treatments. *Curr. Hematol. Malig. Rep.* 16, 345–356 (2021).
19. Turtle, C. J. *et al.* CD19 CAR-T cells of defined CD4+:CD8+ composition in adult B cell ALL patients. *J. Clin. Invest.* 126, 2123–2138 (2016).
20. Good, Z. *et al.* Post-infusion CAR TReg cells identify patients resistant to CD19-CAR therapy. *Nat. Med.* 28, 1860–1871 (2022).
21. Khaled, S. K. *et al.* Adult Patients with ALL Treated with CD62L+ T

Naïve/Memory-Enriched T Cells Expressing a CD19-CAR Mediate Potent Antitumor Activity with a Low Toxicity Profile. *Blood* 132, 4016–4016 (2018).

22. Eyquem, J. *et al.* Targeting a CAR to the TRAC locus with CRISPR/Cas9 enhances tumour rejection. *Nature* 543, 113–117 (2017).
23. Hyrenius-Wittsten, A. *et al.* SynNotch CAR circuits enhance solid tumor recognition and promote persistent antitumor activity in mouse models. *Sci. Transl. Med.* 13, (2021).
24. Rodriguez-Marquez, P. *et al.* CAR density influences antitumoral efficacy of BCMA CAR T cells and correlates with clinical outcome. *Sci Adv* 8, eabo0514 (2022).
25. Pietrobon, V. *et al.* Improving CAR T-Cell Persistence. *Int. J. Mol. Sci.* 22, (2021).
26. Fraietta, J. A. *et al.* Determinants of response and resistance to CD19 chimeric antigen receptor (CAR) T cell therapy of chronic lymphocytic leukemia. *Nat. Med.* 24, 563–571 (2018).
27. Leko, V. & Rosenberg, S. A. Identifying and Targeting Human Tumor Antigens for T Cell-Based Immunotherapy of Solid Tumors. *Cancer Cell* 38, 454–472 (2020).
28. Caruso, H. G., Heimberger, A. B. & Cooper, L. J. N. Steering CAR T cells to distinguish friend from foe. *Oncoimmunology* 8, e1271857 (2019).
29. Marofi, F. *et al.* Hurdles to breakthrough in CAR T cell therapy of solid tumors. *Stem Cell Res. Ther.* 13, 140 (2022).
30. Newick, K., O'Brien, S., Moon, E. & Albelda, S. M. CAR T Cell Therapy for Solid Tumors. *Annu. Rev. Med.* 68, 139–152 (2017).
31. Labani-Motlagh, A., Ashja-Mahdavi, M. & Loskog, A. The Tumor Microenvironment: A Milieu Hindering and Obstructing Antitumor Immune Responses. *Front. Immunol.* 11, 940 (2020).
32. Cha, J.-H., Chan, L.-C., Li, C.-W., Hsu, J. L. & Hung, M.-C. Mechanisms Controlling PD-L1 Expression in Cancer. *Mol. Cell* 76, 359–370 (2019).

33. Parsons, B. L. Multiclonal tumor origin: Evidence and implications. *Mutat. Res. - Rev. Mut. Res.* 777, 1–18 (2018).
34. Brentjens, R. J. *et al.* Safety and persistence of adoptively transferred autologous CD19-targeted T cells in patients with relapsed or chemotherapy refractory B-cell leukemias. *Blood* 118, 4817–4828 (2011).
35. Porter, D. L., Levine, B. L., Kalos, M., Bagg, A. & June, C. H. Chimeric Antigen Receptor–Modified T Cells in Chronic Lymphoid Leukemia. *N. Engl. J. Med.* 365, 725–733 (2011).
36. Chimeric Antigen Receptor-Modified T Cells in Chronic Lymphoid Leukemia; Chimeric Antigen Receptor-Modified T Cells for Acute Lymphoid Leukemia; Chimeric Antigen Receptor T Cells for Sustained Remissions in Leukemia. *N. Engl. J. Med.* 374, 998 (2016).
37. Grupp, S. A. *et al.* Chimeric antigen receptor-modified T cells for acute lymphoid leukemia. *N. Engl. J. Med.* 368, 1509–1518 (2013).
38. Sykulev, Y., Joo, M., Vturina, I., Tsomides, T. J. & Eisen, H. N. Evidence that a single peptide-MHC complex on a target cell can elicit a cytolytic T cell response. *Immunity* 4, 565–571 (1996).
39. Huang, J. *et al.* A single peptide-major histocompatibility complex ligand triggers digital cytokine secretion in CD4(+) T cells. *Immunity* 39, 846–857 (2013).
40. Harris, D. T. *et al.* Comparison of T Cell Activities Mediated by Human TCRs and CARs That Use the Same Recognition Domains. *J. Immunol.* 200, 1088–1100 (2018).
41. Hamieh, M. *et al.* CAR T cell trogocytosis and cooperative killing regulate tumour antigen escape. *Nature* doi:10.1038/s41586-019-1054-1.
42. Salter, A. I. *et al.* Comparative analysis of TCR and CAR signaling informs CAR designs with superior antigen sensitivity and in vivo function. *Sci. Signal.* 14, (2021).

43. Baeuerle, P. A. *et al.* Synthetic TRuC receptors engaging the complete T cell receptor for potent anti-tumor response. *Nat. Commun.* 10, 2087 (2019).
44. Mansilla-Soto, J. *et al.* HLA-independent T cell receptors for targeting tumors with low antigen density. *Nat. Med.* 28, 345–352 (2022).
45. Chockley, P. J., Ibanez-Vega, J., Krenciute, G., Talbot, L. J. & Gottschalk, S. Synapse-tuned CARs enhance immune cell anti-tumor activity. *Nat. Biotechnol.* (2023) doi:10.1038/s41587-022-01650-2.
46. Wang, E. *et al.* Generation of Potent T-cell Immunotherapy for Cancer Using DAP12-Based, Multichain, Chimeric Immunoreceptors. *Cancer Immunol Res* 3, 815–826 (2015).
47. Barber, D. L. *et al.* Restoring function in exhausted CD8 T cells during chronic viral infection. *Nature* 439, 682–687 (2006).
48. Blackburn, S. D. *et al.* Coregulation of CD8+ T cell exhaustion by multiple inhibitory receptors during chronic viral infection. *Nat. Immunol.* 10, 29–37 (2009).
49. Jin, H.-T. *et al.* Cooperation of Tim-3 and PD-1 in CD8 T-cell exhaustion during chronic viral infection. *Proc. Natl. Acad. Sci. U. S. A.* 107, 14733–14738 (2010).
50. Oliveira, G. & Wu, C. J. Dynamics and specificities of T cells in cancer immunotherapy. *Nat. Rev. Cancer* 23, 295–316 (2023).
51. Wherry, E. J. T cell exhaustion. *Nat. Immunol.* 12, 492–499 (2011).
52. Wherry, E. J. & Kurachi, M. Molecular and cellular insights into T cell exhaustion. *Nature Reviews Immunology 2015 15:8* 15, 486–499 (2015).
53. Kouro, T., Himuro, H. & Sasada, T. Exhaustion of CAR T cells: potential causes and solutions. *J. Transl. Med.* 20, 239 (2022).
54. Fraietta, J. A. *et al.* Disruption of TET2 promotes the therapeutic efficacy of CD19-targeted T cells. *Nature* 558, 307–312 (2018).

55. Shah, N. N. *et al.* Clonal expansion of CAR T cells harboring lentivector integration in the CBL gene following anti-CD22 CAR T-cell therapy. *Blood Adv* 3, 2317–2322 (2019).
56. Carnevale, J. *et al.* RASA2 ablation in T cells boosts antigen sensitivity and long-term function. *Nature* 609, 174–182 (2022).
57. Rupp, L. J. *et al.* CRISPR/Cas9-mediated PD-1 disruption enhances anti-tumor efficacy of human chimeric antigen receptor T cells. *Sci. Rep.* 7, 737 (2017).
58. Wiede, F. *et al.* PTPN2 phosphatase deletion in T cells promotes anti-tumour immunity and CAR T-cell efficacy in solid tumours. *EMBO J.* 39, e103637 (2020).
59. Freitas, K. A. *et al.* Enhanced T cell effector activity by targeting the Mediator kinase module. *Science* 378, eabn5647 (2022).
60. Fan, J., Das, J. K., Xiong, X., Chen, H. & Song, J. Development of CAR-T Cell Persistence in Adoptive Immunotherapy of Solid Tumors. *Front. Oncol.* 10, 574860 (2020).
61. Dranoff, G. Experimental mouse tumour models: what can be learnt about human cancer immunology? *Nat. Rev. Immunol.* 12, 61–66 (2011).
62. Ito, M. *et al.* NOD/SCID/gamma(c)(null) mouse: an excellent recipient mouse model for engraftment of human cells. *Blood* 100, 3175–3182 (2002).
63. Zhong, W. *et al.* Comparison of the molecular and cellular phenotypes of common mouse syngeneic models with human tumors. *BMC Genomics* 21, 2 (2020).
64. Gopinathan, A. & Tuveson, D. A. The use of GEM models for experimental cancer therapeutics. *Dis. Model. Mech.* 1, 83–86 (2008).
65. Mou, H., Kennedy, Z., Anderson, D. G., Yin, H. & Xue, W. Precision cancer mouse models through genome editing with CRISPR-Cas9. *Genome Med.* 7, 53 (2015).
66. Deycmar, S., Gomes, B., Charo, J., Ceppi, M. & Cline, J. M. Spontaneous, naturally occurring cancers in non-human primates as a translational model for cancer

immunotherapy. *J Immunother Cancer* 11, (2023).

67. Cauvin, A. J., Peters, C. & Brennan, F. Chapter 19 - Advantages and Limitations of Commonly Used Nonhuman Primate Species in Research and Development of Biopharmaceuticals. in *The Nonhuman Primate in Nonclinical Drug Development and Safety Assessment* (eds. Bluemel, J., Korte, S., Schenck, E. & Weinbauer, G. F.) 379–395 (Academic Press, 2015).
68. Harding, J. D. Nonhuman Primates and Translational Research: Progress, Opportunities, and Challenges. *ILAR J.* 58, 141–150 (2017).
69. Junttila, M. R. & de Sauvage, F. J. Influence of tumour micro-environment heterogeneity on therapeutic response. *Nature* 501, 346–354 (2013).
70. Combes, A. J. *et al.* Discovering dominant tumor immune archetypes in a pan-cancer census. *Cell* 185, 184–203.e19 (2022).
71. Bagaev, A. *et al.* Conserved pan-cancer microenvironment subtypes predict response to immunotherapy. *Cancer Cell* 39, 845–865.e7 (2021).
72. Banik, G. *et al.* High-dimensional multiplexed immunohistochemical characterization of immune contexture in human cancers. *Methods Enzymol.* 635, 1–20 (2020).
73. Sorin, M. *et al.* Single-cell spatial landscapes of the lung tumour immune microenvironment. *Nature* 614, 548–554 (2023).
74. Karimi, E. *et al.* Single-cell spatial immune landscapes of primary and metastatic brain tumours. *Nature* 614, 555–563 (2023).
75. Goltsev, Y. *et al.* Deep Profiling of Mouse Splenic Architecture with CODEX Multiplexed Imaging. *Cell* 174, 968–981.e15 (2018).
76. Pelka, K. *et al.* Spatially organized multicellular immune hubs in human colorectal cancer. *Cell* 184, 4734–4752.e20 (2021).
77. Li, J. *et al.* Tumor Cell-Intrinsic Factors Underlie Heterogeneity of Immune Cell Infiltration

and Response to Immunotherapy. *Immunity* 49, 178–193.e7 (2018).

78. Mariathasan, S. *et al.* TGFβ attenuates tumour response to PD-L1 blockade by contributing to exclusion of T cells. *Nature* 554, 544–548 (2018).
79. Srivastava, S. *et al.* Logic-Gated ROR1 Chimeric Antigen Receptor Expression Rescues T Cell-Mediated Toxicity to Normal Tissues and Enables Selective Tumor Targeting. *Cancer Cell* 35, 489–503.e8 (2019).
80. Giavridis, T. *et al.* CAR T cell–induced cytokine release syndrome is mediated by macrophages and abated by IL-1 blockade. *Nat. Med.* 24, 731–738 (2018).
81. Norelli, M. *et al.* Monocyte-derived IL-1 and IL-6 are differentially required for cytokine-release syndrome and neurotoxicity due to CAR T cells. *Nat. Med.* 24, 739–748 (2018).
82. Choi, G., Shin, G. & Bae, S. Price and Prejudice? The Value of Chimeric Antigen Receptor (CAR) T-Cell Therapy. *Int. J. Environ. Res. Public Health* 19, (2022).
83. Prinzing, B. *et al.* Deleting DNMT3A in CAR T cells prevents exhaustion and enhances antitumor activity. *Sci. Transl. Med.* 13, 272 (2021).
84. Wei, J. *et al.* Targeting REGNASE-1 programs long-lived effector T cells for cancer therapy. *Nature* 576, 471–476 (2019).
85. Mai, D. *et al.* Combined disruption of T cell inflammatory regulators Regnase-1 and Roquin-1 enhances antitumor activity of engineered human T cells. *Proc. Natl. Acad. Sci. U. S. A.* 120, e2218632120 (2023).
86. Zhu, I. *et al.* Design and modular assembly of synthetic intramembrane proteolysis receptors for custom gene regulation in therapeutic cells. *bioRxiv* 2021.05.21.445218 (2021) doi:10.1101/2021.05.21.445218.
87. Choe, J. H. *et al.* SynNotch-CAR T cells overcome challenges of specificity, heterogeneity, and persistence in treating glioblastoma. *Sci. Transl. Med.* 13, (2021).

88. Allen, G. M. *et al.* Synthetic cytokine circuits that drive T cells into immune-excluded tumors. *Science* 378, eaba1624 (2022).
89. Juillerat, A. *et al.* An oxygen sensitive self-decision making engineered CAR T-cell. *Sci. Rep.* 7, 39833 (2017).
90. Tousley, A. M. *et al.* Coopting T cell proximal signaling molecules enables Boolean logic-gated CAR T cell control. *bioRxiv* 2022.06.17.496457 (2022) doi:10.1101/2022.06.17.496457.
91. Levin, A. M. *et al.* Exploiting a natural conformational switch to engineer an interleukin-2 'superkine'. *Nature* 484, 529–533 (2012).
92. Zhu, I. *et al.* Modular design of synthetic receptors for programmed gene regulation in cell therapies. *Cell* 185, 1431–1443.e16 (2022).
93. Zhou, T. *et al.* IL-18BP is a secreted immune checkpoint and barrier to IL-18 immunotherapy. *Nature* 583, 609–614 (2020).
94. Wang, N. *et al.* Efficacy and safety of CAR19/22 T-cell cocktail therapy in patients with refractory/relapsed B-cell malignancies. *Blood* 135, 17–27 (2020).
95. Zah, E., Lin, M.-Y., Silva-Benedict, A., Jensen, M. C. & Chen, Y. Y. T Cells Expressing CD19/CD20 Bispecific Chimeric Antigen Receptors Prevent Antigen Escape by Malignant B Cells. *Cancer Immunology Research* vol. 4 498–508 Preprint at https://doi.org/10.1158/2326-6066.cir-15-0231 (2016).
96. Ghafouri, S. N. *et al.* Abstract CT007: CD19/CD20 bispecific chimeric antigen receptor (CAR) in naive/memory T-cells for the treatment of relapsed or refractory B-cell lymphomas. *Cancer Res.* 81, CT007–CT007 (2021).
97. Cordoba, S. *et al.* CAR T cells with dual targeting of CD19 and CD22 in pediatric and young adult patients with relapsed or refractory B cell acute lymphoblastic leukemia: a phase 1 trial. *Nat. Med.* 27, 1797–1805 (2021).

98. Spiegel, J. Y. *et al.* CAR T cells with dual targeting of CD19 and CD22 in adult patients with recurrent or refractory B cell malignancies: a phase 1 trial. *Nat. Med.* 27, 1419–1431 (2021).
99. Ruella, M. *et al.* Dual CD19 and CD123 targeting prevents antigen-loss relapses after CD19-directed immunotherapies. *J. Clin. Invest.* 126, 3814–3826 (2016).
100. Hegde, M. *et al.* Tandem CAR T cells targeting HER2 and IL13Rα2 mitigate tumor antigen escape. *J. Clin. Invest.* 126, 3036–3052 (2016).
101. Mei, H. *et al.* A bispecific CAR-T cell therapy targeting BCMA and CD38 in relapsed or refractory multiple myeloma. *J. Hematol. Oncol.* 14, 161 (2021).
102. Zah, E. *et al.* Systematically optimized BCMA/CS1 bispecific CAR-T cells robustly control heterogeneous multiple myeloma. *Nat. Commun.* 11, 2283 (2020).
103. Liang, Z. *et al.* Tandem CAR-T cells targeting FOLR1 and MSLN enhance the antitumor effects in ovarian cancer. *Int. J. Biol. Sci.* 17, 4365–4376 (2021).
104. Lamers, C. H. *et al.* Treatment of metastatic renal cell carcinoma with CAIX CAR-engineered T cells: clinical evaluation and management of on-target toxicity. *Mol. Ther.* 21, 904–912 (2013).
105. Mantovani, A., Allavena, P., Marchesi, F. & Garlanda, C. Macrophages as tools and targets in cancer therapy. *Nat. Rev. Drug Discov.* 21, 799–820 (2022).
106. Cassetta, L. & Pollard, J. W. A timeline of tumour-associated macrophage biology. *Nat. Rev. Cancer* 23, 238–257 (2023).
107. Pittet, M. J., Michielin, O. & Migliorini, D. Clinical relevance of tumour-associated macrophages. *Nat. Rev. Clin. Oncol.* 19, 402–421 (2022).
108. Ruffell, B. & Coussens, L. M. Macrophages and therapeutic resistance in cancer. *Cancer Cell* 27, 462–472 (2015).
109. Sánchez-Paulete, A. R. *et al.* Targeting Macrophages with CAR T Cells Delays Solid

Tumor Progression and Enhances Antitumor Immunity. *Cancer Immunology Research* vol. 10 1354–1369 Preprint at https://doi.org/10.1158/2326-6066.cir-21-1075 (2022).

110. Batlle, E. & Massagué, J. Transforming Growth Factor-β Signaling in Immunity and Cancer. *Immunity* 50, 924–940 (2019).
111. Tang, N. *et al.* TGF-β inhibition via CRISPR promotes the long-term efficacy of CAR T cells against solid tumors. *JCI Insight* vol. 5 Preprint at https://doi.org/10.1172/jci.insight.133977 (2020).
112. Kloss, C. C. *et al.* Dominant-Negative TGF-β Receptor Enhances PSMA-Targeted Human CAR T Cell Proliferation And Augments Prostate Cancer Eradication. *Mol. Ther.* 26, 1855–1866 (2018).
113. Hou, A. J., Chang, Z. L., Lorenzini, M. H., Zah, E. & Chen, Y. Y. TGF-β-responsive CAR-T cells promote anti-tumor immune function. *Bioeng Transl Med* 3, 75–86 (2018).
114. Wagner, D. L. *et al.* Immunogenicity of CAR T cells in cancer therapy. *Nat. Rev. Clin. Oncol.* 18, 379–393 (2021).
115. Heng, G. *et al.* Sustained Therapeutic Efficacy of Humanized Anti-CD19 Chimeric Antigen Receptor T Cells in Relapsed/Refractory Acute Lymphoblastic Leukemia. *Clin. Cancer Res.* 26, 1606–1615 (2020).
116. Cao, J. *et al.* Potent anti-leukemia activities of humanized CD19-targeted Chimeric antigen receptor T (CAR-T) cells in patients with relapsed/refractory acute lymphoblastic leukemia. *Am. J. Hematol.* 93, 851–858 (2018).
117. Ewaisha, R. & Anderson, K. S. Immunogenicity of CRISPR therapeutics-Critical considerations for clinical translation. *Front Bioeng Biotechnol* 11, 1138596 (2023).
118. Gilbert, L. A. *et al.* Genome-Scale CRISPR-Mediated Control of Gene Repression and Activation. *Cell* 159, 647–661 (2014).
119. Spitzer, M. H. *et al.* Systemic Immunity Is Required for Effective Cancer Immunotherapy.

Cell 168, 487–502.e15 (2017).

120. Rahim, M. K. *et al.* Dynamic CD8+ T cell responses to cancer immunotherapy in human regional lymph nodes are disrupted in metastatic lymph nodes. *Cell* 186, 1127–1143.e18 (2023).

121. Peranzoni, E., Ingangi, V., Masetto, E., Pinton, L. & Marigo, I. Myeloid Cells as Clinical Biomarkers for Immune Checkpoint Blockade. *Front. Immunol.* 11, 1590 (2020).

122. Klement, J. D. *et al.* Tumor PD-L1 engages myeloid PD-1 to suppress type I interferon to impair cytotoxic T lymphocyte recruitment. *Cancer Cell* 41, 620–636.e9 (2023).

123. Hiam-Galvez, K. J., Allen, B. M. & Spitzer, M. H. Systemic immunity in cancer. *Nat. Rev. Cancer* 21, 345–359 (2021).

124. Craddock, J. A. *et al.* Enhanced tumor trafficking of GD2 chimeric antigen receptor T cells by expression of the chemokine receptor CCR2b. *J. Immunother.* 33, 780–788 (2010).

125. Moon, E. K. *et al.* Expression of a functional CCR2 receptor enhances tumor localization and tumor eradication by retargeted human T cells expressing a mesothelin-specific chimeric antibody receptor. *Clin. Cancer Res.* 17, 4719–4730 (2011).

126. Rapp, M. *et al.* C-C chemokine receptor type-4 transduction of T cells enhances interaction with dendritic cells, tumor infiltration and therapeutic efficacy of adoptive T cell transfer. *Oncoimmunology* 5, e1105428 (2016).

127. Di Stasi, A. *et al.* T lymphocytes coexpressing CCR4 and a chimeric antigen receptor targeting CD30 have improved homing and antitumor activity in a Hodgkin tumor model. *Blood* 113, 6392–6402 (2009).

128. Schomer, N. T., Jiang, Z. K., Lloyd, M. I., Klingemann, H. & Boissel, L. CCR7 expression in CD19 chimeric antigen receptor-engineered natural killer cells improves migration toward CCL19-expressing lymphoma cells and increases tumor control in mice with

human lymphoma. *Cytotherapy* 24, 827–834 (2022).

129. Liu, G. *et al.* CXCR2-modified CAR-T cells have enhanced trafficking ability that improves treatment of hepatocellular carcinoma. *Eur. J. Immunol.* 50, 712–724 (2020).

130. Itoh-Nakadai, A. *et al.* CXCR4-Expressing Anti-CD25 CAR T-Cells Effectively Eliminate Human AML Cells In Vivo. *Blood* 136, 35–36 (2020).

131. Park, J. S. *et al.* Synthetic control of mammalian-cell motility by engineering chemotaxis to an orthogonal bioinert chemical signal. *Proc. Natl. Acad. Sci. U. S. A.* 111, 5896–5901 (2014).

132. Caruana, I. *et al.* Heparanase promotes tumor infiltration and antitumor activity of CAR-redirected T lymphocytes. *Nat. Med.* 21, 524–529 (2015).

133. Kakarla, S. *et al.* Antitumor effects of chimeric receptor engineered human T cells directed to tumor stroma. *Mol. Ther.* 21, 1611–1620 (2013).

134. Zhang, Y. & Brekken, R. A. Direct and indirect regulation of the tumor immune microenvironment by VEGF. *J. Leukoc. Biol.* 111, 1269–1286 (2022).

135. Frafjord, A. *et al.* The Immune Landscape of Human Primary Lung Tumors Is Th2 Skewed. *Front. Immunol.* 12, 764596 (2021).

136. Qin, L. *et al.* Co-expression of a PD-L1-specific chimeric switch receptor augments the efficacy and persistence of CAR T cells via the CD70-CD27 axis. *Nat. Commun.* 13, 6051 (2022).

137. Liu, X. *et al.* A Chimeric Switch-Receptor Targeting PD1 Augments the Efficacy of Second-Generation CAR T Cells in Advanced Solid Tumors. *Cancer Res.* 76, 1578–1590 (2016).

138. Oda, S. K. *et al.* A Fas-4-1BB fusion protein converts a death to a pro-survival signal and enhances T cell therapy. *J. Exp. Med.* 217, (2020).

139. Lange, S. *et al.* A chimeric GM-CSF/IL18 receptor to sustain CAR T-cell function. *Cancer*

Discov. 11, 1661–1671 (2021).

140. Noh, K.-E. *et al.* TGF-β/IL-7 Chimeric Switch Receptor-Expressing CAR-T Cells Inhibit Recurrence of CD19-Positive B Cell Lymphoma. *Int. J. Mol. Sci.* 22, (2021).

141. Hirschhorn, D. *et al.* T cell immunotherapies engage neutrophils to eliminate tumor antigen escape variants. *Cell* 186, 1432–1447.e17 (2023).

142. Beatty, G. L. *et al.* Mesothelin-specific chimeric antigen receptor mRNA-engineered T cells induce anti-tumor activity in solid malignancies. *Cancer Immunol Res* 2, 112–120 (2014).

143. Choi, B. D. *et al.* CAR-T cells secreting BiTEs circumvent antigen escape without detectable toxicity. *Nat. Biotechnol.* 37, 1049–1058 (2019).

144. Kueberuwa, G., Kalaitsidou, M., Cheadle, E., Hawkins, R. E. & Gilham, D. E. CD19 CAR T Cells Expressing IL-12 Eradicate Lymphoma in Fully Lymphoreplete Mice through Induction of Host Immunity. *Mol Ther Oncolytics* 8, 41–51 (2018).

145. Etxeberria, I. *et al.* Intratumor Adoptive Transfer of IL-12 mRNA Transiently Engineered Antitumor CD8+ T Cells. *Cancer Cell* 36, 613–629 (2019).

146. Adachi, K. *et al.* IL-7 and CCL19 expression in CAR-T cells improves immune cell infiltration and CAR-T cell survival in the tumor. *Nat. Biotechnol.* 36, 346–351 (2018).

147. Lai, J. *et al.* Adoptive cellular therapy with T cells expressing the dendritic cell growth factor Flt3L drives epitope spreading and antitumor immunity. *Nat. Immunol.* 21, 914–926 (2020).

148. Kuhn, N. F. *et al.* CD40 Ligand-Modified Chimeric Antigen Receptor T Cells Enhance Antitumor Function by Eliciting an Endogenous Antitumor Response. *Cancer Cell* 35, 473–488.e6 (2019).

149. Huang, R., Wen, Q. & Zhang, X. CAR-NK cell therapy for hematological malignancies: recent updates from ASH 2022. *J. Hematol. Oncol.* 16, 35 (2023).

150. Liu, E. *et al.* Use of CAR-Transduced Natural Killer Cells in CD19-Positive Lymphoid Tumors. *N. Engl. J. Med.* 382, 545–553 (2020).
151. Kruschinski, A. *et al.* Engineering antigen-specific primary human NK cells against HER-2 positive carcinomas. *Proc. Natl. Acad. Sci. U. S. A.* 105, 17481–17486 (2008).
152. Schmidt, D. *et al.* Engineering CAR-NK cells: how to tune innate killer cells for cancer immunotherapy. *Immunother Adv* 2, ltac003 (2022).
153. Jiang, H. *et al.* Activating Immune Recognition in Pancreatic Ductal Adenocarcinoma via Autophagy Inhibition, MEK Blockade, and CD40 Agonism. *Gastroenterology* 162, 590–603.e14 (2022).
154. Zhang, L. *et al.* Single-Cell Analyses Inform Mechanisms of Myeloid-Targeted Therapies in Colon Cancer. *Cell* 181, 442–459.e29 (2020).
155. Kaczanowska, S. *et al.* Genetically engineered myeloid cells rebalance the core immune suppression program in metastasis. *Cell* 184, 2033–2052.e21 (2021).
156. De Palma, M. *et al.* Tumor-targeted interferon-alpha delivery by Tie2-expressing monocytes inhibits tumor growth and metastasis. *Cancer Cell* 14, 299–311 (2008).
157. Morrissey, M. A. *et al.* Chimeric antigen receptors that trigger phagocytosis. *Elife* 7, (2018).
158. Klichinsky, M. *et al.* Human chimeric antigen receptor macrophages for cancer immunotherapy. *Nat. Biotechnol.* 38, 947–953 (2020).
159. Reiss, K. A. *et al.* A phase 1, first-in-human (FIH) study of the anti-HER2 CAR macrophage CT-0508 in subjects with HER2 overexpressing solid tumors. *J. Clin. Orthod.* 40, 2533–2533 (2022).

Chapter 2

Naturally occurring mutations in human T cell lymphomas enhance engineered T cell therapies

Material for this chapter comes from the following work:

Garcia, J.*, Daniels, J.*, Lee, Y., Zhu, I., Cheng, K., Liu, Q., Goodman, D., Burnett, C., Law, C., Thienpont, C., Alavi, J., Azimi, C., Montgomery, G., Roybal, K. T.†, Choi, J†. Naturally occurring mutations in human T cell lymphomas enhance engineered T cell therapies. *Nature*. (2023). In Review.

*These authors contributed equally to this work.

†Corresponding authors.

2.1. Abstract

Adoptive T cell therapies have produced exceptional responses in a subset of cancer patients. However, therapeutic efficacy can be hindered by poor T cell persistence and function. In human T cell cancers, evolution of the disease positively selects for mutations that improve fitness of T cells in challenging situations analogous to those faced by therapeutic T cells. Therefore, we hypothesized that many of these mutations could be co-opted to improve T cell therapies. We systematically screened the effects of 71 mutations from T cell lymphomas on T cell signaling, cytokine production, and *in vivo* persistence in tumors. We identify a gene fusion, CARD11-PIK3R3, found in a CD4+ cutaneous T cell lymphoma that augments CARD11-BCL10-MALT1 complex signaling to increase anti-tumor efficacy of therapeutic T cells in multiple immunotherapy refractory models. Our results indicate that exploiting naturally occurring mutations represents a promising approach to explore the extremes of T cell biology and discover how solutions derived from evolution of malignant T cells can improve a broad range of T cell therapies.

2.2. Introduction

T cell therapies, including chimeric antigen receptor (CAR) T cells, have revolutionized cancer therapy[1]. However, impressive responses are limited to a subset of patients with hematological cancers and have not been unlocked in patients with solid tumors, which represent 90% of adult cancers[2,3]. Adoptive T cell therapy in both treatment-resistant hematological malignancies and solid cancers is limited by a complex combination of factors, including poor *in vivo* persistence, immunosuppressive environmental factors, and T cell

exhaustion[4-6]. New solutions to overcome these limitations are needed to address the significant unmet need for effective cell therapies.

Other groups have performed unbiased screens to identify modifications that improve T cell fitness *in vitro* and/or *in vivo*[7-13]. Due to limitations in technology, many of these screening efforts have focused on modifying expression of endogenous wild-type genes via CRISPR/Cas9, shRNA or cDNA overexpression. Other screening studies have thus far been limited in scope to prior knowledge-based design[14].

To overcome this engineering problem, we turned to spontaneously occurring T cell cancers. Over time, T cells, like other cells in the adult, acquire somatic mutations[15]. When these mutations increase the fitness of the T cell, T cell clones emerge via positive selection. These T cell cancers develop genetic means to overcome similar cell-intrinsic and cell-extrinsic immunosuppressive factors facing anti-tumor T cells. For example, resistance to TGF-b signaling and T cell exhaustion[16,17]. The potential power of this approach is highlighted by the observation that other modifications which improve T cell therapies have been identified in T cell lymphomas[17-20]. These include mutations and/or copy number deletions in *PDCD1*, *TET2*, *CBLB*, *DNMT3A*, and *PTPN2*[21-25].

Leveraging mutations from T cell cancers has many potential benefits over current approaches. First, evolution employs any mutation available in nature. Like existing approaches, these mutations can modify gene expression by gene locus duplication or deletion. However, unlike current approaches, gain-of-function point mutations or translocations can be introduced that have unique, outsized effects unachievable by modulation of wild-type gene expression[26]. Additionally, an evolution-based approach pre-selects mutations that are more likely to have effects, improving the signal-to-noise as compared to existing approaches.

Here, we have generated a first-of-its-kind library of 71 mutations and 45 wildtype overexpression controls. We introduce these mutations into human and mouse T cells and assess their effects on T cell phenotypes *in vitro* and *in vivo* using arrayed and pooled screens. Through these efforts, we have identified a fusion of caspase recruitment domain-containing protein 11 (CARD11) and phosphoinositide-3-kinase regulatory subunit 3 (PIK3R3) that dramatically increases AP-1 and NF-kB signaling, IL-2 production and tumor killing *in vitro* and *in vivo*. CARD11-PIK3R3 improves CAR- and T cell receptor (TCR)-T anti-tumor activity, reduces T cell dose requirements, and relieves the requirement for harsh preconditioning.

2.3. T cell lymphoma mutations reprogram CAR signaling and functional outputs

First, we utilized statistical analysis as well as manual curation of published and in-house T cell lymphoma genomic datasets to identify mutations that occur more often than expected by chance alone, implying positive selection. These mutations served as the basis for a mutation library (Supplementary Table 1)[17,26,27]. We identified and cloned 61 point mutations (encoding non-synonymous amino acid substitutions and putative gain-of-function truncating mutations) in 40 different genes. For each point mutation included in the library, a wild-type control of the same gene was generated to control for the effects of overexpression of the wild-type form of the gene. In addition, we identified 10 gene fusions and included 5 control genes (Fig. 2.1a). These targets were cloned into a barcoded lentiviral construct to enable pooled screening. In total, this library for T cell mutation screening consisted of 116 unique constructs.

The effects of most of the mutations have not been fully characterized in the context of T cell signaling and effector function. To elucidate their functions, we generated a Jurkat reporter cell line that expresses three different fluorescent reporter genes in response to NFAT, NF-kB,

and AP-1 pathway activation[28]. These triple reporter cells were transduced with a CD19-CD28z or a CD19-BBz-CAR (Extended Data Fig. 2.1a). We then transduced triple reporter lines with each construct in the library and co-cultured them with K562 cells that expressed the cognate antigen, CD19, or control K562 cells that lacked the CD19 antigen (Extended Data Fig. 2.1a). Twenty-four hours later, these co-cultures were subject to flow cytometry to measure activation of the three T cell signaling pathways (Extended Data Fig. 2.1b-c). Supernatants were collected from these co-cultures to assess for IL-2 production. For the CD19-BBz-CAR screen, PD-1 levels were also assessed. Collectively, these assays enabled elucidation of the mutations' effects on biochemical signaling pathways, the effects of antigen, and evaluation of effector cytokine production.

In vitro screening uncovered numerous mutations with significant impacts on CAR signaling and cytokine production (Fig. 2.1b, Extended Data Fig. 2.1d). These screens were highly reproducible across two experimental replicates (Extended Data Fig. 2.1e-f). Similar effects were observed when mutations were paired with either the CD28z-CAR or BBz-CAR (Extended Data Fig. 2.1g). Mutations previously reported to upregulate TCR dependent signaling (e.g. PLCG1[29-32]) had effects that were consistent with previous findings, suggesting our assay captures known positive regulators of TCR signaling. In addition, expression of the negative control construct DGKZ, a known inhibitor of TCR signaling, significantly reduced CAR dependent signaling, as expected[33] (Fig. 2.1b).

To identify patterns of effects on canonical T cell signaling, we performed unbiased K means clustering (Fig. 2.1b). Gain-of-function mutations in the same genes (e.g. PLCG1, CARD11) tended to cluster together and activate or inhibit similar pathways although to varying extents. The mutations produced a striking diversity of effects on TCR-dependent signaling (Fig. 2.1c). For the BBz-CAR, a total of 10 different combinations of signaling pathway up- or down-regulation induced by mutations were observed. Some of these signaling modifications

may be desirable. For example, imbalances between NFAT and AP-1 signaling may contribute to T cell exhaustion[34]. Therefore, mutations that increase AP-1 but not NFAT may be beneficial to T cell therapies. 24 different point mutation constructs showed significant differences versus their wild-type counterparts, demonstrating substantial increases or decreases of signaling endowed by the mutations not attributable to overexpression of the wild-type genes (Extended Data Fig. 2.2a-c).

Moreover, these mutations provide effect sizes unachievable with changes in gene expression alone, enabling tunable modifications over wide dynamic ranges. As an example of this tunability, AP-1 reporter expression could be tuned down or up over a range of 0.4 fold to nearly 3 fold the levels induced by CAR activation (mCherry) in controls (Fig. 2.1d). These outsized effects are more profoundly seen in IL-2 production, with 9 different mutations producing higher levels of IL-2 than achievable with any wild-type gene tested (Fig. 2.1e). Mutations can abolish IL-2 expression or increase secretion by 396-fold. While mutations in the same gene tend to have similar qualitative effects, the effect size can vary widely. For example, mutations in BRAF and CARD11 have large dynamic ranges of IL-2 production depending on the mutation. IL-2 increased from 15-396 fold amongst BRAF mutations and 114-359 fold for CARD11 mutations (Fig. 2.1e). Lastly, specific mutations led to significant up- or down-regulation of PD-1 expression upon antigen exposure (Fig. 2.1e).

Previous work[26] has suggested some of the mutations require antigen stimulation to exert their effects. Antigen-specificity is critical to minimize off-target effects of the CAR-T cells. The requirement for antigen restricts T cell effector functions to the tumor microenvironment. Particularly for the BBz-CAR, the mutations had significantly less effects without antigen compared to with antigen (Extended Data Fig. 2.2d). Collectively, this T cell mutation library provides a powerful and tunable toolkit for rewiring the balance and strength of different T cell signaling and functional outputs in response to CAR signaling.

A major barrier to the success of cell therapy is the accumulation and persistence of T cells within tumors[35]. These mutations are recurrent in humans because they are positively selected for *in vivo* in patients. We hypothesized these mutations could be beneficial to *in vivo* persistence of human CAR-T cells in the tumor microenvironment. Therefore, we systematically screened mutations in primary human CAR T cells in a xenograft model. To uncover mutations that improve persistence in highly adverse conditions, we utilized a fast-growing K562 subcutaneous tumor model in which T cell efficacy is limited (Extended Data Fig. 2.3a). To screen mutations *in vivo*, primary human CD3+ T cells were individually co-transduced with a CD19-BBz-CAR and the T cell mutation constructs. Cells expressing both the CAR and the mutation constructs were pooled, sorted, then injected into immunodeficient mice bearing subcutaneous K562-CD19 tumors. A sample of this pre-injection pooled library was taken for baseline sequencing of barcodes (Extended Data Fig. 2.3b). Barcode frequency in tumors were compared to the pre-injection T cell pool to determine constructs which were depleted or enriched *in vivo*. The single most depleted construct in the library was PDCD1, which encodes the co-inhibitory receptor and immunotherapy target PD-1[36], suggesting that our *in vivo* screen was successfully able to identify therapeutically relevant targets (Fig. 2.1f). Constructs identified as significantly enriched in tumor infiltrating T cells included MYCN p.P44L, CARD11-PIK3R3 gene fusion, CCND3 p.P284S, wild-type MYCN, STAT3 p.G618R, and RLTPR p.Q575E (Fig. 2.1f, Extended Data Fig. 2.3c).

2.4. CARD11-PIK3R3 enhances CARD11-BCL10-MALT1 signaling

We next examined the *in vitro* CAR signaling of the top hits from our *in vivo* screen and found that CCND3 p.P284S and MYCN p.P44L showed downregulated antigen-dependent

NFAT, NF-κB, and AP-1 signaling despite increased enrichment *in vivo* (Extended Data Fig. 2.3d). Prior work in other cell types suggests[37,38] that these constructs may activate proliferative programs without increasing effector functions. In contrast, CARD11-PIK3R3 showed dramatically enhanced NF-κB, AP-1 signaling and IL-2 production, without increasing NFAT or PD-1 (Extended Data Fig. 2.3d). Of note, previous work has suggested that increased signaling through NF-κB and AP-1[8,39] but not NFAT[34] could help to counter T cell dysfunction. Additionally, recent studies have demonstrated improved maintenance of memory phenotypes and effector functions in CD8+ T cell subsets that produce high levels of IL-2[40]. These favorable *in vitro* features coupled with the improved persistence of CARD11-PIK3R3 cells *in vivo* led us to select CARD11-PIK3R3 for further functional validation and mechanistic testing. CARD11-PIK3R3 was initially reported in a single patient with CD4+ cutaneous T cell lymphoma[41]. To our knowledge, it has not been functionally assessed *in vitro* or *in vivo*. Notably, this perturbation linking portions of two genes together would not have been identified by previous screening approaches.

In normal T cells, T cell receptor (TCR) signaling activates PKCθ, which in turn promotes the assembly of the CARD11-BCL10-MALT1 (CBM) signalosome[42] (Fig. 2.2a). CBM complex components are essential for normal T cell activation and function in response to antigen[42]. The CBM complex subsequently has three major outputs: NF-κB and AP-1 transcriptional activity and MALT1 proteolytic activity[42]. In the absence of TCR signaling, an inhibitory domain present in wild-type CARD11 prevents CARD11 binding to the other members of the CBM complex (Fig. 2.2b). Upon TCR signaling, the inhibitory domain is phosphorylated, enabling oligomerization of CARD11 protein and recruitment of BCL10-MALT1 filaments to form a functional CBM complex[43]. Though specific functions in T cells have not been elucidated for PIK3R3, it contains two SH2 domains which bind to tyrosine phosphorylated proteins[44] (Fig. 2.2b). The product of the translocation between CARD11 and PIK3R3 results in a gene fusion of the N-terminal

CARD11 protein CARD domain, coiled-coil domain, and part of the inhibitory domain with an SH2 domain from the C-terminus of PIK3R3 (Fig. 2.2b). To determine which domains of CARD11-PIK3R3 are required for the observed phenotype, we deleted specific domains and tested their ability to induce NF-κB signaling (Fig. 2.2c). Deletion of the PIK3R3 or the CARD11 component of CARD11-PIK3R3 abolished signaling activity, suggesting both partners are required for function (Fig. 2.2c). In CARD11, the coiled-coil domain and the CARD11 domain but not the truncated portion of the inhibitory domain are necessary to activate NF-kB (Fig. 2.2c).

We next hypothesized that CARD11-PI3KR3, like endogenous CARD11, recruits the CBM complex. We had already demonstrated that CARD11-PIK3R3 induces elevated NF-κB and AP-1 signaling (Extended Data Fig. 2.3d), consistent with increased CBM complex signaling. Thus, we sought to test whether CARD11-PIK3R3 induces MALT1 paracaspase activity. Western blotting of canonical MALT1 substrates CYLD and HOIL-1[45] indicated increased tonic and stimulation-induced cleavage of these proteins in the presence of CARD11-PIK3R3 (Fig. 2.2d). MALT1 inhibitor treatment abrogated these effects, demonstrating cleavage of these proteins was indeed dependent on the MALT1 paracaspase (Fig. 2.2d).

Next, we sought to determine whether CARD11 or BCL10 were required for the function of CARD11-PIK3R3 through CRISPR knockout experiments. In unstimulated, CAR-stimulated, and pharmacological TCR stimulated conditions we observed a reliance of CARD11-PIK3R3 on BCL10 but not wild-type CARD11 (Fig. 2.2e). In contrast, control cells relied on both CARD11 and BCL10 for TCR-triggered activation of NF-κB as expected. Interestingly, cells lacking CARD11-PIK3R3 did not depend on either CARD11 or BCL10 for CAR-dependent signaling (Fig. 2.2e). To further elucidate the function of BCL10 in mediating CARD11-PIK3R3 function, we generated a mutant version of CARD11-PIK3R3 with an amino acid substitution at the BCL10 binding interface (p.R28A), which was previously shown to abolish CARD11-BCL10

binding[46]. We observed that BCL10 binding was critical for both tonic NF-κB and antigen-dependent NF-κB and AP-1 signaling (Fig. 2.2f).

Finally, given the requirement for the PIK3R3 component of CARD11-PIK3R3 (Fig. 2.2c), we determined whether phospho-tyrosine binding capacity of the SH2 region of PIK3R3 is required for CARD11-PIK3R3 signaling. To ablate binding, we generated an arginine to alanine mutation in the phospho-tyrosine binding pocket of the PIK3R3 SH2 region[47] and observed a significant reduction in NF-κB signaling (Fig. 2.2g). Altogether, these data indicate that CARD11-PIK3R3 enhances CBM complex signaling in a manner dependent on BCL10 and PIK3R3 SH2-dependent binding of phospho-tyrosine residues.

2.5. CARD11-PIK3R3 expression enhances CAR T cells in vitro

We next sought to characterize the effects of CARD11-PIK3R3 expression in primary human CAR T cells. To examine effects on gene expression, we performed RNA-sequencing of human CD4+ and CD8+ T cells from three donors, with and without antigenic stimulation (Supplemental Table 2). Principal component analysis demonstrated the most dramatic transcriptional differences were induced by CAR-dependent stimulation, suggesting that CARD11-PIK3R3 expression is not sufficient to cause primary cells to adopt a fully antigen activated phenotype (Extended Data Fig. 2.5a). By comparing transcripts upregulated in both CD4+ and CD8+ T cells upon CAR stimulation, we identified a core group of 43 genes modulated by CARD11-PIK3R3 (Fig. 2.3a) These included several transcripts with important roles in CAR T cell function and effector cytokine production (Fig. 2.3a), including activation markers (IL2RA), cytotoxic and effector molecules (IFNG, TNF, IL4, IL5, IL13), chemokines

(CCL4), and co-stimulatory molecules (ICOS, TNFRSF4[OX40]). Several of these genes, such as ICOS[48] and OX40[49], have been previously suggested to favorably impact anti-tumor responses. Interestingly, CARD11-PIK3R3 expressing CD4+ T cells were enriched for gene signatures related to cell cycle as compared to CD8+ T cells, which were enriched most for RNA metabolism, cytokine signaling, and translation signatures (Fig. 2.3b). Consistent with our biochemical analyses, gene set enrichment identified enrichment of NF-κB, AP-1, and MALT1 paracaspase signatures[50] (Fig. 2.3b).

Because we observed basal NF-κB signaling in CARD11-PIK3R3 expressing Jurkat cells and upregulation of proliferation-associated gene pathways in CD4+ T cells, we determined if CARD11-PIK3R3 could induce cytokine independent growth in primary CAR T cells. To do so, we co-transduced primary T cells with a CD19-BBz-CAR and CARD11-PIK3R3. After removing anti-CD3/CD28 stimulation and sorting for a purified population, cells were expanded and rested in culture with IL-2. CARD11-PIK3R3 improved the expansion of CAR-T cells in the presence of IL-2, however removal of IL-2 either early or late in the culture led to rapid T cell population contraction (Extended Data Fig. 2.4a-c). Next, we sought to understand how increased CBM complex signaling affects the activation state and effector phenotypes in primary CAR T cells. To do so, we co-transduced primary T cells with a CD19-BBz or CD19-CD28z-CAR and CARD11-PIK3R3. To assess antigen induced activation states, we co-cultured transduced CD4+ or CD8+ T cells with K562-CD19 targets for 24 hours, then determined expression of activation markers via flow cytometry.

We observed equivalent expression of some activation markers (PD-1, CD39) in CD19-BBz-CAR T cells with and without CARD11-PIK3R3 (Fig. 2.3c). Consistent with our bulk RNAseq data, we found CD25 (IL2RA) and ICOS to be significantly upregulated in

CARD11-PIK3R3 CD19-BBz CAR T cells as compared to CAR T cells alone (Fig. 2.3d, Extended Data Fig. 2.5b).

These observations were similar in the CD19-CD28z-CAR setting (Extended Data Fig. 2.5c), though CARD11-PIK3R3 CD19-CD28z CAR T cells also had higher expression of PD-1 and CD39, while CD25 trended upwards but was not significant. Interestingly, while expression of CARD11-PIK3R3 leads to higher basal transcriptional activity of NF-κB in Jurkats, primary CD8+ T cells transduced with CARD11-PIK3R3 alone did not show significantly higher expression of activation markers compared to untransduced control T cells, though CD4+ T cells transduced with CARD11-PIK3R3 did have increased ICOS expression (Extended Data Fig. 2.5d). This data, in conjunction with the lack of IL-2 independent growth (Extended Data Fig. 2.4b-c), would suggest that while CARD11-PIK3R3 may induce some basal NF-κB signaling, it is not sufficient to cause full antigen independent activation or proliferation of untransformed primary T cells.

Bulk RNAseq analysis of antigen stimulated CARD11-PIK3R3 CD19-BBz-CAR T cells identified numerous upregulated cytokine transcripts (Fig. 2.3a). To confirm these findings at the protein level we co-cultured transduced CD4+ or CD8+ T cells with CD19-K562 targets for 48 hours and assessed cytokine production. Consistent with the Jurkat ELISA results, we found that CARD11-PIK3R3 induced higher secretion of IL-2, in addition to inflammatory cytokines such as IFN-γ and TNF-α (Fig. 2.3d). The Th2 cytokine IL- 5 was also significantly increased indicating that CARD11-PIK3R3 induces a unique cytokine profile (Fig. 2.3d). Surprisingly, cytokine secretion was substantially increased in CD8+ CARD11-PIK3R3 CAR T cells, while less so in CD4+ CARD11-PIK3R3 CAR T cells, despite being originally observed in a CD4+ T cell cancer (Fig. 2.3d). Similar trends were observed in CD8+ T cells with the CD19-CD28z-CAR, though in some cases, these trends did not reach statistical significance

(Extended Data Fig. 2.5e). Cytokine secretion was antigen dependent. Like control cells, T cells expressing CARD11-PIK3R3 alone did not induce cytokine release (Extended Data Fig. 2.5f).

Next, we determined how expression of CARD11-PIK3R3 effects CAR T cell cytotoxicity and growth. Tumor microenvironments often lack pro-survival signaling required by cytotoxic T cells, such as IL-2[51]. However, *in vitro* cytotoxicity assays often incorporate exogenous IL-2, which fails to recapitulate the lack of IL-2 experienced by T cells in tumors. Therefore, we co-cultured transduced CD8+ T cells with CD19-K562s at a 1:1 ratio and maintained in culture for two weeks with or without supplemental IL-2. After two weeks of culture supplemented with IL-2 both the CARD11-PIK3R3 CD19-BBz CAR T cells and CD19-BBz CAR T cells alone were able to efficiently clear the CD19-K562 targets. However, when cultured without supplemental IL-2, only the CARD11-PIK3R3 CD19-BBz CAR T cells were able to efficiently clear the CD19-K562 targets. We found that for one T cell donor, the CD19-BBz-CAR T cells failed to fully eliminate the CD19-K562 targets even with IL-2; however, the addition of CARD11-PIK3R3 enabled tumor cell clearance with and without IL-2 (Fig. 2.3e). This suggests that the expression of CARD11-PIK3R3 may rescue the cytotoxic capacity of poor T cell donors, which may be of benefit in the autologous clinical setting where patient T cells are often less effective[52]. Less dramatic differences in cytotoxicity were observed for the CD19-CD28z-CAR T cells in the long co-culture killing assay, which may be a result of the known propensity for CD28z-CARs to drive more IL-2 production (Extended Data Fig. 2.5g)[53]. Additionally, we assessed cytotoxicity at decreasing effector to target ratios and found that at every ratio tested, the CD19-BBz or CD19-28z-CAR T cells with CARD11-PIK3R3 exhibited superior control of tumor cell growth compared to the CAR controls (Extended Data Fig. 2.5h-i). Beyond enhanced cytotoxicity, CARD11-PIK3R3 expression led to increased expansion of both CD19-BBz and CD19-28z-CAR

T cells after two stimulations over two weeks in culture (Extended Data Fig. 2.5j), suggesting greater proliferative potential of CARD11-PIK3R3 CAR T cells when activated by antigen.

2.6. CARD11-PIK3R3 improves CAR T cells in vivo

We next determined if CARD11-PIK3R3 promotes the therapeutic efficacy of CD19-BBz-CAR T cells in the CD19+ NALM-6 xenograft leukemia model. We dosed NSG mice with 5 x 10^5 luciferase expressing Nalm6 on day 0, then treated with 1 x 10^6 CAR+ transduced human T cells on day 5 (Extended Data Fig. 2.6a,b). NALM-6 cancer burden was assessed twice weekly using IVIS imaging (Fig. 2.4a). We found that when the TCR was expressed (TCR replete), the CD19-BBz-CAR T cells with CARD11-PIK3R3 controlled NALM-6 leukemia, but the mice experienced lethal weight loss consistent with accelerated graft-versus-host disease (GVHD) (Extended Data Fig. 2.6c,d). GVHD is common in xenograft settings if the TCR is not knocked out; however, GVHD is often 35-40 days post adoptive T cell transfer[54]. We mitigated the early onset GVHD with TCR knockout in the CAR T cells using CRISPR/Cas9 (Extended Data Fig. 2.6a,b). Under TCR knockout conditions, the CD19-BBz-CAR T cell treatment failed to control the NALM-6 leukemic burden resulting in a median overall survival of 24 days, while CD19-BBz CAR with CARD11-PIK3R3T cells eliminated NALM-6 leukemia, with 100% survival at 35 days (Fig. 2.4a).

The improved efficacy of CD19-BBz-CAR T cells was also observed at higher doses of 7 x 10^6 CAR+ T cells, where 4 of 7 CD19-BBz-CAR treated animals that initially controlled tumor began relapsing with NALM-6 disease, while 7 of 7 CARD11-PIK3R3 CD19-BBz-CAR T cell treated animals did not relapse (Fig. 2.4b, Extended Data Fig. 2.7a). We also determined that

CARD11-PIK3R3 expressing T cells alone had no anti-tumor effect, demonstrating that the anti-tumor effects observed are antigen-specific, and dependent on CAR activity (Fig. 2.4b). To address safety concerns, we also determined that NALM-6 bearing animals that controlled tumors with CAR or CARD11-PIK3R3 CAR T cell treatment gained weight over the course of 100 days, losing weight only when NALM-6 relapse occurred (Fig. 2.4b, Extended Data Fig. 2.7b). Similarly, non-tumor bearing mice tolerated high doses of control T cells, CAR T cells, CAR + CARD11-PIK3R3 T cells (Extended Data Fig. 2.7c). Finally, upon 5 x 10^5 NALM-6 tumor rechallenge (to animals that had eliminated the leukemia and had not developed symptoms of GVHD), we found that CD19-BBz-CAR treated animals succumbed to NALM-6 disease at a similar rate as naïve age matched controls, while CARD11-PIK3R3 CD19-BBz-CAR T cells prevented leukemic growth(Extended Data Fig. 2.7d). These data indicate that CARD11-PIK3R3 enhances therapeutic efficacy while maintaining safety, even at high T cell doses, *in vivo*.

In vitro data indicated that CARD11-PIK3R3 CD19-CD28z-CAR T cells had similar though a less drastic phenotype as compared to CARD11-PIK3R3 CD19-BBz-CAR T cells (Extended Data Fig. 2.5). However, we next determined whether CARD11-PIK3R3 could improve CD19-CD28z-CAR T cell activity at low doses in the NALM6 leukemia model described above. We thus dosed NALM6-bearing mice with 4 x 10^5 CD19-CD28z-CAR T cells, or CARD11-PIK3R3 CD19-CD28z-CAR T cells (Extended Data Fig. 2.8a) and found that CAR T cell treated animals succumbed to disease, while CARD11-PIK3R3 CAR T cells cleared an initial NALM6 tumor challenge, and a rechallenge (injected on Day 77 post initial tumor implantation) (Fig. 2.4c,d, Extended Data Fig. 2.8b). Therefore, the anti-tumor efficacy of CARD11-PIK3R3 expression is not limited to CARs with 4-1BB costimulatory domains, but also improves those with CD28 domains, suggesting that CARD11-PIK3R3 expression could broadly benefit CAR T cell therapies.

Finally, we sought to determine how CARD11-PIK3R3 could perform in a xenograft solid tumor model. Here, we used the subcutaneous model of mesothelioma (M28), which naturally expresses the tumor associated antigen MCAM[55]. We manufactured and dosed tumor bearing animals with 5 x 10^5 MCAM targeted CD28z-CAR T cells with or without CARD11-PIK3R3, or control T cells (Extended Data Fig. 2.8c). Animals maintained weight throughout the study (Extended Data Fig. 2.8d), indicating therapy was well tolerated. While MCAM-CD28z-CAR treatment delayed tumor growth compared to the control, both control and CAR T cell treated tumors progressively increased in size (Fig. 2.4e). In contrast, CARD11-PIK3R3 MCAM-CD28z-CAR T cell treated animals controlled M28 tumor growth over the course of approximately 70 days (Fig. 2.4e). Therefore, CARD11-PIK3R3 safely improves the long-term therapeutic efficacy of human CAR T cells *in vivo* in both hematological and solid tumor settings. Furthermore, CARD11-PIK3R3 CAR T cells protect from relapse (rechallenge) as compared to CAR T cells alone.

Given the improved therapeutic efficacy in xenografts, we wanted to determine if CARD11-PIK3R3 improves CAR T cell efficacy in an immunotherapy refractory, fully immunocompetent *in vivo* setting with an intact immunosuppressive tumor microenvironment[56]. To accomplish this, we expressed human CD19 on B16-F10 melanoma (B16-hCD19+).

We utilized OT-I T cells, which express the transgenic TCR that recognizes OVA peptide, as donor T cells for CAR transduction to exclude any effects of the endogenous TCR. We transduced CD45.2+ OT-I CD8+ T cells with the human CD19 targeted murinized BBz CAR with or without CARD11-PIK3R3 (Extended Data Fig. 2.8e). As there is high homology between human and murine CARD11 we did not murinize CARD11-PIK3R3[KR1] . Animal weight was maintained throughout the study (Extended Data Fig. 2.8f). Five days post adoptive transfer of 4 x 10^6 CAR T cells, we observed significantly higher number of CARD11-PIK3R3

CD19-BBz-CART cells in the tumor and spleen as compared to the CD19-BBz-CAR T cells, suggesting greater *in vivo* expansion and/or persistence of CARD11-PIK3R3 CD19-BBz-CAR T cells (Fig. 2.4f, Extended Data Fig. 2.8g). We found that the CARD11-PIK3R3 CD19-BBz CAR T cell treatment controlled B16-hCD19+ tumor growth compared to untransduced (control) or CD19-BBz CAR T cells (Fig. 2.4g). In fact, in 5/5 animals treated with CD19-BBz CAR with CARD11-PIK3R3 T cells tumors regressed at least 30% from their largest volume, while all CD19-BBz-CAR treated animals had tumors that increased in size at every measurement. After a dramatic initial response, the B16-hCD19+ tumors relapsed in CARD11-PIK3R3 CD19-BBz CAR T cell treated animals. In a repeated study, CD19-BBz-CAR and CARD11-PIK3R3 CD19-BBz-CAR T cell treated tumors were assessed at tumor endpoint by flow cytometry. CD19-BBz-CAR treated tumors maintained CD19 expression, while CARD11-PIK3R3 CD19-BBz-CAR T cell treated tumors were uniformly CD19 negative, suggesting antigen loss as the mechanism of relapse (Extended Data Fig. 2.8h). Overall, CARD11-PIK3R3 CD19-BBz CAR T cell therapy resulted in significantly improved survival compared to CD19-BBz-CAR T cell therapy (Fig. 2.4g). Notably, this anti-tumor activity was achieved without lymphodepletion. Lymphodepletion regimens increase the availability of homeostatic cytokines that signal through the common gamma chain and thus have been shown to significantly improve CAR T cell engraftment and efficacy[57]. We conclude that CARD11-PIK3R3 CAR T cells drive a potent anti-tumor response in a solid tumor model highly resistant to immunotherapy.

2.7. CARD11-PIK3R3 improves TCR-transgenic T cells in vivo

While CAR therapies are heavily pursued as cellular therapeutics, many groups have employed TCR-based T cell therapies particularly for the treatment of solid tumors[58]. Therefore,

we sought to assess the efficacy of the CARD11-PIK3R3 T cells in a TCR-transgenic tumor model. To accomplish this, we utilized the B16-F10 melanoma model wherein the melanoma cells express chicken ovalbumin (OVA)[59] (Fig. 2.5a). CD45.1+ OT-I CD8+ T cells were transduced with either control (GFP) or CARD11-PIK3R3 (mCherry) retroviruses, enabling tracking of adoptively transferred cells in CD45.2+ C57BL/6J hosts bearing B16-OVA melanoma tumors.

First, we utilized a recently described dual-transfer system to determine the relative fitness of cells expressing control vector or the CARD11-PIK3R3[7]. We used CD45.1+ OT-I T cells in which approximately 10% of the cells were mCherry positive (corresponding to CARD11-PIK3R3 expressing cells), which were mixed with control cells expressing GFP. Strikingly, we observed a 145-fold increase in cell number (normalized to input) of CARD11-PIK3R3 expressing cells compared to control cells among the TILs 7 days following transfer (Fig. 2.5b). This corresponded to a significantly increased fraction of transferred cells among total CD8+ T cells, even without normalization to input numbers (Extended Data Fig. 2.9a). Therefore, within the same tumor microenvironment, CARD11-PIK3R3 expressing T cells have dramatically improved accumulation compared to control cells. We attempted to assess longer term persistence of the mixed population graft (i.e 100,000 CARD11-PIK3R3 OT-Is with 900,000 control OT-Is) at 21 days post T cell transfer, but unexpectedly 4/5 tumors were cleared, preventing characterization of TILs at this time point (Extended Data Fig. 2.9b). We confirmed enhanced competitive accumulation of CARD11-PIK3R3 in a second transgenic TCR mouse model, pmel-1 T cells (which recognize gp100, an endogenous melanoma antigen) against B16-F10 tumors (Extended Data Fig. 2.9c-e). We performed this assay with both the wild-type CARD11-PIK3R3 and the R28A mutant to assess the dependence of the *in vivo*

phenotypes on BCL10 interactions. Mutating the R28A binding site reduced accumulation *in vivo* by 1257-fold (Extended Data Fig. 2.9c-e).

We next characterized the phenotype of cells following adoptive transfer of either CARD11-PIK3R3 or control transduced OT-I cells. Seven days after adoptive transfer, there was a significant reduction in tumor growth in mice treated with 1 x 10^6 CARD11-PIK3R3 OT-I cells compared to control OT-I T cells, suggesting enhanced efficacy (Extended Data Fig. 2.9f). In accordance with the data obtained from the competitive dual-transfer assay, there was also enhanced accumulation of CARD11-PIK3R3 OT-I T cells in the tumor when transferred separately (Extended Data Fig. 2.9f). In addition, we detected a higher proportion of CARD11-PIK3R3 OT-I cells compared to control OT-I cells in the spleen and tumor draining lymph node, though to a lesser extent than observed in the tumor (Fig. 2.5c).

Ex vivo restimulation with PMA/Ionomycin and intracellular cytokine staining of CARD11-PIK3R3 OT-I cells revealed enhanced stemness and effector functions of CARD11-PIK3R3 expressing cells. CARD11-PIK3R3 expression increased the expression of the stemness-associated transcription factor TCF-1 in TILs (Fig. 2.5c). However, TCF-1 was not elevated in spleen or tumor draining lymph node CARD11-PIK3R3 cells, suggesting tumor-specific remodeling of T cell phenotype (Extended Data Fig. 2.9g). Functionally, CARD11-PIK3R3 TILs showed increased production of TNF-α, IFN-γ, and IL-2 (Fig. 2.5d, Extended Data Fig. 2.9h), and the proportion of polyfunctional cells producing all three of these effector cytokines was significantly elevated in CARD11-PIK3R3 OT-I cells (Fig. 2.5d). Together, these results indicate that CARD11-PIK3R3 expression promotes the intra-tumoral accumulation of highly functional, stem-like T cells.

Finally, we determined the effects of CARD11-PIK3R3 on the therapeutic efficacy of T cells in an immunocompetent system. On day 12 following B16-OVA implantation, mice were treated with PBS control or 2 x 10^6 OT-I cells transduced with either control or CARD11-PIK3R3, without pre-conditioning or lymphodepletion. CARD11-PIK3R3 OT-I T cells mediated significantly enhanced control of tumor growth (Extended Data Fig. 2.9i). In addition, CARD11-PIK3R3 OT-I cells promoted prolonged overall survival. Strikingly, 60% of mice (3/5) receiving CARD11-PIK3R3 achieved complete clearance of tumors at over three months following tumor challenge, at which point no PBS or control OT-I T cell treated mice survived (Extended Data Fig. 2.9i). Of note, we did not observe weight loss, ataxia, or other systemic symptoms in the CARD11-PIK3R3 treated mice compared to controls (Extended Data Fig. 2.9j).

The long-term persistence experiment suggested that low doses of CARD11-PIK3R3 cells may be sufficient to induce tumor clearance (Extended Data Fig. 2.9b). This was a provocative finding for two reasons. Reduced cell numbers are routinely used as “stress tests” to quantify relative efficacy of modified T cell therapies[60]. Moreover, these data suggest that CARD11-PIK3R3 may overcome one key limitation of cell therapies, the ability to manufacture sufficient cells for therapeutic efficacy in humans. To test this, we compared therapeutic efficacy of 20,000 and 100,000 CARD11-PIK3R3 positive OT-I cells against 2 x 10^6 control OT-I cells in B16-OVA tumor bearing mice, again without lymphodepletion. Strikingly, CARD11-PIK3R3 enabled superior tumor control with both a 20-fold (4/4 cleared) and 100-fold (5/5 cleared) lower dose than control cells (Fig. 2.5e).

We sought to determine if CARD11-PIK3R3 OT-I cells persist after clearance of the initial tumor challenge. Current T cell therapies often lack long term persistence, failing to form memory populations after clearance of the primary tumor, resulting in high incidence of relapse[61]. After more than two weeks of initial tumor clearance, CARD11-PIK3R3 OT-I T cell

treated animals treated with low cell doses or naïve controls were rechallenged with B16-OVA tumor cells in the contralateral flank. The CARD11-PIK3R3 OT-I T cell treated were protected from tumor development compared to naïve, untreated mice at both low dose levels (Fig. 2.5e). The rejection of a secondary tumor challenge suggests that CARD11-PIK3R3 OT-I T cells can respond to and suppress tumor re-occurrence, though future studies are required to determine if this long-term protection is OT-I mediated. These functional properties are highly desirable in cancer therapies, allowing for a single engineered therapy to respond to primary tumors and to prevent relapse, inducing durable clinical remission.

To further extend these TCR efficacy findings to human engineered TCR T cells, we developed a human TCR-based xenograft model. KRAS p.G12D, a common mutation present in human solid tumors, can be presented on various human HLA alleles and has been targeted by adoptive T cell therapies in small studies in humans[62]. Utilizing HLA-C*08:02 over-expressing SNU-1 gastric carcinoma cells which harbor a KRAS p.G12D mutation and a clinically validated TCR against HLA-C*08:02 presented KRAS p.G12D, we observed significantly enhanced tumor clearance with CARD11-PIK3R3 expression (Fig. 2.5f). Therefore, CARD11-PIK3R3 expression enhances the function of both human and mouse therapeutic TCR cells. Altogether, these data indicate that CARD11-PIK3R3 expressing T cells have superior therapeutic function *in vivo* in multiple immunotherapy refractory tumor models, including CAR and TCR-transgenic based models.

To address concerns of toxicity or transformation, we monitored the mice from Fig. 2.5e and Extended Data Fig. 2.9i for up to 418 days after T cell transfer (Extended. Data Fig. 2.10a). Throughout this time, CARD11-PIK3R3 OT-I T cell treated animals gained weight similarly to that of published controls (Extended Data Fig. 2.10b). To assess for occult disease, we performed necropsy on three mice on day 240 after T cell transfer. Their spleens were of normal

weight and gross appearance (Extended Data Fig. 2.10c,d). Additionally, CARD11-PIK3R3 OT-I T cells made up less than 1% of total CD8+ T cells in the spleen and blood (Extended Data Fig. 2.10e). We performed hematoxylin and eosin (H&E) staining of common extra-nodal sites of lymphoma, as well as the spleen and lymph nodes. Pathology review failed to identify any evidence of nuclear atypia, destruction of normal cellular architecture, or neoplastic disease (Extended Data Fig. 2.10f).

For the remaining 9 animals, we monitored the blood for evidence of leukemic disease for 330-418 after adoptive transfer. There were no atypical cells in the blood. Moreover, tail bleeds of CARD11-PIK3R3 OT-I treated animals revealed CARD11-PIK3R3 OT-I T cells were present at less than 1% of the overall CD8 population (Extended Data Fig. 2.10g-j). This data suggests contraction of CARD11-PIK3R3 OT-I T cell population after exposure to initial or rechallenge tumors. Altogether, these data demonstrate a favorable safety profile of CARD11-PIK3R3 expressing anti-tumor T cells and a lack of evidence of malignant transformation *in vivo* over long time periods.

2.8. Discussion

By screening T cell lymphoma mutations through both *in vitro* and *in vivo* arrayed assays, we identified how individual mutations can tune T cell signaling, improve cytotoxic T cell functions, and promote *in vivo* accumulation. This approach identified a novel gene fusion, CARD11-PIK3R3, which dramatically enhances therapeutic T cell function and efficacy. Transcriptional profiling of CD4+ and CD8+ CAR T cells demonstrated significant effects of the CARD11-PIK3R3. Interestingly, CARD11-PIK3R3, though discovered in a CD4+ T cell

lymphoma, had outsized effects in CD8+ T cells, increasing function *in vitro* and tumor control *in vivo* in syngeneic models. Future work is required to better understand the mechanistic differences of CARD11-PIK3R3 signaling in CD4+ and CD8+ T cells. In particular, PIK3R3 SH2 interactions should be mapped, and quantitative studies to determine effects of CARD11-PIK3R3 on critical signaling cascades in T cells must be performed. These detailed analyses will allow for further insights into how CBM signaling can sculpt T cell activation and can be regulated to enhance a variety of T cell therapeutic modalities.

Expression of CARD11-PIK3R3 enables superior tumor control in human and mouse T cells in CAR models. CARD11-PIK3R3 demonstrated improved anti-tumor efficacy in both 4-1BB and CD28 CAR T cell models, suggesting the mechanism of CARD11-PIK3R3 enhancement is not limited by CAR architecture, and allowing for future application to a broad array of CAR designs. Furthermore, while we demonstrated improved anti-tumor efficacy in both hematological and solid xenograft tumors models, these findings were expanded upon in syngeneic settings, where CARD11-PIK3R3 expressing T cells exhibited improved tumor control without the requirement of lymphodepletion.

Inclusion of CARD11-PIK3R3 in TCR therapies proved to also drive superior anti-tumor efficacy. Even at 100-fold lower cell doses and upon re-challenge, TCR transgenic cells expressing CARD11-PIK3R3 have improved tumor control in a fully immunocompetent murine model without lymphodepletion. Importantly, TCR knockout highlighted the TCR/CAR dependence of signaling through CARD11-PIK3R3. Furthermore, we did not observe evidence of T cell lymphomagenesis *in vivo*, even at over one year post adoptive T cell transfer. Notably, the gene fusion we identified would be inaccessible through previous T cell screening efforts such as loss of function, CRISPR activation, or wild-type gene overexpression screens[7-10]. Therefore, naturally occurring mutations which have undergone positive selection in humans *in*

vivo represent a powerful set of tools to enhance cell therapy. Our findings support further testing of mutations identified in T cell lymphomas, or even other somatic mutations occurring in other expanded T cell clones, such as in autoimmune disease, may hold promise for identifying additional tools to enhance T cell function. Our approach provides a platform for modifying other immune cell types with naturally occurring mutations for cell therapy, such as macrophages[63], NK cells[64], gamma delta T cells[65], or B cells[66]. The potential utility of this approach is highlighted by the surprising fact that while originally discovered in malignant CD4+ T cells, CARD11-PIK3R3 dramatically enhances CD8+ T cell activity.

Future work will explore how to optimally ensure the safety of T cell therapeutics combined with CARD11-PIK3R3 or other naturally occurring T cell mutations. Numerous studies to date have employed knockout of T cell lymphoma tumor suppressors to enhance T cell therapy without evidence of malignant transformation, including knockout of PD-1 in a phase I trial[21]. Our *in vitro* studies demonstrated that cytokines can support CARD11-PIK3R3 CAR-T cell growth. To elucidate implications for manufacturing and for safety, further studies will be required to assess the necessity or sufficiency of cytokines to enable growth with clinically relevant CAR designs. Our long-term *in vivo* xenograft and syngeneic studies, performed in multiple models and at high T cell doses, showed no signs of lymphomagenesis, even at 418 days after adoptive T cell transfer. However, we cannot entirely rule out the possibility of malignant transformation; therefore, CARD11-PIK3R3 or other mutations may be candidates for controlled expression, such as with synNotch or synthetic intramembrane proteolysis receptor (SNIPR) circuits, which we have previously used for antigen specific transcriptional regulation of payloads[67-69]. Furthermore, we discovered that CARD11-PIK3R3 signals downstream of the TCR, presenting safety concerns for enhanced autoimmunity in the autologous setting, or

GVHD in the allogeneic setting. Nonetheless, we observed this toxicity can be controlled through CRISPR knockout of the TCR.

Finally, our results implicate the CBM signalosome as a key regulator of therapeutic T cell function. Several individual outputs of CBM signaling such as inducing AP-1 and NF-κB transcriptional activity[8,39], and downregulation of MALT1 cleavage substrates REGNASE-1 and ROQUIN[7,70], have each been implicated independently as approaches to improve T cell therapy. This raises the possibility that a unifying feature of these various approaches is that they partly address a relative deficiency of CBM signaling in tumor infiltrating lymphocytes. CARD11-PIK3R3 expression represents a powerful engineering solution to enhance each of these separate CBM outputs simultaneously. Further investigation of T cell lymphoma mutations in the context of adoptively transferred T cells has the promise to both improve cellular therapies and to elucidate new T cell biology.

2.9. Methods

Receptor and Mutation Screening Construct Construction

Intracellular domains containing the appropriate costimulatory domain, CD3zeta domain, Gal4VP64 and GSlinkers were synthesized by Twist. Receptors were built by fusing the CD19 scFv [71] to the corresponding receptor scaffold and intracellular tail. All receptors contain an n-terminal CD8α signal peptide (MALPVTALLLPLALLLHAARP) for membrane targeting and a flag-tag (DYKDDDDK) for easy determination of surface expression with α-flag PE (Biolegend 637310). In some cases the receptors additionally contained a T2A self-cleaving sequence followed by a tNGFR sequence, used in downstream applications for T cell isolations. The

receptors were cloned into a modified pHR'SIN:CSW vector containing a PGK promoter for all primary T cell experiments. Wildtype genes of the mutation library were ordered as plasmids through DNASU, and point mutations were introduced through PCR site directed mutagenesis. Some mutated genes were synthesized by Twist. Wild type or mutated gene fragments were cloned into a modified pHR'SIN:CSW vector containing a PGK promoter followed by a T2A self-cleaving sequence, a unique barcode and the fluorescent tag mCherry used to identify transduced cells. Wild type or mutant gene fragments were cloned via a Sbf1 site in the multiple cloning site 3′ to the PGK promoter sequence. All constructs were cloned via Infusion cloning (Clontech #ST0345) or Gibson assembly.

Primary Human T cell Isolation and Culture

Primary CD3+, CD4+ and CD8+ T cells were isolated from anonymous donor blood after apheresis by negative selection (STEMCELL Technologies #15062 & 15063). Blood was obtained from Blood Centers of the Pacific (San Francisco, CA) as approved by the University Institutional Review Board. T cells were cryopreserved in RPMI-1640 (UCSF cell culture core) with 20% human AB serum (Valley Biomedical Inc., #HP1022) and 10% DMSO. After thawing, T cells were cultured in human T cell medium consisting of X-VIVO 15 (Lonza #04-418Q), 5% Human AB serum and 10 mM neutralized N-acetyl L-Cysteine (Sigma-Aldrich #A9165) supplemented with 30 units/mL IL-2 (NCI BRB Preclinical Repository) for all experiments unless otherwise noted. *In vivo* experiments were completed with bulk CD3+ cells isolated in a similar manner.

Lentiviral Transduction of Human T cells

Pantropic VSV-G pseudotyped lentivirus was produced via transfection of Lenti-X 293T cells (Clontech #11131D) with a pHR'SIN:CSW transgene expression vector and the viral packaging plasmids pCMVdR8.91 and pMD2.G using Mirus TransIT-Lenti (Mirus #MIR 6606). Primary T cells were thawed the same day, and after 24 hours in culture, were stimulated with Human T-Activator CD3/CD28 Dynabeads (Life Technologies #11131D) at a 1:3 cell:bead ratio. At 48 hours, viral supernatant was harvested and the primary T cells were exposed to the virus for 24 hours. In some cases, previously prepared and frozen concentrated virus was used in place of fresh. At day 5 post T cell stimulation, the Dynabeads were removed, T cells were sorted, and the T cells expanded until day 10-14 when they were rested and could be used *in vitro* or *in vivo* assays. T cells were sorted for assays with a Beckton Dickinson (BD) FACS ARIA II.

TCR KO and Lentiviral Transduction of Human T Cells

For TCR KO experiments, primary T cells were cultured in human T cell medium consisting of X-VIVO 15 (Lonza #04-418Q), 5% Human AB serum and 10 mM neutralized N-acetyl L-Cysteine (Sigma-Aldrich #A9165) supplemented with 100 units/mL IL-7 (Miltenyi #130-095-362) and 100 units/mL IL-15 (Miltenyi #130-095-765). Primary T cells were thawed, rested for 1 hour then stimulated with Human T-Activator CD3/CD28 Dynabeads (Life Technologies #11131D) at a 1:3 cell:bead ratio. One day after activation, T cells were transduced with concentrated virus. 24 hours later, virus and Dynabeads were removed, cells were rested for 24 hours, then resuspended at 1 x 100^6 cells per mL in P3 electroporation buffer (Lonza #V4SP-3960) with gRNA (CAGGGTTCTGGATATCTGT) targeting the human TRAC

locus and Cas9. 23 uL of this mixture was aliquoted to each well of a 96 well nucleofection plate (Lonza #V4SP-3960) and immediately electroporated using a 4-D Lonza Nucleofector with program EH115. Cells were resuspended in pre-warmed human T cell medium and recovered for 30 minutes in the incubator before being transferred to culture. Electroporated cells were assessed for TCR KO and lentiviral transduction via flow before injection to mice.

Cell lines

The cancer cell lines used were K562 myelogenous leukemia cells (ATCC #CCL-243), Jurkat cells (Clone E6-1, ATCC# TIB-152), B16-F10 melanoma cells (ATCC #CRL-6475), M28 epithelioid cells (originally obtained from Dr. Brenda Gerwin's lab at the National Cancer Institute), A549 lung epithelial carcinoma cells (ATCC #CCL-18), and SNU-1 (ATCC #CRL-5971). K562s and A549s were lentivirally transduced to stably express human CD19. CD19 levels were determined by flow cytometry (Biolegend, clone HIB19). A549s were additionally transduced to express the nuclear stain mKate2. SNU-1 cells were transduced with HLA-C*08:02. Jurkat cells were transduced with retroviruses encoding fluorescent reporter constructs [28] (Addgene 118095, 118094, and 118031) and stimulated with PMA/ionomycin to sort a line with high induction of each reporter. To enable screening with our mCherry expressing lentiviral constructs, an iRFP fluorescent reporter was subcloned to replace mCherry in the previously described AP1-mCherry construct. Triple reporter cells were then transduced with a CD19 28z-CAR or CD19 BBz-CAR. Jurkat, SNU-1 and K562 cells were cultured in RPMI + 10% FBS with penicillin/streptomycin and sodium pyruvate. B16-OVA, B16-F10 and A549 cells were cultured in DMEM + 10% FBS with penicillin/streptomycin. All cell lines were routinely tested for mycoplasma contamination (Southern Biotech).

In vitro Primary T Cell Assays

For *in vitro* co-culture assays, transduced primary T cells were co-cultured with target cells at the indicated effector to target ratios and co-culture time courses. For Luminex assays, cells were co-cultured in media lacking exogenous IL-2, supernatants were collected 48 hours after start, frozen at -80C and sent for analysis to Eve Technologies. For repeat stimulation assay, transduced T cells were co-cultured on the adherent CD19 expressing A549 cell line, and after 1 week T cells were removed from co-culture without disturbing adherent cells, counted and replated on CD19 expressing A549 cells seeded 24 hours prior. For co-culture assays performed over a period of days to weeks, media was supplemented regularly. All primary T cell *in vitro* assays were performed with three donors, unless otherwise noted in figure legend.

Flow Cytometry

For all *in vitro* primary T cell assays, cells were washed with PBS 2% FBS twice, stained with surface staining markers at room temperature for 20 minutes, washed twice, and resuspended in PBS 2% FBS with DRAQ7 (diluted 1:1000) before analysis on a BD FACSymphony X-50 Flow Cytometer. The following antibodies were used: CD8 (SK1), CD25 (M-A251), CD39 (A1), CD69 (FN50), CD271 (ME20.4), CD278 (C398.4A), CD279 (EH12.2H7).

In vivo Xenograft Assays

NOD.Cg-Prkdc^{scid} Il2rg^{tm1Wjl}/SzJ (NSG) mice were dosed tumor cells via subcutaneous injection (solid tumor) or tail vein injection (Nalm6). Mice with similar sized tumor burden were randomized to receive treatments of CAR T cells. Engineered or control T cells were dosed via retro-orbital injection. Subcutaneous tumors were measured with digital calipers twice weekly, and tumor volume was calculated using the following formulas: (length x width^2)/2 (CD19 K562, M28) or length × width × [(length × width)$^{0.5}$] × π/6 as previously described [7] (SNU-1). For subcutaneous tumors death was defined as a progressively growing tumor that reaches 15mm (SNU-1) or 20mm (CD19 K562, M28) in its longest axis or that develops ulceration or necrosis. For Nalm6 leukemic model, death was defined hind limb loss, poor body score, or loss of 15% of more of body weight, whichever occurred first. Animal drinking water was supplemented with Clavomox to prevent bacterial infections.

Jurkat reporter screening and analysis

CAR triple reporter Jurkat cells were transduced in 96 well plate format with individual T cell lymphoma mutation lentiviruses. 48 hours post-transduction, cells were plated at approximately a 1:1 ratio with K562 or K562-CD19 cells. Plates were spun at 300g for 2 minutes to promote interaction of CAR cells and target cells. Following 24 hours of co-culture, supernatants were removed for IL-2 ELISA (ELISA MAX™ Deluxe Set Human IL-2, Biolegend) and cells were washed in FACS buffer (PBS + 2% FBS) and analyzed by FACS. For the BBz-CAR screen, cells were stained with anti-PD-1 (Biolegend, clone EH12.2H7) prior to FACS analysis. Each screen was performed in biological replicate with separate lentiviral transductions. For analysis, the percentage positive for each reporter in each condition (i.e.

each CAR and co-culture cell type) was compared to the mCherry only controls and the corresponding wild-type gene control when available by T test followed by Bonferroni correction. Z scores were calculated for each condition as $(x – \mu) / \sigma$ (where x is the observed value, μ is the mean, and σ is the standard deviation). Constructs were excluded if insufficient mCherry+ cells were obtained for FACS analysis or if they failed sequencing verification.

In vivo screening and analysis

Human CD3+ T cells were lentivirally co-transduced with a CD19-BBZ CAR with tNGFR and the mutant construct library in an arrayed fashion. CD3+ T cells were assessed via flow for CD19-BBZ CAR (FLAG) and mutant construct (mCherry) expression. T cells were pooled based on mCherry expression and sorted for a purified dual positive population. 6e6 library T cells were injected to 15 CD19-K562 tumor bearing animals. T cells were isolated from the tumor and spleen by positive selection using the tNGFR (CELLection™ Biotin Binder Kit) at 7, 14, and 21 days post injection. gDNA was isolated from these T cells (NucleoSpin Tissue, Machery Nagel), and quantified by NanoDrop Spectrophotometry and adjusted to 8ng/uL. PCR amplification of the samples was performed using primers (Table 1) to enrich for the mutation barcodes (PCR1). PCRs were performed with Kapa HiFi, in reaction volumes of 50 µL with between 10 and 1090 ng of gDNA, all reactions underwent 7 cycles of amplification. For the subsequent PCR to add Illumina barcodes and adapters to the products (PCR2), all products from PCR1 were quantified with a Qubit 1X dsDNA High Sensitivity Assay kit (Invitrogen) and up to 10ng of template was used in a 25 µL reaction with Kapa Hifi. Different forward and reverse primers were used for each sample for PCR2 to add unique custom Illumina I5 and I7 barcode sequences to each sample. Finally, PCR2 products were again quantified using Qubit, and these products were

pooled at 1:1 molar ratio, diluted, loaded, and run on a MiniSeq 75 cycle cartridge using the standard manufacturer protocols. MAGECK software (https://sourceforge.net/projects/mageck/) was utilized to identify significantly enriched or depleted barcodes. Constructs with less than 10^2 reads in the pre-injection sample were excluded from analysis.

Bulk RNAseq and analysis

For bulk RNAseq, T cells from 3 independent healthy donors transduced with the indicated constructs were either unstimulated or stimulated via co-culture with CD19 expressing A549 cells for 8 hours. RNA was then isolated (Nucleospin RNA XS, Machery-Nagel and cDNA libraries were constructed using SMART-Seqv4 Ultra Low Input RNA Kit (Takara Bio) and Nextera XT (Illumina). Sequencing reads were aligned using STAR, transcripts quantified using HT-Seq, and differentially expressed genes were identified using DESeq2 as previously described[17].

Immunoblot analysis

Jurkat cells (1-5 x 10^6) were pre-treated for 30 minutes with the MALT1 inhibitor Z-VRPR-FMK (75 uM) or vehicle control. Cells were then treated with PMA/ionomycin as indicated for 2 hours. Whole-cell lysates were generated and analyzed by immunoblotting with the following antibodies: anti-HOIL1 (Millipore Sigma, MABC576), anti-CYLD (Santa Cruz, sc-74435), and anti-β-actin (Cell Signaling Technologies, 4967).

CARD11 and BCL10 CRISPR knock-out

CRISPR knockout was performed in triple reporter Jurkat cells using the SE Cell Line 4D-Nucleofector Kit (Lonza). 1 x 10^6 cells were nucleofected with Cas9 only or ribonuclear protein complexes of Cas9 with CARD11 gRNA (CAATGACCTTACACTGACGC) or BCL10 gRNA (TCGCCGAATAGATTCAACAA).

Mouse T cell purification and retroviral transduction

CD8+ T cells were isolated from the spleens of CD45.1+ or CD45.2+ OT-I mice using a mouse CD8+ T cell isolation kit (Stemcell Technologies) or Mouse Pan CD3+ T cell isolation kit (Biolegend). T cells were then cultured with 100 U/mL recombinant human IL-2 (Peprotech), anti-CD3e (1 ug/mL) and anti-CD28 (0.5 ug/mL) overnight. For CAR experiments, T cells were stimulated overnight with anti-CD3/CD28 beads (ThermoFisher). Retroviral supernatants were added to T cells in Retronectin (Takara) coated plates and spinduction was performed for 1 hour at 2000 rpm at 30°C. Following transduction, T cells were resuspended and cultured in fresh media containing 100 U/mL IL-2 until adoptive transfer. Transduction efficiency was determined by flow cytometry prior to adoptive transfer.

B16 melanoma tumor model

Female C57BL/6 mice age 6-8 weeks were injected subcutaneously with 5 x 10^5 B16-OVA or B16-F10 melanoma cells. Mice with similar sized tumors were randomized to receive treatments of OT-I or pmel-1 T cells. 100 uL of T cells (or PBS control) were

retro-orbitally injected on day 8-12 post tumor inoculation. For dual-transfer competitive assay and tumor infiltrating lymphocyte analysis experiments, 1 x 10^6 T cells were transferred. For anti-tumor efficacy, 2 x 10^6 T cells were transferred. For dose response experiments, the indicated number of cells were transferred. For rechallenge experiments, B16-OVA cells were injected subcutaneously on the opposite flank. Tumor lengths and widths were determined every 2-3 days by digital caliper measurement and tumor volume was calculated as length × width × $[(\text{length} \times \text{width})^{0.5}] \times \pi/6$ as previously described [7]. Death was defined as a progressively growing tumor that reaches 15mm in its longest axis or that develops ulceration or necrosis. For anti-tumor efficacy experiments, measurement of tumors and determination of survival endpoint was blinded to experimental condition. Experiments were performed in accordance with Northwestern University Institutional Animal Care and Use Committee approved protocols.

Mouse necropsy

Necropsy was performed utilizing protocols outlined by the Northwestern University Center for Comparative Medicine (CCM). Three mice were euthanized. Mice and spleens were weighed at the time of necropsy. Half the spleen and blood samples were taken for RBC Lysis followed by FACS analysis of transferred cells. After removal of the spleen, the mice were perfused with 10% neutral buffered formalin. Mouse blood, skin, heart, lung, brain, liver, stomach, kidney, intestine, colon, pancreas, lymph nodes, bone, spleen, bladder were removed and fixed at room temperature for 48 hours in 10% neutral buffered formalin, followed by 24 hours in 70% ethanol. After 24 hours in 70% ethanol, all tissues were embedded by the Mouse Histology and Phenotyping Laboratory at Northwestern University (MHPL). Slides were

evaluated by Dr. Jared T. Ahrendsen, Director of MHPL and Assistant Professor of Pathology at Northwestern University for signs of nuclear atypia, cellular architecture, and presence of neoplastic disease.

CD19-B16 melanoma tumor model

Male B6.SJL-Ptprca Pepcb/BoyJ mice age 6-12 weeks were injected subcutaneously with 1 x 10^5 CD19-B16 melanoma cells. Mice with similar sized tumors were randomized to receive treatments of CAR T cells. 100 uL of T cells (or PBS control) were retro-orbitally injected on day 12 post tumor inoculation. Tumor lengths and widths were determined every 2-3x per week by digital caliper measurement and tumor volume was calculated using the following formula: (length x $width^2$)/2. Death was defined as a progressively growing tumor that reaches, 2000mm^3 or 20mm in its longest axis, whichever comes first.

B16 tumor infiltrating lymphocyte (TIL) isolation and analysis

To isolate TILs, B16-F10-Ova tumors were excised, minced, and digested using collagenase IV (1 mg/mL) and DNAseI (50 ug/mL) for 30 minutes at 37°C in a shaking incubator at 200 rpm. TILs were filtered through a 70 uM cell strainer, in some cases lymphocytes were isolated over Percoll density centrifugation. For dual-transfer experiments, the isolated TILs were subjected to Fc receptor blocking, live/dead staining (Live/Dead Violet) and surface marker staining for flow cytometric analysis. For intracellular cytokine staining, cells were restimulated *ex vivo* in media containing brefeldin and monensin (Invitrogen), phorbol myristate acetate, and ionomycin for four hours. Following Fc blocking, live/dead staining, and cell surface marker

staining, cells were fixed (BD CytoFix), permeabilized (Invitrogen 10x Perm), and stained for intracellular proteins.

2.10. Figures

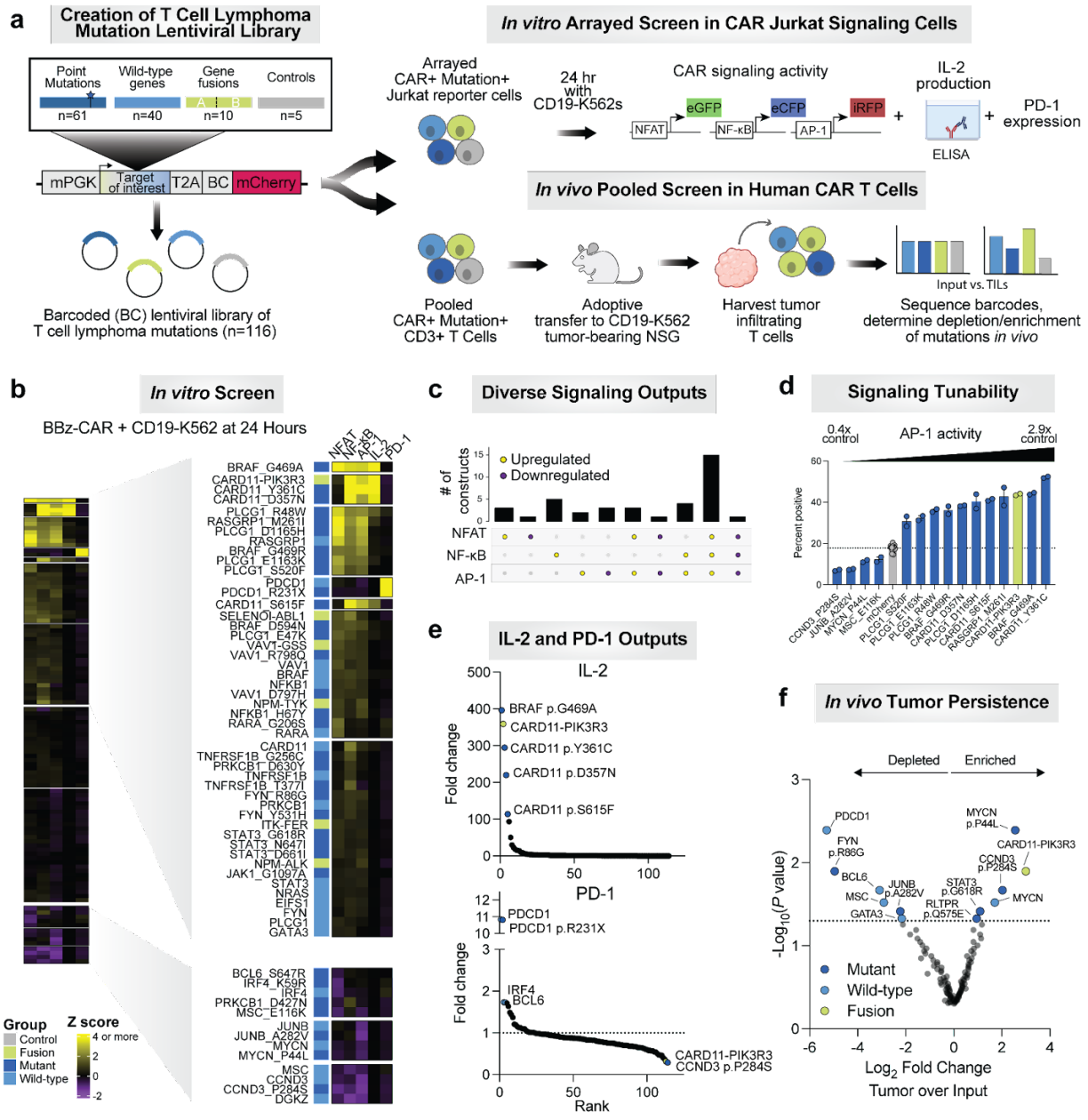

Figure 2.1 In vitro and in vivo screening identifies T cell lymphoma mutations which reprogram CAR signaling and functional outputs.

(a) Schematic indicating approach to development and screening of T cell mutation library. **(b)** Heatmap of reporter activity Z score for each of the indicated T cell mutation constructs in the BBz-CAR CD19-K562 screen. Clustering was determined using K-means. Z score indicates the mean Z score, normalized to mCherry only controls, of two independent experimental replicates. Select clusters with pronounced effects on outputs are highlighted. (Figure legend continued on the next page.)

(Figure legend continued from the previous page.) **(c)** Upset plot demonstrating unique signaling outputs of mutations in the BBz-CAR CD19-K562 screen. **(d)** Bar graph indicating percent AP-1 signaling in BBz-CAR cells upon CD19-K562 stimulation of select mutations. Each point represents an experimental replicate, mean + s.e.m. depicted. **(e)** IL-2 and PD-1 fold change in BBz-CAR CD19-K562 screen. Select constructs are labeled. Fold change represents mean of two independent experimental replicates as compared to mCherry controls. **(f)** Volcano plot indicating enrichment or depletion in vivo for each construct as determined by MAGeCK. Positive $\log_2$ fold change indicates increased persistence in tumors compared to input.

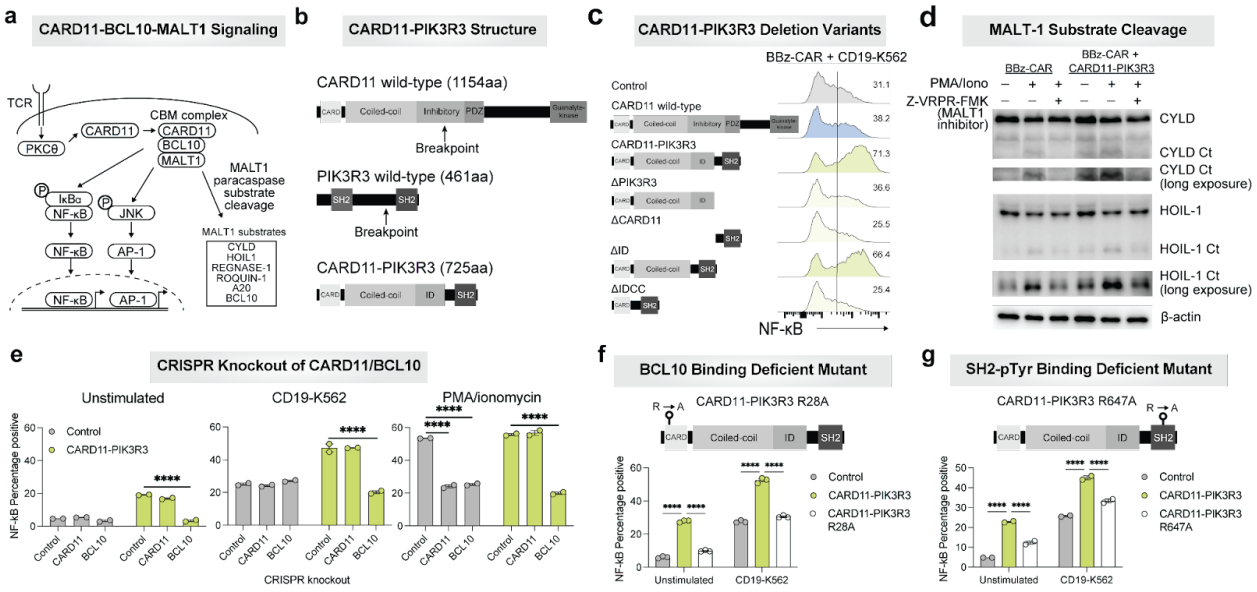

Figure 2.2 CARD11-PIK3R3 enhances CARD11-BCL10-MALT1 complex signaling

(a) Schematic indicating CARD11-BCL10-MALT1 (CBM) signaling in normal T cells. **(b)** Diagram of the structure and domains of wild-type CARD11, wild-type PIK3R3, and CARD11-PIK3R3. **(c)** NF-κB reporter activity of BBz-CAR CARD11-PIK3R3 variant Jurkat cells co-cultured with K562-CD19 cells. Data representative of two independent experiments. **(d)** Western blotting of MALT1 substrates in control or CARD11-PIK3R3 expressing BBz-CAR Jurkat cells. PMA/Iono indicates phorbol myristate acetate/ionomycin treatment. Ct indicates the C-terminal cleavage product. Data representative of 2 independent experiments. **(e)** NF-κB reporter activity of control, CARD11, or BCL10 CRISPR knockout BBz-CAR Jurkat cells. Each point represents an experimental replicate, mean + s.e.m. depicted. **(f-g)** Diagram and BBz-CAR Jurkat reporter activity of BCL10 binding-deficient and phospho-tyrosine (pTyr) binding-deficient CARD11-PIK3R3 mutants, respectively. Each data point indicates an experimental replicate, mean + s.e.m. depicted. **** indicates P value < 0.0001, one-way ANOVA followed by Tukey's multiple comparison test.

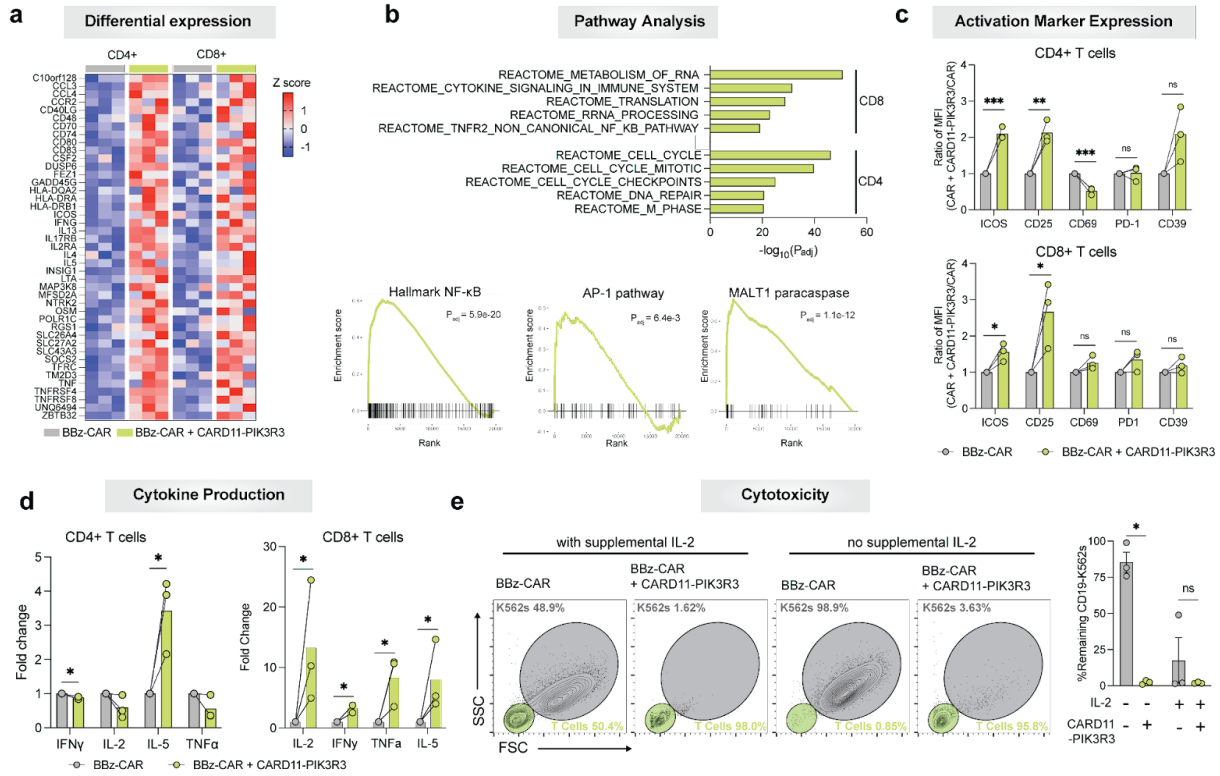

Figure 2.3 CARD11-PIK3R3 expression leads to signaling, transcriptional, and functional enhancements in primary human CD8+ T cells.

(a) Heatmap of significantly upregulated genes in CARD11-PIK3R3 compared to control BBz-CAR T cells after stimulation with CD19 antigen shared among both CD4+ and CD8+ T cells, each column indicates an independent donor. **(b)** Top 5 Reactome pathways enriched in CD4+ and CD8+ T cells (top) and NF-kB, AP-1, and MALT1 gene signature enrichment in CARD11-PIK3R3 expressing CD8+ BBz-CAR T cells after stimulation (bottom). **(c)** Activation markers expressed on transduced CD4 and CD8 T cells 24 hours post 1:1 co-culture with CD19-K562s. Ratio of MFI in CARD11-PIK3R3 relative to control shown. Each data point indicates an independent donor, mean + s.e.m. depicted. P values determined by unpaired T test. **(d)** Cytokine secretion of transduced CD4+ and CD8+ T cells 48 hours post 1:1 co-culture with CD19-K562s, represented as fold change relative to control. Each data point indicates an independent donor[JD1] . P values determined by ratio paired T test. **(e)** Flow cytometry plots depicting CD8+ T cell and CD19-K562 populations after 14-day co-culture with and without supplemental IL-2. Bar graph summarizing population percentages from three independent donors, mean + s.e.m. depicted. P values determined by paired T test. * indicates P value < 0.05, ** indicates P value < 0.01, *** indicates P values < 0.001, **** indicates P value < 0.0001.

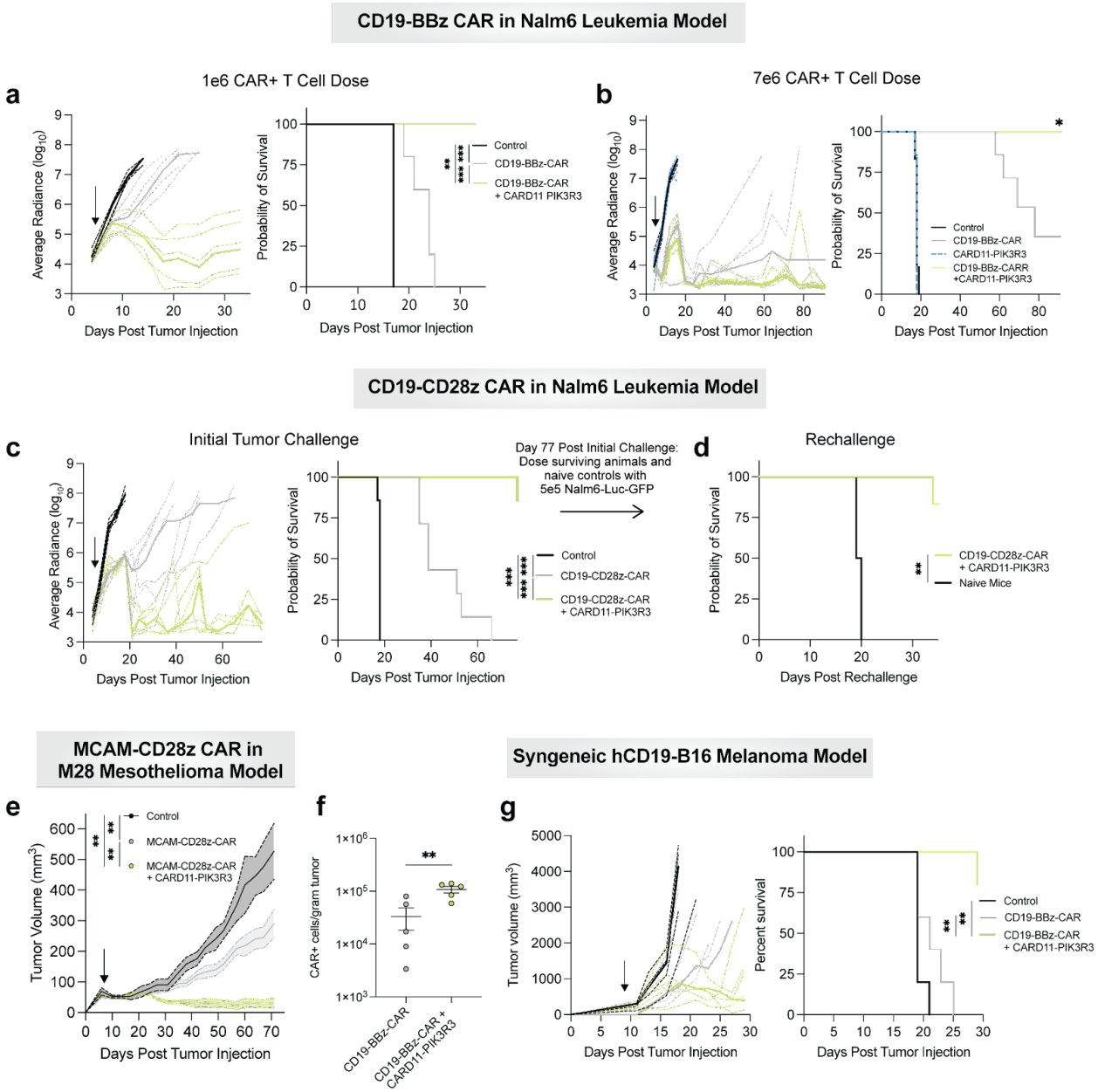

Figure 2.4 CARD11-PIK3R3 improves the therapeutic efficacy of human and mouse CAR T cells *in vivo*.

(a-c) Radiance (right panels) and survival analysis (left panels) of Nalm6-Luc-GFP tumor bearing animals. Radiance measured via IVIS and used as a proxy for tumor burden. Animals treated with T cells 5 days post Nalm6 tumor engraftment. **(a)** Control (n=5), CD19-BBz-CAR (n=6), CD19-BBz-CAR + CARD11-PIK3R3 (n=5) T cells dosed at 1e6 CAR+ T cells. **(b)** Control (n=6), CD19-BBz-CAR (n=7), CD19-BBz-CAR + CARD11-PIK3R3 (n=7) dosed at 7e6 CAR+ T cells. CARD11-PIK3R3 T cell (n=7) dose was equivalent to the total number of CARD11-PIK3R3 expressing T cells dosed in the CD19-BBz-CAR + CARD11-PIK3R3 group. (Figure legend continued on the next page.)

(Figure legend continued from the previous page.) **(c)** Control (n=7), CD19-CD28z-CAR (n=7), CD19-CD28z-CAR + CARD11-PIK3R3 (n=7) T cells dosed at 4e5 CAR+ T cells. **(d)** Survival analysis of part (c) surviving CD19-CD28z-CAR + CARD11-PIK3R3 (n=6) animals or naïve mice (n=4) rechallenged with 5e5 Nalm6-Luc-GFP tumors on day 77 post initial tumor injection. **(e)** Tumor volumes of M28 tumor bearing animals treated with control (n=5), MCAM-CD28z-CAR (n=5), or MCAM-CD28z-CAR + CARD11-PIK3R3 (n=5). T cells dosed at 5e5 CAR+ cells. **(f)** Accumulation of CD19-BBz-CAR T cells in hCD19-B16 tumor 5 days post adoptive cell transfer. Each data point indicates individual mouse, mean + s.e.m. depicted. P values determined using unpaired t test. **(g)** Tumor volume (right panel) and survival analysis (left panel) of hCD19-B16 tumor bearing animals treated with control (n=5), CD19-BBz-CAR (n=5) or CD19-BBz-CAR +CARD11-PIK3R3 (n=5) OT-1 T cells. T cells dosed at 4e6 CAR+ cells. Arrow indicates date of T cell injection. Dotted lines indicate individual mice, bold line indicates median. P values determined by one-way ANOVA followed by Tukey's multiple comparisons test (tumor volume) or Log-rank Mantel-Cox (survival). * indicates P value < 0.05, ** indicates P value <0.01, *** indicates P values < 0.001.

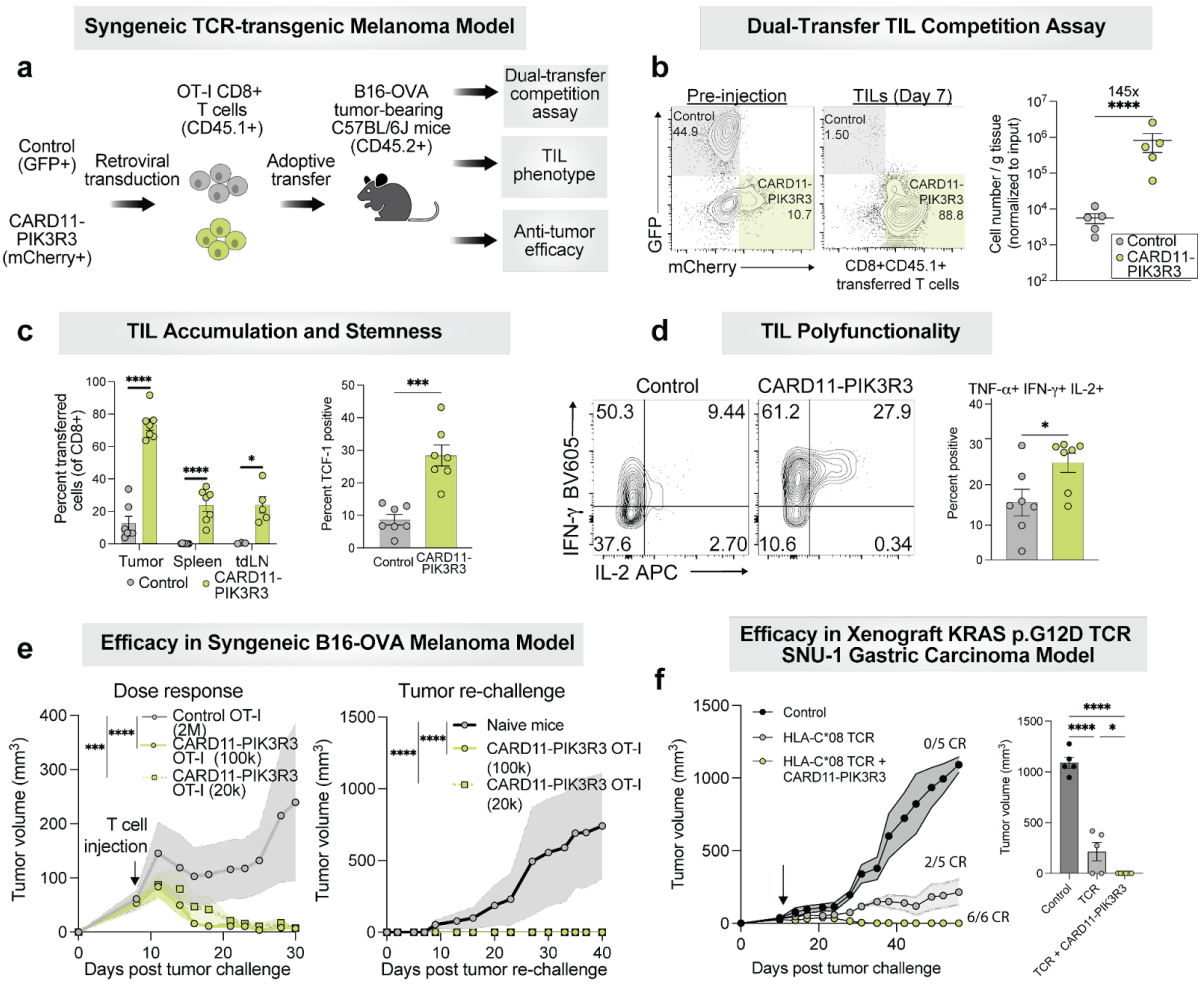

Figure 2.5 CARD11-PIK3R3 enhances the therapeutic efficacy of mouse and human TCR-transgenic T cells *in vivo*.

(a) Diagram of *in vivo* syngeneic melanoma model. **(b)** Accumulation of TILs in the dual-transfer competition assay 7 days post T cell transfer. Each data point indicates individual mouse, mean + s.e.m. depicted. P values determined by ratio paired T test. **(c)** Cell accumulation in control OT-I and CARD11-PIK3R3 OT-I treated mice, TCF-1 expression in tumor infiltrating OT-I cells. Each data point indicates individual mouse, mean + s.e.m. depicted. P values determined by unpaired T test. **(d)** Ex vivo cytokine production with PMA/Ionomycin stimulation of control OT-I or CARD11-PIK3R3 OT-I TILs 7 days post T cell transfer. Each data point indicates individual mouse, mean + s.e.m. depicted. P values determined by unpaired T test. **(e)** Tumor size of B16-OVA melanoma bearing mice treated with OT-1 CARD11-PIK3R3 T cells at 100,000 (n=4) or 20,000 (n=5) T cell dose as compared to 2 x 10^6 control OT-1 T cells (n=5) (left) and mice with cleared tumors from the dose response experiment rechallenged with B16-OVA melanoma tumors subcutaneously on the contralateral flank (right). P values determined by one-way ANOVA followed by Tukey's multiple comparisons test. (Figure legend continued on the next page.)

(Figure legend continued from the previous page.) **(f)** Tumor size of SNU-1 HLA-C*08:02 gastric cancer xenograft bearing mice treated with control (n=5), KRAS p.G12D-specific TCR T cells (n=5), or KRAS p.G12D-specific TCR CARD11-PIK3R3 T cells (n=6), mean + s.e.m. depicted. Complete response (CR) was defined as an absence of a detectable tumor. * indicates P value < 0.05, *** indicates P values < 0.001, **** indicates P value < 0.0001.

2.11. Extended Data Figures

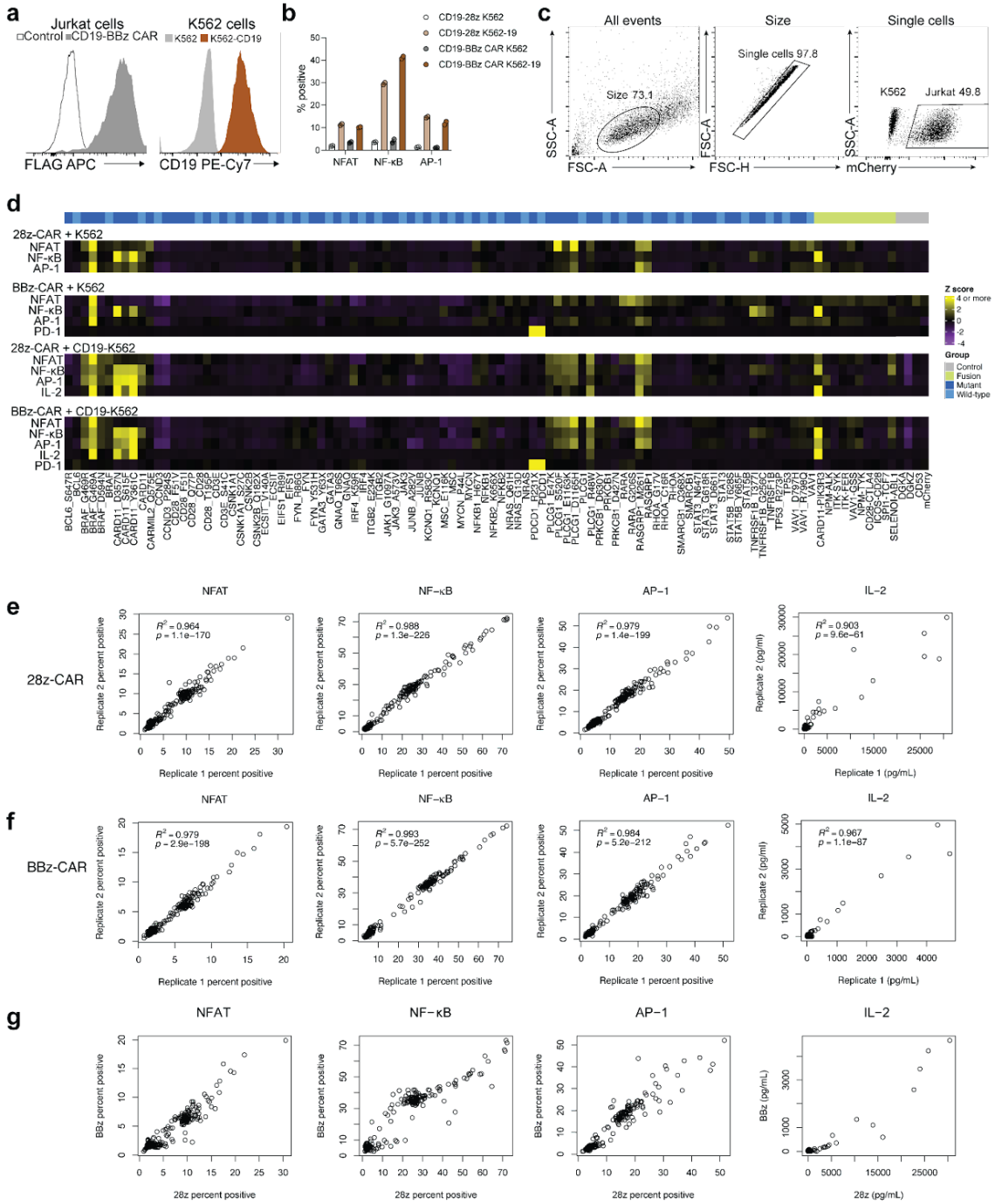

Extended Data Figure 2.1 *In vitro* screening of 28z-CAR and BBz-CAR triple reporter Jurkat cells.

(a) CAR and CD19 expression in cell lines utilized for screening. **(b)** Percent positive for the indicated reporter construct in 28z-CAR or BBZ-CAR transduced Jurkat cells co-cultured with the indicated cell line. **(c)** Gating strategy to identify library construct transduced Jurkat cells in co-culture. **(d)** Heatmaps depicting Z scores *in vitro* screens. Z scores represent mean of two experimental replicates. Z scores are calculated on a row-by-row basis and thus represent different percentage positive values across different experimental conditions, such as with or without CD19 antigen. **(e)** Reproducibility of screening in 28z-CAR Jurkat cells. **(f)** Reproducibility of screening in BBz-CAR Jurkat cells. Each replicate indicates an independent lentiviral transduction of Jurkat cells with T cell lymphoma mutation screening constructs. **(g)** Scatterplot indicating CD19-28z CAR (x-axis) and CD19-BBz CAR (y-axis) percent positive for reporter constructs and IL-2 production.

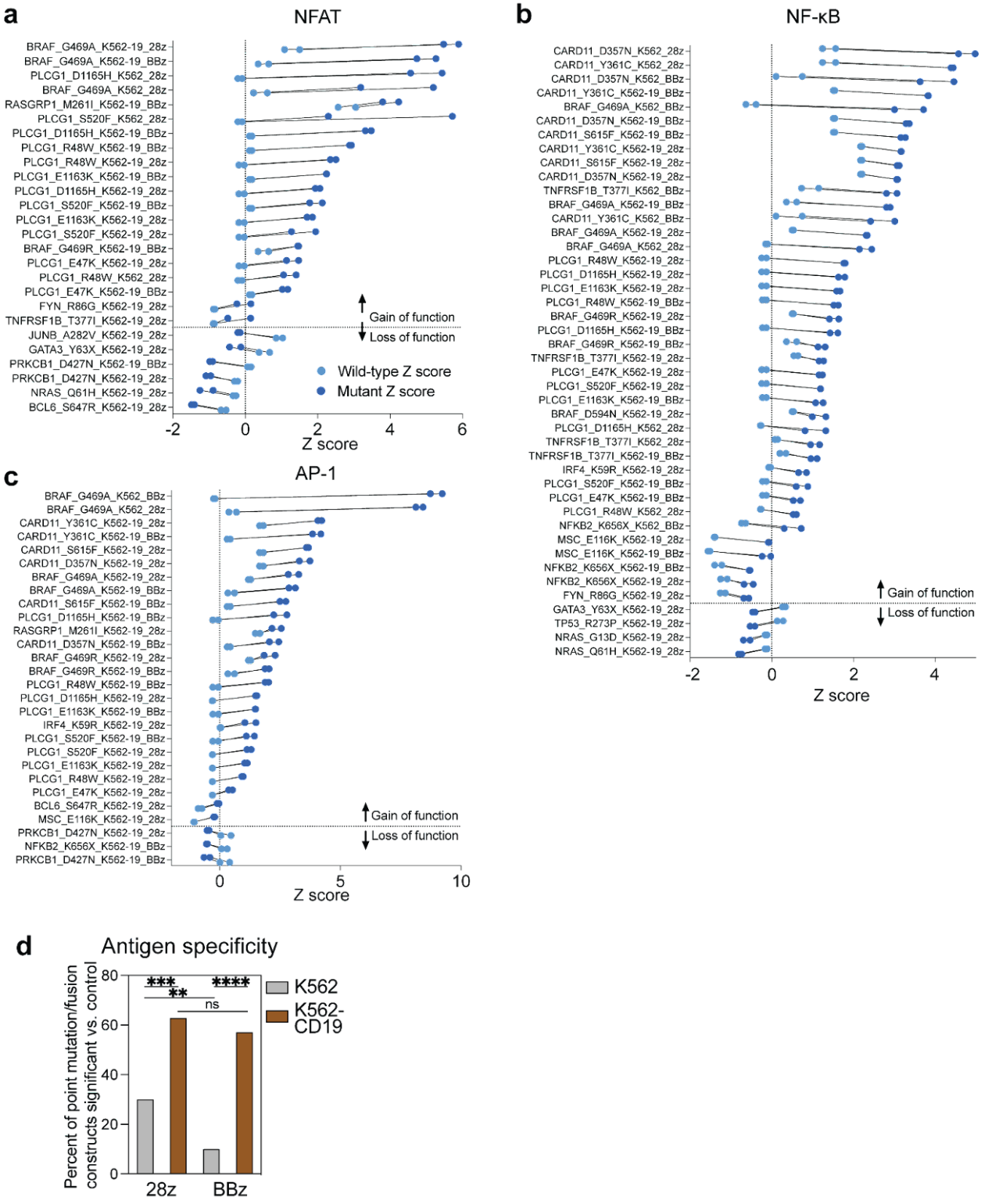
a
NFAT
BRAF_G469A_K562-19_28z
BRAF_G469A_K562-19_BBz
PLCG1_D1165H_K562_28z
BRAF_G469A_K562_28z
RASGRP1_M261I_K562-19_BBz
PLCG1_S520F_K562_28z
PLCG1_D1165H_K562-19_BBz
PLCG1_R48W_K562-19_BBz
PLCG1_R48W_K562-19_28z
PLCG1_E1163K_K562-19_BBz
PLCG1_D1165H_K562-19_28z
PLCG1_S520F_K562-19_BBz
PLCG1_E1163K_K562-19_28z
PLCG1_S520F_K562-19_28z
BRAF_G469R_K562-19_BBz
PLCG1_E47K_K562-19_28z
PLCG1_R48W_K562_28z
PLCG1_E47K_K562-19_BBz
FYN_R86G_K562-19_28z
TNFRSF1B_T377I_K562-19_28z
JUNB_A282V_K562-19_28z
GATA3_Y63X_K562-19_28z
PRKCB1_D427N_K562-19_BBz
PRKCB1_D427N_K562-19_28z
NRAS_Q61H_K562-19_28z
BCL6_S647R_K562-19_28z
Gain of function
Loss of function
Wild-type Z score
Mutant Z score
-2
0
2
4
6
Z score
b
NF-κB
CARD11_D357N_K562_28z
CARD11_Y361C_K562_28z
CARD11_D357N_K562_BBz
CARD11_Y361C_K562-19_BBz
BRAF_G469A_K562_BBz
CARD11_D357N_K562-19_BBz
CARD11_S615F_K562-19_BBz
CARD11_Y361C_K562-19_28z
CARD11_S615F_K562-19_28z
CARD11_D357N_K562-19_28z
TNFRSF1B_T377I_K562_BBz
BRAF_G469A_K562-19_BBz
CARD11_Y361C_K562_BBz
BRAF_G469A_K562-19_28z
BRAF_G469A_K562_28z
PLCG1_R48W_K562-19_28z
PLCG1_D1165H_K562-19_28z
PLCG1_E1163K_K562-19_28z
PLCG1_R48W_K562-19_BBz
BRAF_G469R_K562-19_28z
PLCG1_D1165H_K562-19_BBz
BRAF_G469R_K562-19_BBz
TNFRSF1B_T377I_K562-19_28z
PLCG1_E47K_K562-19_28z
PLCG1_S520F_K562-19_28z
PLCG1_E1163K_K562-19_BBz
BRAF_D594N_K562-19_28z
PLCG1_D1165H_K562_28z
TNFRSF1B_T377I_K562_28z
TNFRSF1B_T377I_K562-19_BBz
IRF4_K59R_K562-19_28z
PLCG1_S520F_K562-19_BBz
PLCG1_E47K_K562-19_BBz
PLCG1_R48W_K562_28z
NFKB2_K656X_K562_BBz
MSC_E116K_K562-19_28z
MSC_E116K_K562-19_BBz
NFKB2_K656X_K562-19_BBz
NFKB2_K656X_K562-19_28z
FYN_R86G_K562-19_28z
GATA3_Y63X_K562-19_28z
TP53_R273P_K562-19_28z
NRAS_G13D_K562-19_28z
NRAS_Q61H_K562-19_28z
Gain of function
Loss of function
-2
0
2
4
Z score
c
AP-1
BRAF_G469A_K562_BBz
BRAF_G469A_K562_28z
CARD11_Y361C_K562-19_28z
CARD11_Y361C_K562-19_BBz
CARD11_S615F_K562-19_28z
CARD11_D357N_K562-19_28z
BRAF_G469A_K562-19_28z
BRAF_G469A_K562-19_BBz
CARD11_S615F_K562-19_BBz
PLCG1_D1165H_K562-19_BBz
RASGRP1_M261I_K562-19_28z
CARD11_D357N_K562-19_BBz
BRAF_G469R_K562-19_28z
BRAF_G469R_K562-19_BBz
PLCG1_R48W_K562-19_BBz
PLCG1_D1165H_K562-19_28z
PLCG1_E1163K_K562-19_BBz
IRF4_K59R_K562-19_28z
PLCG1_S520F_K562-19_BBz
PLCG1_S520F_K562-19_28z
PLCG1_E1163K_K562-19_28z
PLCG1_R48W_K562-19_28z
PLCG1_E47K_K562-19_28z
BCL6_S647R_K562-19_28z
MSC_E116K_K562-19_28z
PRKCB1_D427N_K562-19_28z
NFKB2_K656X_K562-19_BBz
PRKCB1_D427N_K562-19_BBz
Gain of function
Loss of function
0
5
10
Z score
d
Antigen specificity
Percent of point mutation/fusion constructs significant vs. control
80
60
40
20
0
***
**
****
ns
K562
K562-CD19
28z
BBz

Extended Data Figure 2.2 Point mutations with statistically significant differences compared to wild-type constructs and antigen specificity of mutations.

(a-c) NFAT, NF-κB, and AP-1 reporter activity. Mutations with a statistically significant difference from the wild-type construct are shown. Each row indicates the mutation construct, co-culture condition and CAR construct. Gain of function indicates mutations which increased reporter activity relative to wild-type, while loss of function refers to mutations with lower reporter activity than the wild-type counterpart. Each dot indicates one biological replicate. **(d)** Percent of constructs with significant effects in the indicated CAR and co-culture condition. ** indicates P value < 0.01, *** indicates P < 0.001, **** indicates P < 0.0001, Chi-squared test.

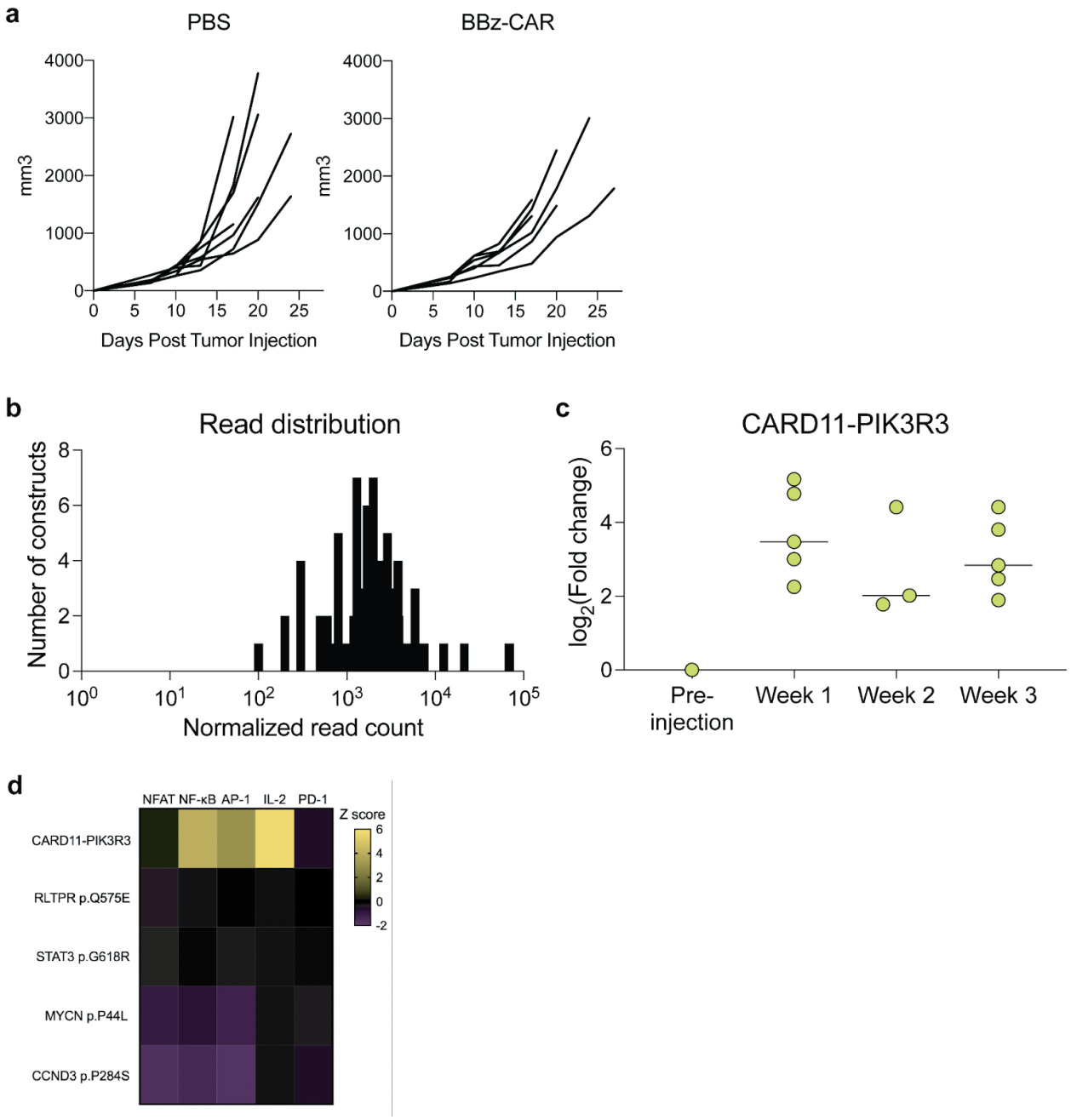

Extended Data Figure 2.3 Pooled human CAR T cell *in vivo* persistence screening of T cell lymphoma mutation library.

(a) Tumor growth curve for mice bearing CD19-K562 subcutaneous tumors treated with vehicle (PBS, control) or 1 x 106 CAR+ T cells. **(b)** Histogram of normalized read count distribution of pre-injection constructs. Constructs with a pre-injection normalized read count of $<10^2$ were excluded from analysis. (Figure legend continued on the next page.)

(Figure legend continued from the previous page.)**(c)** Log_2 fold change of CARD11-PIK3R3 normalized reads at each indicated time point in the pooled *in vivo* experiment. **(d)** *In vitro* screen Z scores of mutation constructs identified as positive hits from *in vivo* screening. Z score represents the mean Z score of two experimental replicates.

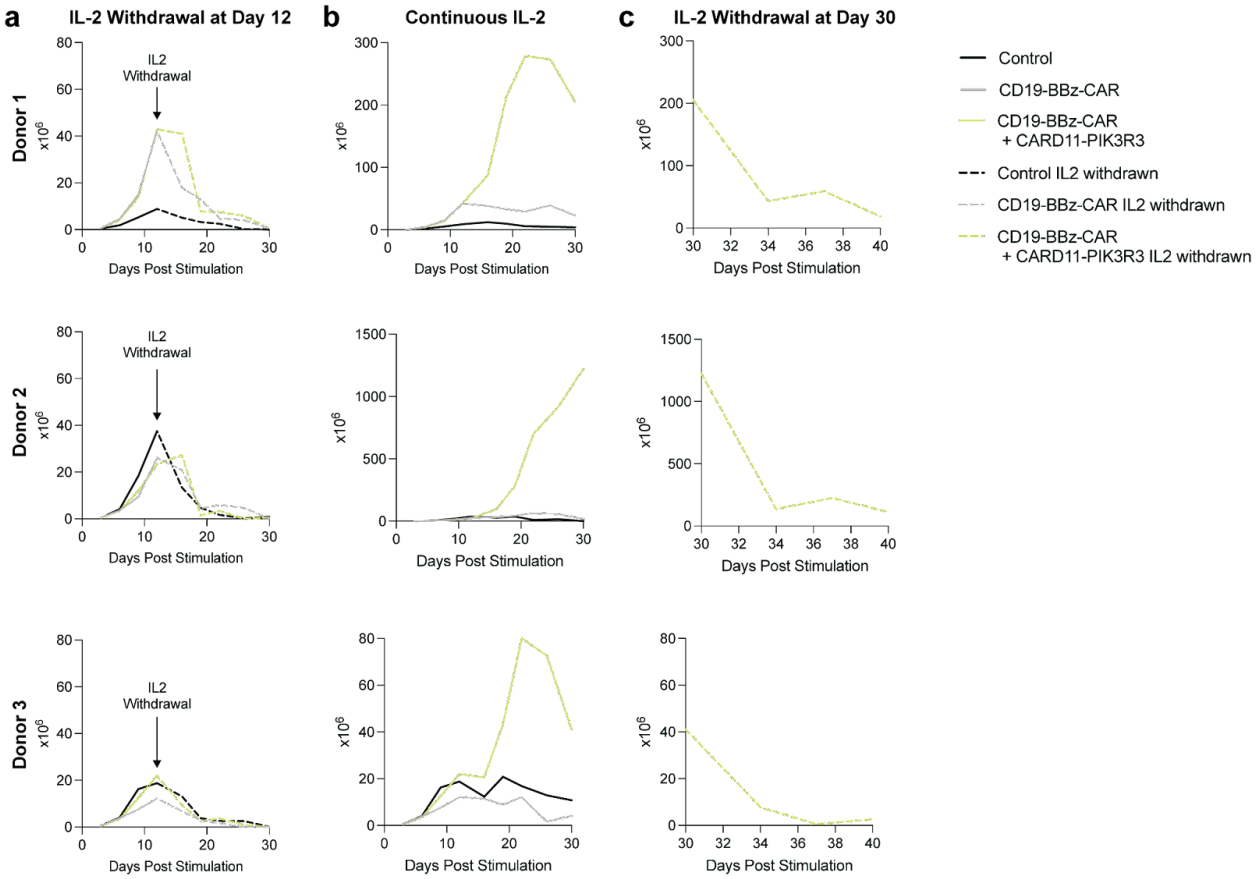

Extended Data Figure 2.4 *In vitro* Expansion of CD19-BBz-CAR T cells with and without CARD11-PIK3R3

(a,b) CAR or CAR + CARD11-PIK3R3 were sorted for purity, then expanded with IL-2 for 12 days. On Day 12, cultures were split, reseeding each group without IL-2 **(a)** and with IL-2 **(b)**. Cells were counted and split from day 12 to day 30. **(c)** On Day 30, CD19-BBz-CAR + CARD11-PIK3R3 T cells that were cultured with IL-2 were reseeded without IL-2 and counted and split for an additional 10 days.

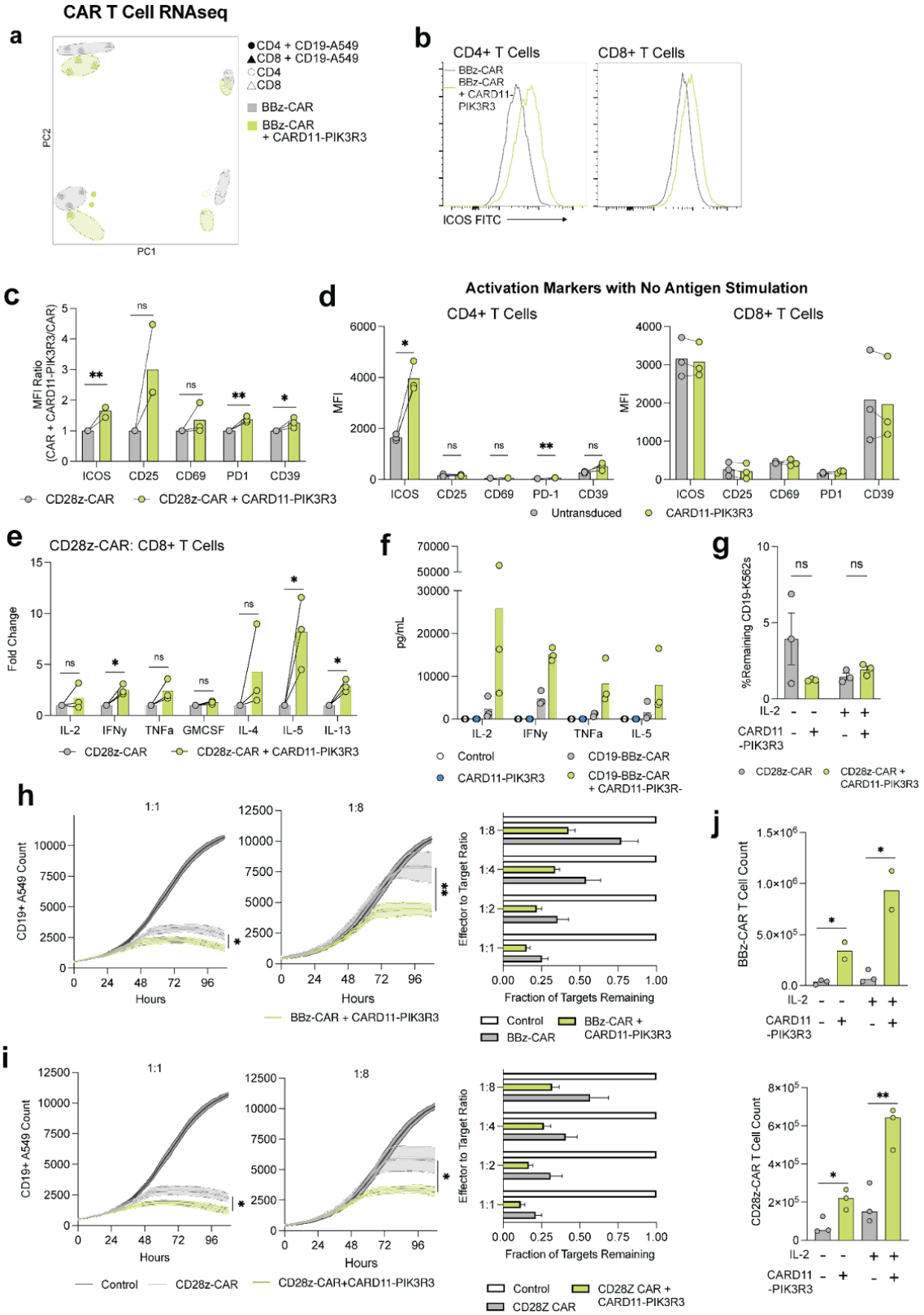
CAR T Cell RNAseq
a
●CD4 + CD19-A549
▲CD8 + CD19-A549
○CD4
△CD8
BBz-CAR
BBz-CAR + CARD11-PIK3R3
PC1
PC2
b
CD4+ T Cells
CD8+ T Cells
BBz-CAR
BBz-CAR + CARD11-PIK3R3
ICOS FITC
c
MFI Ratio (CAR + CARD11-PIK3R3/CAR)
ICOS
CD25
CD69
PD1
CD39
CD28z-CAR
CD28z-CAR + CARD11-PIK3R3
d
Activation Markers with No Antigen Stimulation
CD4+ T Cells
CD8+ T Cells
MFI
PD-1
Untransduced
CARD11-PIK3R3
e
CD28z-CAR: CD8+ T Cells
Fold Change
IL-2
IFNy
TNFa
GMCSF
IL-4
IL-5
IL-13
f
pg/mL
Control
CD19-BBz-CAR
CARD11-PIK3R3
CD19-BBz-CAR + CARD11-PIK3R-
g
%Remaining CD19-K562s
IL-2
CARD11 -PIK3R3
h
1:1
1:8
CD19+ A549 Count
Hours
BBz-CAR + CARD11-PIK3R3
Effector to Target Ratio
Fraction of Targets Remaining
BBz-CAR
BBz-CAR + CARD11-PIK3R3
i
CD28z-CAR
CD28z-CAR+CARD11-PIK3R3
CD28Z CAR
CD28Z CAR + CARD11-PIK3R3
j
BBz-CAR T Cell Count
CD28z-CAR T Cell Count

Extended Data Figure 2.5 *In vitro* analysis of CARD11-PIK3R3 expressing T cells.

(a) Principal component analysis of transcriptomes of human BBz-CAR T cells, three independent donors depicted. **(b)** Representative histogram of ICOS expression on CD19-BBz-CAR T cells 24 hours after co-culture with CD19-K562s. **(c)** Activation markers expressed on CD8+ CD19-28z-CAR T cells after 24 hours co-cultured with CD19-K562s. Ratio of MFI (CAR + CARD11-PIK3R3/CAR) shown. P values determined by unpaired T test. **(d)** Activation markers expressed on untransduced and CARD11-PIK3R3 CD4+ and CD8+ T cells after 24 hours co-cultured with CD19-K562s. **(e)** Cytokine secretion of CD8+ CD19-CD28z-CAR T cells 48 hours post 1:1 co-culture with CD19-K562s. **(f)** Cytokine secretion of control, CARD11-PIK3R3, CD19-BBz-CAR and CD19-BBz-CAR + CARD11-PIK3R3 CD8+ T cells 48 hours post 1:1 co-culture with CD19-K562s. Select graphs represented as fold change between comparisons. P values determined by ratio paired T test. **(g)** Bar graph summarizing CD19-K562 population percentages after 14-day co-culture of CD19-CD28z-CAR T cells with and without CARD11-PIK3R3, and supplemental IL-2. P values determined by paired T test. **(h-i)** Cell counts of CD19-A549 mKate2+ targets co-cultured with CD8+ **(h)** CD19-BBz-CAR T cells or **(i)** CD19-CD28z-CAR T cells over 108 hour period. Bar graph indicates target cell counts at hour 108, standardized to control. **(j)** Cell counts of CD8+ CD19-BBz-CAR T cells or CD19-CD28z-CAR T cells on Day 13 after two stimulations with CD19-K562 targets. P values determined by unpaired T test. P values calculated by 1-way ANOVA followed by Tukey's multiple comparison test, performed on cell count at 108 hours. Each data point indicates an independent donor, mean + s.e.m. depicted. * indicates P value < 0.05, ** indicates P value < 0.01.

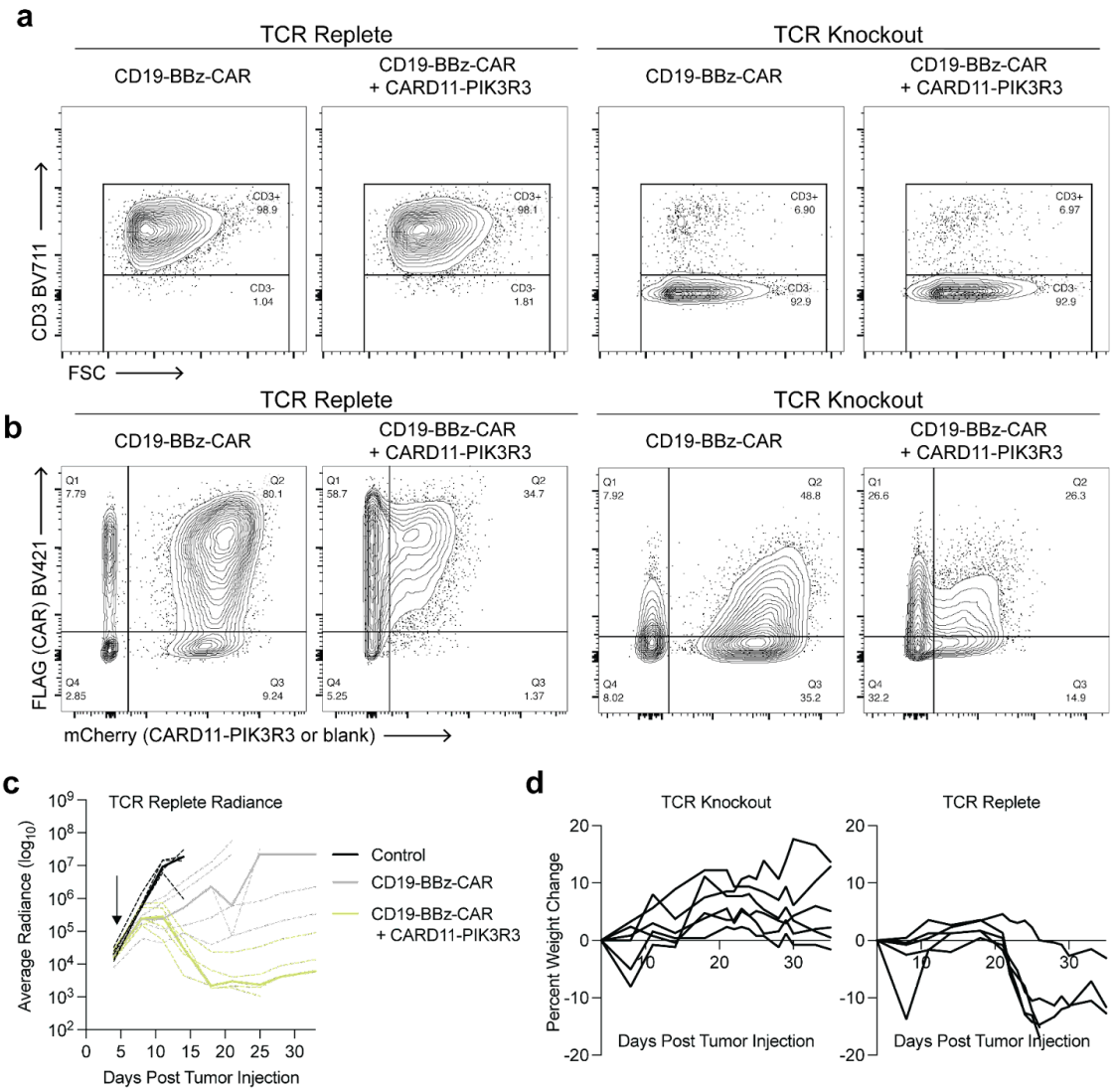

Extended Data Figure 2.6 Weight loss of CD19-BBz-CAR + CARD11-PIK3R3 treated animals ameliorated with TCR Knockout

(a) Flow cytometry plots indicating CD3 expression of TCR replete or TCR knockout groups after electroporation with TRAC targeted RNPs. **(b)** Flow cytometry plots indicating CAR (FLAG) and CARD11-PIK3R3 or control blank construct (mCherry) expression in human CD3 T cells. **(c)** Radiance of Nalm6-Luc-GFP tumor bearing animals treated with Control (n=5), CD19-BBz-CAR (n=5), CD19-BBz-CAR + CARD11-PIK3R3 (n=5) TCR replete T cells dosed at 1e6 CAR+ T cells, control cells dosed equivalent to highest total T cell dose in other treatment groups. Dotted lines indicate individual mice, bold line indicates median. Arrow indicates date T cells were injected. **(d)** Percent weight change from baseline of TCR Knockout or TCR replete CD19-BBz-CAR + CARD11-PIK3R3 treated Nalm6 bearing animals.

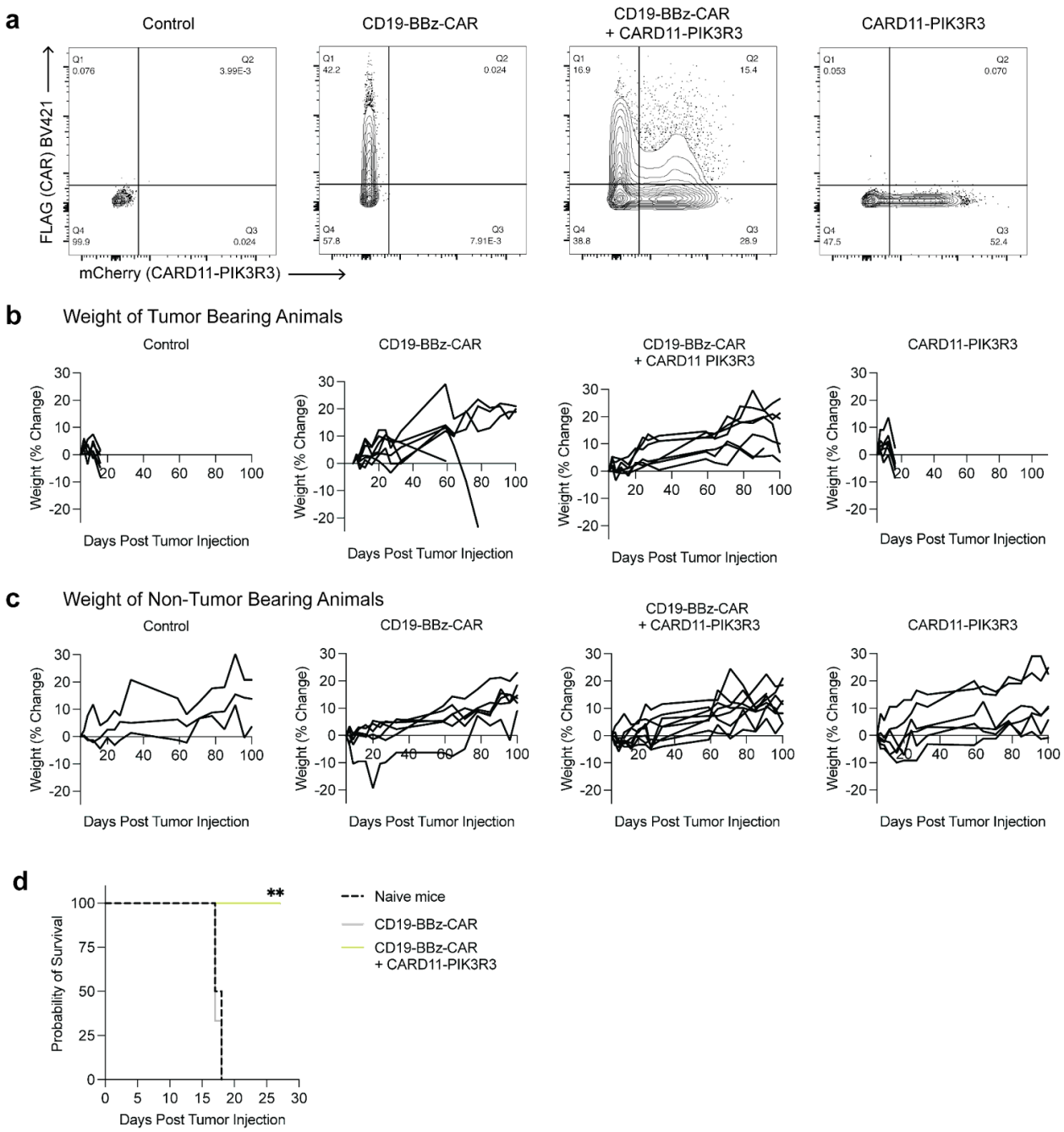

Extended Data Figure 2.7 CD19-BBz-CAR + CARD11-PIK3R3 is well tolerated and effective at high doses

(a) Flow cytometry plots indicating CAR (FLAG) and CARD11-PIK3R3 (mCherry) expression in human CD3 T cells. **(b-c)** Percent weight change from baseline of (b) tumor bearing or **(c)** non-tumor bearing animals treated with control, CD19-BBz-CAR, CD19-BBz-CAR+CARD11-PIK3R3 or CARD11-PIK3R3 (Figure legend continued on the next page.)

(Figure legend continued from the previous page.) **(d)** Survival analysis of Fig 4b surviving CD19-BBz-CAR (n=3), CD19-BBz-CAR + CARD11-PIK3R3 (n=4) animals or naïve mice (n=4) rechallenged with 5e5 Nalm6-Luc-GFP tumors. P values determined by Log-rank Mantel-Cox. ** indicates P value < 0.01.

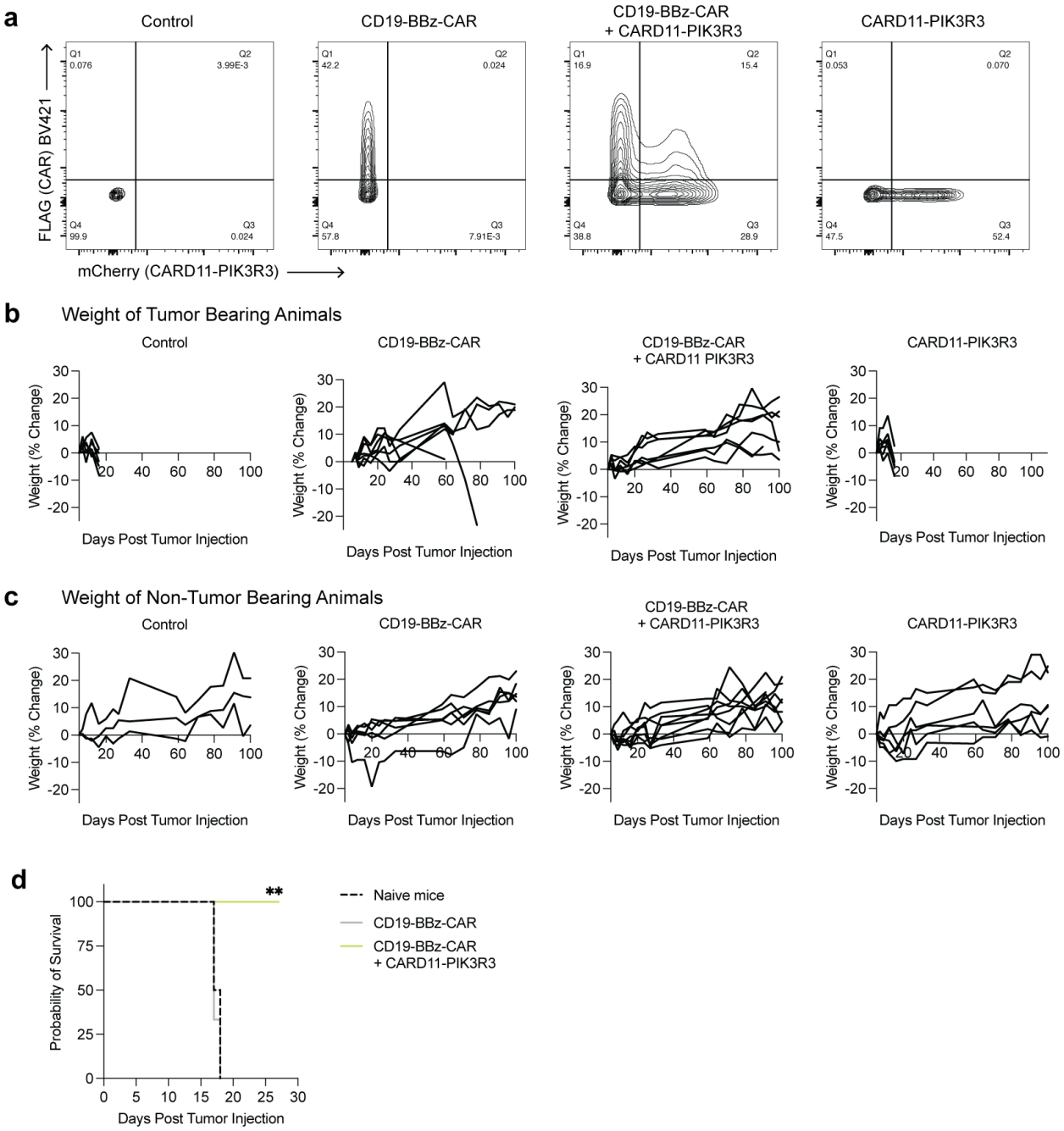

Extended Data Figure 2.8 *In vivo* analysis of CARD11-PIK3R3 expressing CAR T cells

(a,c) Flow cytometry plots indicating FLAG (CAR) and mCherry (CARD11-PIK3R3) expression in human CD3 T cells. **(b)** Percent weight change from baseline of control, CD19-CD28z-CAR or BBz-CAR + CARD11-PIK3R3 treated Nalm6 tumor bearing animals. **(d)** Percent weight change from baseline of control, MCAM-CD28z-CAR or MCAM-CD28z-CAR + CARD11-PIK3R3 treated M28 tumor bearing animals. **(e)** Flow cytometry plots indicating GFP (CAR) and CARD11-PIK3R3 (mCherry) expression in mouse OT-I T cells. (Figure legend continued on the next page.)

(Figure legend continued from the previous page.) **(f)** Percent weight change from baseline of control, CD19-BBz-CAR or CD19-BBz-CAR + CARD11-PIK3R3 treated hCD19-B16 tumor bearing animals. **(g)** Accumulation of CD19-BBz-CAR T cells in spleen of hCD19-B16 tumor bearing animals 5 days post adoptive cell transfer. Each data point indicates one mouse, mean + s.e.m. depicted. P values determined using unpaired t test. **(h)** Histograms indicating human CD19 ligand expression on hCD19-B16 tumors, CD19-BBz-CAR or CD19-BBz-CAR+CARD11-PIK3R3 treated with that had reach euthanasia endpoint, compared to known CD19 positive B16 tumor sample. * indicates P value < 0.05.

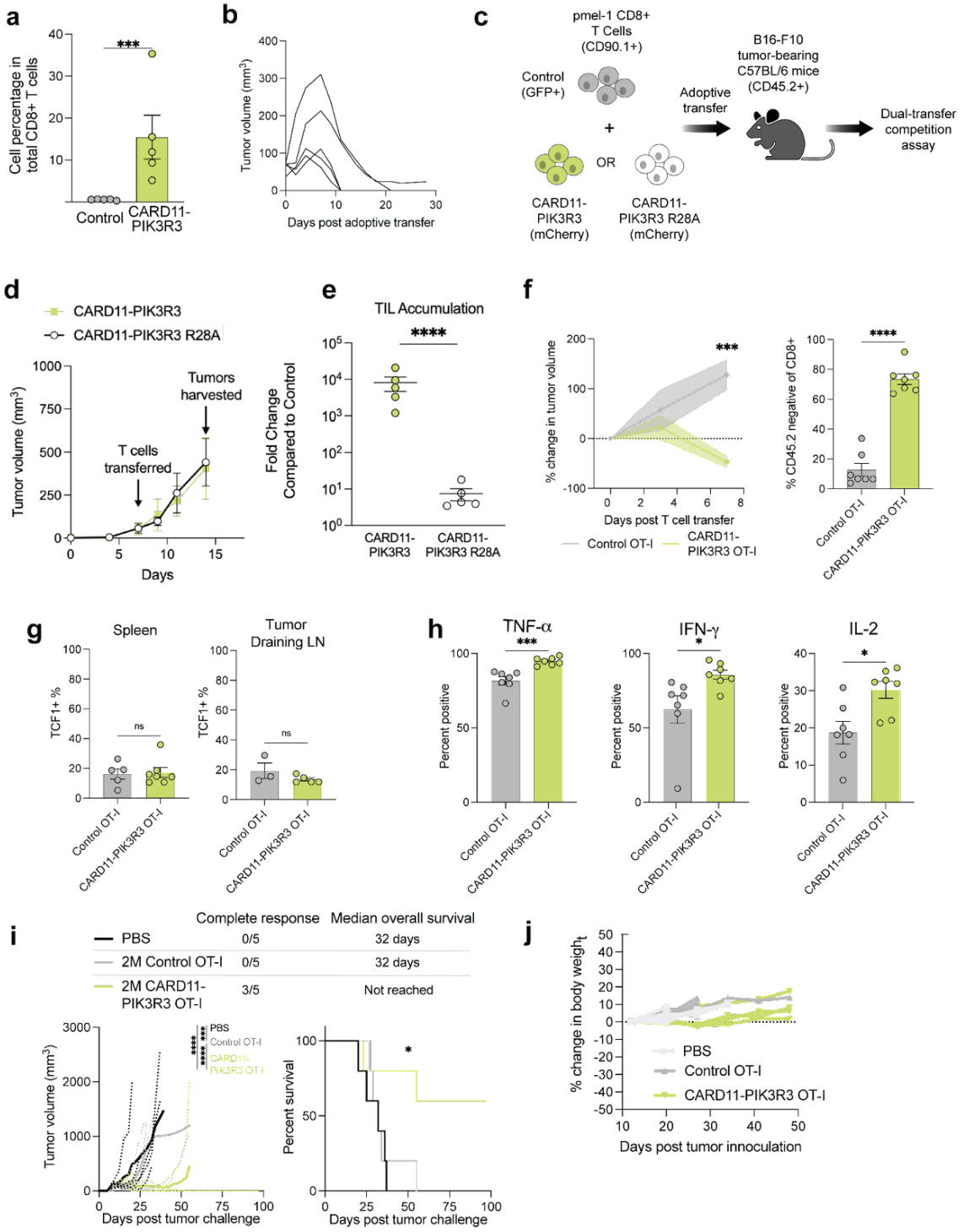

Extended Data Figure 2.9 *In vivo* analysis of CARD11-PIK3R3 expressing OT-I T cells.

(a) Cell percentage in total CD8+ T cells of control or CARD11-PIK3R3 OT-I T cells in dual transfer experiment. **(b)** Tumor growth curve for mice bearing B16-OVA tumors treated with 1 x 10^6 OT-I T cells (10% CARD11-PIK3R3 positive). (Figure legend continued on the next page.)

(Figure legend continued from the previous page.) **(c)** Schematic of competition experiments with CARD11-PIK3R3 and CARD11-PIK3R3 R28A pmel-1 CD8 T cells in B16-F10 tumor model. **(d)** Tumor growth curves of mice described in (c). **(e)** Fold-enrichment in the tumor of wild-type CARD11-PIK3R3 or CARD11-PIK3R3 (p.R28A) expressing pmel-1 CD8 T cells compared to vector control 7 days after adoptive transfer. Mean + s.e.m. depicted. All P values determined by ratio paired T test. **(f)** Percent change in tumor volume and proportion of transferred cells in control OT-I (n=8) and CARD11-PIK3R3 OT-I (n=9) mice bearing B16-OVA subcutaneous tumors. Each data point indicates one mouse, mean + s.e.m. depicted. **(g)** Frequency of TCF-1+ OT-I cells in spleen and tumor draining lymph node (LN) of mice bearing B16-OVA subcutaneous tumors. **(h)** Ex vivo cytokine production with PMA/Ionomycin stimulation of control OT-I or CARD11-PIK3R3 OT-I TILs 7 days post T cell transfer. P values determined by unpaired T test. **(i)** Tumor volume and survival analysis in B16-OVA melanoma bearing mice treated with PBS (n=5), control OT-I cells (2×10^6) (n=5), or CARD11-PIK3R3 OT-I cells (2×10^6) (n=5) day 12 after tumor inoculation. Complete response was defined as an absence of a detectable tumor. P values determined by one-way ANOVA followed by Tukey's multiple comparisons test (tumor volume) or Log-rank Mantel-Cox (survival). **(j)** Percent change in body weight in PBS, control OT-I, or CARD11-PIK3R3 OT-I treated, B16-OVA tumor bearing mice. Each data point indicates one mouse, mean + s.e.m. depicted. ns indicates not significant, *** indicates P values < 0.001, **** indicates P value < 0.0001.

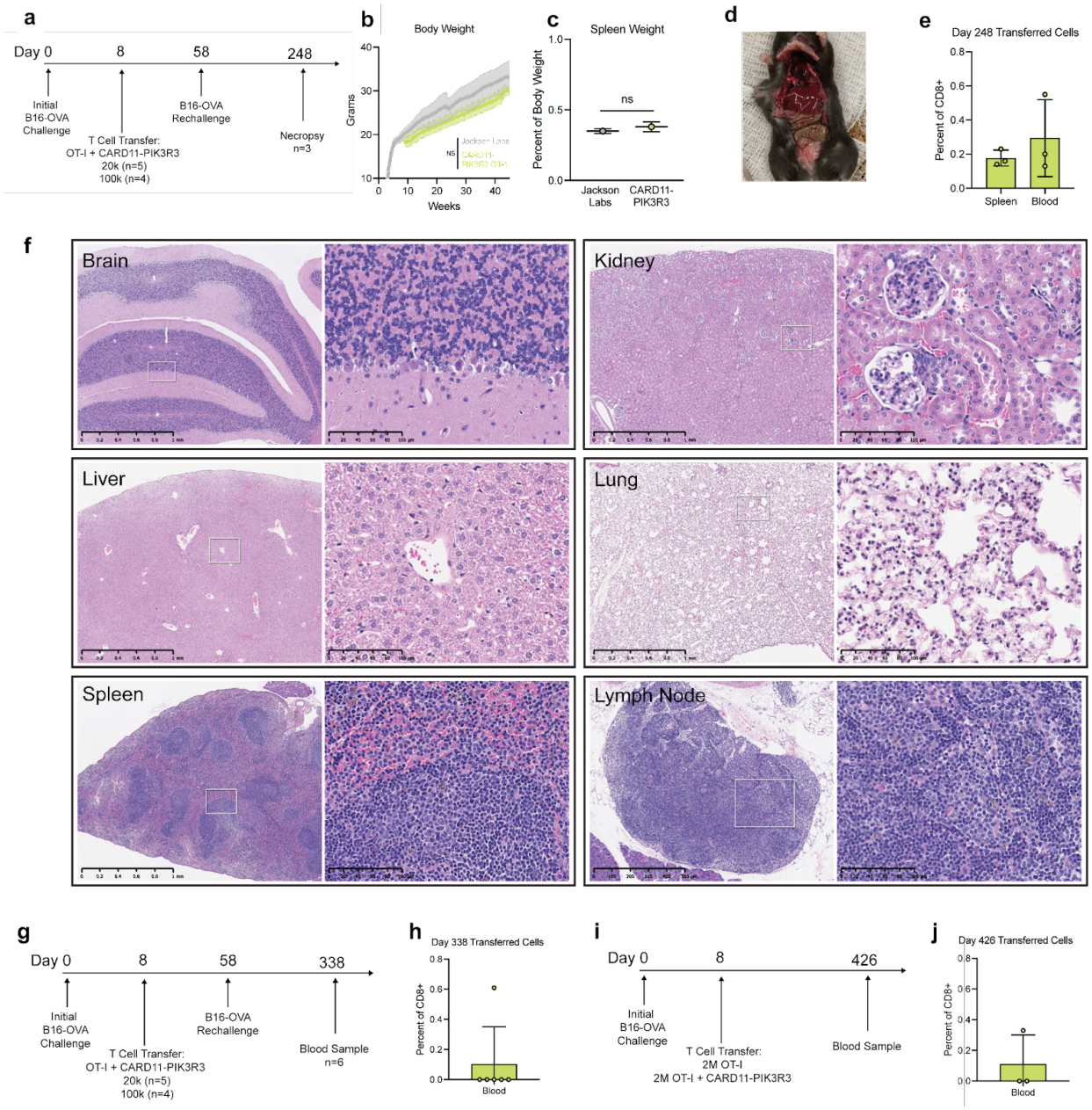

Extended Data Figure 2.10 Long-term evaluation of B6 mice treated with CARD11-PIK3R3 expressing OT-I T cells.

(a) Mice that cleared B16-F10-OVA from Fig. 5e were monitored for up to 240 days after adoptive T cell transfer. Necropsies were performed in as outlined in this schematic. **(b)** Body weights of all CARD11-PIK3R3 infused mice from Fig. 5e and Extended Fig. 9i were measured weekly and compared to expected weight curves published by The Jackson Laboratory Research Institute (Figure legend continued on the next page.)

(Figure legend continued from the previous page.) **(c)** Spleen weight for three animals that underwent necropsy on day 240. This was calculated as percent of body weight and compared to expected spleen weight published by The Jackson Laboratory Research Institute **(d)** Necropsy of one representative animal. None of the three animals had gross pathology. **(e)** Percentage of CD8 T cells in spleen and blood that express CARD11-PIK3R3 240 days after adoptive transfer. **(f)** Representative hematoxylin and eosin-stained tissue sections from select organs where nodal or extranodal lymphomas can occur. Animals were subject to full-body necropsies. Tissues did not show evidence of nuclear atypia, changes in cellular architecture, or presence of neoplastic disease. Representative images at low (left) and high (right) -power magnification are shown with size bars. White box reflects the site of high-magnification image. **(g,i)** Schematic of blood sampling of mice presented in Fig. 5e 330 days after adoptive transfer **(g)** or of 2e6 OT-I CARD11-PIK3R3 treated mice presented in Extended Fig. 9i 418 days after adoptive transfer **(i)**. **(h,j)** Percentage of CD8 T cells in blood that express CARD11-PIK3R3 in the two cohorts described in Fig. 5e or Extended Fig. 9i. Each data point indicates one mouse, mean + s.e.m. depicted.

2.12. References

1. June, C. H., O'Connor, R. S., Kawalekar, O. U., Ghassemi, S. & Milone, M. C. CAR T cell immunotherapy for human cancer. Science 359, 1361-1365 (2018).
2. Hou, A. J., Chen, L. C. & Chen, Y. Y. Navigating CAR-T cells through the solid-tumour microenvironment. Nature Reviews Drug Discovery 20, 531-550 (2021).
3. Larson, R. C. & Maus, M. V. Recent advances and discoveries in the mechanisms and functions of CAR T cells. Nature Reviews Cancer 21, 145-161 (2021).
4. Long, A. H. et al. 4-1BB costimulation ameliorates T cell exhaustion induced by tonic signaling of chimeric antigen receptors. Nat Med 21, 581-590 (2015).
5. Maude, S. L. et al. Chimeric Antigen Receptor T Cells for Sustained Remissions in Leukemia. New England Journal of Medicine 371, 1507-1517 (2014).
6. Kloss, C. C. et al. Dominant-Negative TGF-β Receptor Enhances PSMA-Targeted Human CAR T Cell Proliferation And Augments Prostate Cancer Eradication. Mol Ther 26, 1855-1866 (2018).
7. Wei, J. et al. Targeting REGNASE-1 programs long-lived effector T cells for cancer therapy. Nature 576, 471-476 (2019).
8. Legut, M. et al. A genome-scale screen for synthetic drivers of T cell proliferation. Nature 603, 728-735 (2022).
9. Shifrut, E. et al. Genome-wide CRISPR Screens in Primary Human T Cells Reveal Key Regulators of Immune Function. Cell 175, 1958-1971.e1915 (2018).
10. Schmidt, R. et al. CRISPR activation and interference screens decode stimulation responses in primary human T cells. Science 375, eabj4008 (2022).
11. Sutra Del Galy, A. et al. In vivo genome-wide CRISPR screens identify SOCS1 as intrinsic checkpoint of CD4(+) T(H)1 cell response. Sci Immunol 6, eabe8219 (2021).

12. Dong, M. B. et al. Systematic Immunotherapy Target Discovery Using Genome-Scale In Vivo CRISPR Screens in CD8 T Cells. Cell 178, 1189-1204.e1123 (2019).
13. Zhou, P. et al. In vivo discovery of immunotherapy targets in the tumour microenvironment. Nature 506, 52-57 (2014).
14. Roth, T. L. et al. Pooled Knockin Targeting for Genome Engineering of Cellular Immunotherapies. Cell 181, 728-744.e721 (2020).
15. Mustjoki, S. & Young, N. S. Somatic Mutations in "Benign" Disease. N Engl J Med 384, 2039-2052 (2021).
16. Kadin, M. E. et al. Loss of receptors for transforming growth factor beta in human T-cell malignancies. Proc Natl Acad Sci U S A 91, 6002-6006 (1994).
17. Park, J. et al. Integrated genomic analyses of cutaneous T-cell lymphomas reveal the molecular bases for disease heterogeneity. Blood 138, 1225-1236 (2021).
18. Wartewig, T. et al. PD-1 is a haploinsufficient suppressor of T cell lymphomagenesis. Nature 552, 121-125 (2017).
19. Kataoka, K. et al. Integrated molecular analysis of adult T cell leukemia/lymphoma. Nat Genet 47, 1304-1315 (2015).
20. Kleppe, M. et al. Mutation analysis of the tyrosine phosphatase PTPN2 in Hodgkin's lymphoma and T-cell non-Hodgkin's lymphoma. Haematologica 96, 1723-1727 (2011).
21. Stadtmauer Edward, A. et al. CRISPR-engineered T cells in patients with refractory cancer. Science 367, eaba7365 (2020).
22. Fraietta, J. A. et al. Disruption of TET2 promotes the therapeutic efficacy of CD19-targeted T cells. Nature 558, 307-312 (2018).
23. Kumar, J. et al. Deletion of Cbl-b inhibits CD8⁺ T-cell exhaustion and promotes CAR T-cell function. Journal for ImmunoTherapy of Cancer 9, e001688 (2021).

24. Prinzing, B. et al. Deleting DNMT3A in CAR T cells prevents exhaustion and enhances antitumor activity. Science Translational Medicine 13, eabh0272 (2021).
25. Wiede, F. et al. PTPN2 phosphatase deletion in T cells promotes anti-tumour immunity and CAR T-cell efficacy in solid tumours. The EMBO Journal 39, e103637 (2020).
26. Park, J. et al. Genomic analysis of 220 CTCLs identifies a novel recurrent gain-of-function alteration in RLTPR (p.Q575E). Blood 130, 1430-1440 (2017).
27. Daniels, J. et al. Cellular origins and genetic landscape of cutaneous gamma delta T cell lymphomas. Nature communications 11, 1806-1806 (2020).
28. Jutz, S. et al. Assessment of costimulation and coinhibition in a triple parameter T cell reporter line: Simultaneous measurement of NF-κB, NFAT and AP-1. J Immunol Methods 430, 10-20 (2016).
29. Patel, V. M. et al. Frequent and Persistent PLCG1 Mutations in Sézary Cells Directly Enhance PLCγ1 Activity and Stimulate NFκB, AP-1, and NFAT Signaling. J Invest Dermatol 140, 380-389.e384 (2020).
30. Ungewickell, A. et al. Genomic analysis of mycosis fungoides and Sézary syndrome identifies recurrent alterations in TNFR2. Nature genetics 47, 1056-1060 (2015).
31. Robles-Valero, J. et al. Cancer-associated mutations in VAV1 trigger variegated signaling outputs and T-cell lymphomagenesis. Embo j 40, e108125 (2021).
32. Vallois, D. et al. Activating mutations in genes related to TCR signaling in angioimmunoblastic and other follicular helper T-cell–derived lymphomas. Blood 128, 1490-1502 (2016).
33. Chen, S. S., Hu, Z. & Zhong, X.-P. Diacylglycerol Kinases in T Cell Tolerance and Effector Function. Frontiers in Cell and Developmental Biology 4 (2016).
34. Martinez, G. J. et al. The transcription factor NFAT promotes exhaustion of activated $CD8^+$ T cells. Immunity 42, 265-278 (2015).

35. Rafiq, S., Hackett, C. S. & Brentjens, R. J. Engineering strategies to overcome the current roadblocks in CAR T cell therapy. Nature Reviews Clinical Oncology 17, 147-167 (2020).
36. Sharma, P. & Allison, J. P. Immune checkpoint targeting in cancer therapy: toward combination strategies with curative potential. Cell 161, 205-214 (2015).
37. Schmitz, R. et al. Burkitt lymphoma pathogenesis and therapeutic targets from structural and functional genomics. Nature 490, 116-120 (2012).
38. Liu, Y. et al. The genomic landscape of pediatric and young adult T-lineage acute lymphoblastic leukemia. Nature genetics 49, 1211-1218 (2017).
39. Lynn, R. C. et al. c-Jun overexpression in CAR T cells induces exhaustion resistance. Nature 576, 293-300 (2019).
40. Kahan, S. M. et al. Intrinsic IL-2 production by effector CD8 T cells affects IL-2 signaling and promotes fate decisions, stemness, and protection. Sci Immunol 7, eabl6322 (2022).
41. Wang, L. et al. Genomic profiling of Sézary syndrome identifies alterations of key T cell signaling and differentiation genes. Nature genetics 47, 1426-1434 (2015).
42. Ruland, J. & Hartjes, L. CARD-BCL-10-MALT1 signalling in protective and pathological immunity. Nat Rev Immunol 19, 118-134 (2019).
43. Jattani, R. P., Tritapoe, J. M. & Pomerantz, J. L. Intramolecular Interactions and Regulation of Cofactor Binding by the Four Repressive Elements in the Caspase Recruitment Domain-containing Protein 11 (CARD11) Inhibitory Domain. J Biol Chem 291, 8338-8348 (2016).
44. Burke, J. E. Structural Basis for Regulation of Phosphoinositide Kinases and Their Involvement in Human Disease. Molecular Cell 71, 653-673 (2018).

45. Kutzner, K. et al. Phosphorylation of serine-893 in CARD11 suppresses the formation and activity of the CARD11-BCL10-MALT1 complex in T and B cells. Science Signaling 15, eabk3083 (2022).
46. Li, S., Yang, X., Shao, J. & Shen, Y. Structural Insights into the Assembly of CARMA1 and BCL10. PLOS ONE 7, e42775 (2012).
47. Grossmann, A. et al. Phospho-tyrosine dependent protein-protein interaction network. Mol Syst Biol 11, 794 (2015).
48. Fan, X., Quezada, S. A., Sepulveda, M. A., Sharma, P. & Allison, J. P. Engagement of the ICOS pathway markedly enhances efficacy of CTLA-4 blockade in cancer immunotherapy. Journal of Experimental Medicine 211, 715-725 (2014).
49. Massarelli, E. et al. High OX-40 expression in the tumor immune infiltrate is a favorable prognostic factor of overall survival in non-small cell lung cancer. J Immunother Cancer 7, 351 (2019).
50. Bardet, M. et al. The T-cell fingerprint of MALT1 paracaspase revealed by selective inhibition. Immunol Cell Biol 96, 81-99 (2018).
51. Jiang, T., Zhou, C. & Ren, S. Role of IL-2 in cancer immunotherapy. Oncoimmunology 5, e1163462 (2016).
52. Thommen, D. S. & Schumacher, T. N. T Cell Dysfunction in Cancer. Cancer Cell 33, 547-562 (2018).
53. Guedan, S. et al. Enhancing CAR T cell persistence through ICOS and 4-1BB costimulation. JCI Insight 3 (2018).
54. King, M. A. et al. Human peripheral blood leucocyte non-obese diabetic-severe combined immunodeficiency interleukin-2 receptor gamma chain gene mouse model of xenogeneic graft-versus-host-like disease and the role of host major histocompatibility complex. Clin Exp Immunol 157, 104-118 (2009).

55. Bidlingmaier, S. et al. Identification of MCAM/CD146 as the target antigen of a human monoclonal antibody that recognizes both epithelioid and sarcomatoid types of mesothelioma. Cancer Res 69, 1570-1577 (2009).
56. Li, Q.-X., Feuer, G., Ouyang, X. & An, X. Experimental animal modeling for immuno-oncology. Pharmacology & Therapeutics 173, 34-46 (2017).
57. Kalbasi, A. et al. Potentiating adoptive cell therapy using synthetic IL-9 receptors. Nature 607, 360-365 (2022).
58. Zhang, Y., Liu, Z., Wei, W. & Li, Y. TCR engineered T cells for solid tumor immunotherapy. Experimental Hematology & Oncology 11, 38 (2022).
59. Overwijk, W. W. & Restifo, N. P. B16 as a mouse model for human melanoma. Curr Protoc Immunol Chapter 20, Unit-20.21 (2001).
60. Eyquem, J. et al. Targeting a CAR to the TRAC locus with CRISPR/Cas9 enhances tumour rejection. Nature 543, 113-117 (2017).
61. McLellan, A. D. & Ali Hosseini Rad, S. M. Chimeric antigen receptor T cell persistence and memory cell formation. Immunol Cell Biol 97, 664-674 (2019).
62. Leidner, R. et al. Neoantigen T-Cell Receptor Gene Therapy in Pancreatic Cancer. New England Journal of Medicine 386, 2112-2119 (2022).
63. Klichinsky, M. et al. Human chimeric antigen receptor macrophages for cancer immunotherapy. Nat Biotechnol 38, 947-953 (2020).
64. Rezvani, K. Adoptive cell therapy using engineered natural killer cells. Bone Marrow Transplantation 54, 785-788 (2019).
65. Kabelitz, D., Serrano, R., Kouakanou, L., Peters, C. & Kalyan, S. Cancer immunotherapy with γδ T cells: many paths ahead of us. Cellular & Molecular Immunology 17, 925-939 (2020).

66. Wennhold, K., Shimabukuro-Vornhagen, A. & von Bergwelt-Baildon, M. B Cell-Based Cancer Immunotherapy. Transfusion Medicine and Hemotherapy 46, 36-46 (2019).
67. Zhu, I. et al. Modular design of synthetic receptors for programmed gene regulation in cell therapies. Cell 185, 1431-1443.e1416 (2022).
68. Morsut, L. et al. Engineering Customized Cell Sensing and Response Behaviors Using Synthetic Notch Receptors. Cell 164, 780-791 (2016).
69. Roybal, K. T. et al. Precision Tumor Recognition by T Cells With Combinatorial Antigen-Sensing Circuits. Cell 164, 770-779 (2016).
70. Zhao, H. et al. Genome-wide fitness gene identification reveals Roquin as a potent suppressor of CD8 T cell expansion and anti-tumor immunity. Cell Rep 37, 110083 (2021).
71. Porter, D. L., Levine, B. L., Kalos, M., Bagg, A. & June, C. H. Chimeric Antigen Receptor–Modified T Cells in Chronic Lymphoid Leukemia. New England Journal of Medicine 365, 725-733 (2011).

Chapter 3

The Immunological Impact of CARD11-PIK3R3 CAR T Cell Anti-Tumor Responses in Immunotherapy Refractory Solid Tumors

Material from this chapter comes from the following work:

Burnett, C.*, Garcia J.*, Alavi, J., Guldberg S., Thienpont, C., Tamaka, S., Spitzer, M., Roybal, K. T. The immunological impact of CARD11-PIK3R3 CAR T cell anti-tumor responses in immunotherapy refractory solid tumors. (2023). Manuscript in Preparation.

*These authors contributed equally to this work.

3.1. Abstract

CARD11-PIK3R3 is a novel potency enhancer of engineered cell therapies that was discovered through systematic screening of T cell lymphoma mutations alongside CAR T cells. CARD11-PIK3R3 enhances CARD11-BCL10-MALT1 (CBM) signaling outputs and induces the secretion of high levels of inflammatory cytokines from CD8+ T cells, such as IL-2 and IFN-γ. Inclusion of CARD11-PIK3R3 was discovered to dramatically improve CAR therapy in immunologically cold syngeneic tumor models without the requirement for pre-conditioning. Here, we sought to determine how CARD11-PIK3R3 CAR T cells influence the endogenous immune system both locally within the tumor microenvironment (TME) and systemically. During acute tumor rejection, CARD11-PIK3R3 CAR T cells have improved memory phenotype and accumulation and alter the cytokine and chemokine state of the TME and periphery. The TME of CARD11-PIK3R3 CAR treated animals is marked by significantly fewer pro-tumorigenic suppressive cells and greater numbers of inflammatory myeloid populations. CARD11-PIK3R3 CAR treated animals ultimately succumb to antigen negative tumors, indicating that inclusion of CARD11-PIK3R3 is insufficient for induction of epitope spread. Altogether, CARD11-PIK3R3 CAR therapy potently shifts the TME and should be paired with additional payloads to attain full endogenous immune system engagement, and multi-nodal rejection.

3.2. Introduction

Chimeric Antigen Receptor (CAR) T cell therapies, while highly effective in leukemia and some lymphomas, have yet to make a clinical impact in solid tumors. This is due in part to the unique challenges of solid tumors, which are often highly immunosuppressive, resulting in a lack

of persistence, proliferation, and cytotoxicity of adoptively transferred cell therapies. Furthermore, even when CAR therapy performs well, antigen heterogeneity or loss of the CAR targeted antigen can lead to antigen negative relapse. An ideal solid tumor CAR T cell product must potently target tumor specific antigens and promote endogenous antigen presenting cells (APCs) and polyclonal T cell activation to induce full tumor clearance. In this study we aimed to contrast a functional CARD11-PIK3R3 CAR T cell product with conventional CAR T cells that fail to demonstrate any tumor control to understand the requirements of an effective response and deficits of the current clinical standard.

We have previously described CARD11-PIK3R3, an onco-fusion discovered through systematic screening of lymphoma mutations in CAR T cells, which dramatically improves the anti-tumor efficacy of CAR therapies in multiple *in vivo* tumor models. While our previous studies revealed CARD11-PIK3R3 T cells to have improved CBM signaling, cytokine secretion, and cytotoxicity *in vitro* and *in vivo*, we have yet to determine how CARD11-PIK3R3 CAR T cells influence or engage with the endogenous TME. Here, we show that during acute tumor rejection, CARD11-PIK3R3 improves CAR T cell accumulation and memory phenotype and leads to greater secretion of inflammatory cytokines and immune recruiting chemokines within the tumor microenvironment. CARD11-PIK3R3 CAR treated animals had fewer pro-tumorigenic suppressive cells, such as Tregs, and greater inflammatory myeloid populations within the TME. Finally, we determined that CARD11-PIK3R3 CAR treated animals relapsed with antigen negative tumors, indicating that inclusion of CARD11-PIK3R3 is insufficient for induction of epitope spread, but we note key findings, such as the lack of full DC maturation, an increase in myeloid derived suppressor cells, and heightened PDL1 expression, that could be targets for future additive studies with CARD11-PIK3R3. This data suggests that multi-nodal approaches to solid tumors can be enabled by CARD11-PIK3R3 CAR therapy, which achieves the needed

persistence, cytotoxic potency, and inflammatory profile to make impact on solid tumors. CARD11-PIK3R3 engineered cells can be paired with combination therapies, such as PD-1/PD-L1 checkpoint blockade, or additional payloads, like FLT3-L for DC maturation or IL-27 for amplification of innate and T cell responses, to attain full endogenous immune system engagement, and multi-nodal rejection.

3.3. CARD11-PIK3R3 T Cells Demonstrate Greater Expansion and Increased T Cell Memory Phenotype

Our previous work evaluated CARD11-PIK3R3 CAR T cells in a syngeneic immunocompetent B16-F10 melanoma model. To determine if tumor control was limited to a specific syngeneic model or immune microenvironment, we investigated CARD11-PIK3R3 CAR T cells in multiple immunocompetent solid tumor models. To assess this, we constructed a murinized 4-1BB second generation CAR targeting either hALPPL2 (hALPPL2-CAR) or hCD19 (hCD19-CAR) (Fig. 3.1a, Extended Data Fig. 3.1a). We used retroviral transduction of CAR alone or dual transduction of CAR with CARD11-PIK3R3 to engineer our CAR T graft. We lentivirally transduced target cells lines of B16-F10 melanoma and KPC-Y pancreatic ductal adenocarcinoma to express hCD19 (hCD19-B16-F10, hCD19-KPC-Y-hot, hCD19-KPC-Y-cold), and a murine line of mesothelioma 40L to express hALPPL2 (hALPPL2-40L) as a model antigen targets. We subcutaneously implanted the tumor lines and injected the CAR T products without host preconditioning once tumors reached a measurable volume (Fig. 3.1b, Extended Data Fig. 3.1b). We observed acute tumor control in hCD19-KPC-Y-hot, hCD19-KPC-Y-cold, and hALPPL2-40L models comparable to our previous work in hCD19-B16-F10 (Fig. 3.1c, Extended Data Fig. 3.1c). Additionally, efficacy of CARD11-PIK3R3 CAR T cells across multiple tumor

models, and when paired with CARs targeting either hCD19 or hALPPL2 demonstrates that the anti-tumor potency of CARD11-PIK3R3 modified T cells is not limited by the scFV or the TME. In contrast, tumor control from conventional CAR T cells was comparable to untransduced control T cells, demonstrating their lack of potency in these solid tumor settings without preparative preconditioning.

The dramatic tumor regression induced by CARD11-PIK3R3 CAR T cells suggests significant changes may be occurring within the TME. We sought to further characterize the adoptively transferred T cells within the TME, and peripheral immune compartments of syngeneic mice treated with CAR or CARD11-PIK3R3 CAR treatment. We isolated the tumor, spleen, lymph node and blood of hALPPL2-40L tumor bearing mice at the peak of tumor growth prior to CARD11-PIK3R3 CAR tumor regression and performed mass cytometry by time-of-flight (CyTOF) to assess T cell abundance and phenotype (Fig. 3.1b,c). CARD11-PIK3R3 CAR T cells were more abundant (by % of total CD45 cells) in the spleen, tumor, lymph node and blood as compared to CAR treated animals (Fig 3.1d). CARD11-PIK3R3 CAR T cells expressed high levels of Ki67 in all organs (Fig. 3.1e), suggesting that the increased accumulation is due to greater proliferation, though we cannot rule out the contribution of greater persistence. While overall there were a greater number of both CD4+ and CD8+ CARD11-PIK3R3 CAR T cells as compared to CAR, we also observed that the CARD11-PIK3R3 CAR T cells were slightly more skewed towards a CD8+ phenotype (Fig. 3.1f, Extended Data Fig. 3.2a,b). Higher effector (CD8+) to helper (CD4+) ratios in tumor infiltrating lymphocytes has been used commonly as a prognostic factor that is associated with positive outcomes[2].

While the total number of CARD11-PIK3R3 CAR T cells within the tumor and draining lymph node was significantly higher than that of CAR T alone, both groups had similar numbers of tumor infiltrating naive and central memory T cells. However, CARD11-PIK3R3 CAR treated

tumors and their corresponding draining lymph nodes had significantly higher numbers of effector cells (Fig. 3.1g, Extended Data 3.2c). In the peripheral blood and spleen all manually gated T cell subsets were significantly expanded in the CARD11-PIK3R3 CAR treated animals (Fig. 3.1g, Extended Data 3.2c), suggesting an expanded pool of naive and central memory T cells in the periphery may serve to replenish effectors within the tumor over time.

Finally, we performed unbiased clustering on the CAR T populations within the blood and tumor, which identified 4 distinct CAR T cell clusters of interest. Cluster 1 was significantly expanded within the blood of CARD11-PIK3R3 CAR treated animals, and was dominated by antigen experienced (CD44high), cycling (Ki67high) CD8+ T cells characterized by the expression of CD27 and PD1. In comparison, cluster 5, which is the dominant cluster in peripheral blood of CAR T cell treated animals, expressed higher levels of the inhibitory ligand PD-L1, and memory markers such as CD62L and Ly6C, an expression profile which suggest these low cycling cells consist of non-activated memory T cells (Fig. 3.1h,i).

Within the tumor we observed a significant expansion of cluster 3 cells particularly in CARD11-PIK3R3 CAR T cell treated animals, while CAR T cell treated tumors maintained a higher proportion of non-activated cluster 5 T cells. Similar to cluster 1, cluster 3 was dominated by antigen experienced (CD44high) and cycling (Ki67high) CD8 T cells; however, in cluster 3 these cells were also enriched for CD69, CD25 and Ly6C, indicating a highly activated though memory-like state. Furthermore, cluster 3 had lower expression of senescence or exhaustion markers such as KLRG1, CD39 and PD-L1. Altogether, these data suggest CARD11-PIK3R3 CAR T cells form a productive, activated anti-tumor response, while CAR T cells, though exposed to antigen, struggle to differentiate into effectors.

3.4. CARD11-PIK3R3 CAR T cells secrete higher levels of effector cytokines and chemokines in vitro and induce changes to mediator milieu in vivo

Our previous work demonstrated that human CARD11-PIK3R3 CAR T cells secrete high levels of cytokines, such as IL-2 and IFN-γ, in addition to secretion of Th2 like cytokines, such as IL-4, IL-5 and IL-13. Here, we sought to understand the cytokine secretion profile of mouse CAR T cells expressing CARD11-PIK3R3, and given the CD8+ biased phenotype *in vivo*, determine if CARD11-PIK3R3 has different effects in CD4+ vs. CD8+ T cells. To do this we co-cultured CD4+ or CD8+ CD19-CAR +/- CARD11-PIK3R3 T cells at a 1:1 ratio with hCD19-B16 target cells for 24 hours, collected supernatants and analyzed them with a panel of 32 cytokines and chemokines using Luminex (Fig. 3.2a). We calculated the fold change of CARD11-PIK3R3 CAR cytokine secretion as compared to CAR to determine which mediators were differentially increased when CARD11-PIK3R3 is expressed. Similar to our results in primary human CAR T cells[2], we found that CARD11-PIK3R3 expressing CD8+ T cells demonstrate a greater change in cytokine and chemokine secretion as compared to CD4+ T cells (Fig 3.2b). For CD8+ CARD11-PIK3R3 CAR T cells, we observed an increase in the chemoattractant CXCL9, the inflammatory cytokine IL-6, and Th2 and regulatory cytokines such as IL-4, IL-10 and IL-13.

In contrast, CD4+ CARD11-PIK3R3 CAR T cells increased secretion of just a few analytes, such as IL-17. We observed an increase in IL-2 secretion in both CD8+ and CD4+ CARD11-PIK3R3 CAR T cells (Fig. 3.2b).

We hypothesized that the significant *in vitro* secretion of inflammatory mediators by CARD11-PIK3R3 CAR T cells would result in differences in the cytokine and chemokine milieu *in vivo*. To characterize this, we used the same 32-plex cytokine/chemokine Luminex assay on

the serum of blood, tumor, and spleen from CAR +/- CARD11-PIK3R3 treated mice 7 days after the T cells were transferred (Fig. 3.2c).We observed many elevated cytokines/chemokines across tissue of mice treated with CARD11-PIK3R3 CAR T cells and were particularly interested to find significant increases in T cell chemoattractants CXCL9, CXCL10, and CCL5, as well as monocyte chemoattractants CCL3, CCL4, CCL2 (Fig 3.2d, e). While some of the observed *in vivo* increases, like high levels of CXCL9 in the spleen and blood, may be explained by the high levels of secretion CARD11-PIK3R3 CAR T cells *in vitro* (Fig. 3.2b), other molecules that are elevated but not produced by CARD11-PIK3R3 CAR T cells may be driven by responding endogenous cells. For example CXCL10, a chemokine known to broadly recruit immune cells to inflamed tissue[3], was elevated across all three tissues, though not highly expressed by CARD11-PIK3R3 CAR T cells *in vitro* suggesting possible production by endogenous cells. CCL3 was highly increased in the tumor and spleen, and is known for involvement in recruiting myeloid precursors, as well as other lymphocytes [4]. CCL4, known for its ability to recruit CD103+ dendritic cells to sites of inflammation [5], was elevated across all three tissues. CCL2, a potent chemoattractant of macrophages with roles in both tumor progression and anti-tumor responses, was slightly increased within the spleen and blood [6]. Finally, CCL5 was elevated in the tumor and blood.

Interestingly, across all three tissues we observed a significant increase in IFN-γ in CARD11-PIK3R3 CAR treated mice as compared to CAR alone (Fig. 3.2d,e). While CARD11-PIK3R3 CAR T cells *in vitro* produced higher amounts of IL-2 (Fig. 3.2b), we did not observe increased serum levels of IL-2 in any tissue of CARD11-PIK3R3 CAR T cell treated mice when compared to CAR T cell alone. It is possible that IL-2 may be locally consumed by engineered or endogenous immune cells and is therefore undetectable in the serum *in vivo*.

Altogether, the cytokine and chemokine profiling indicate a widespread immune inflammation and recruitment is occurring in CARD11-PIK3R3 CAR T cell treated animals.

3.5. CARD11-PIK3R3 CAR T cells remodel the tumor microenvironment

We sought to understand the changes to the tumor and peripheral immune populations that occurred when treating CARD11-PIK3R3 CAR T cells. We performed unbiased FlowSOM[7] clustering on the CD45+ fraction of the blood, tumor, spleen and draining lymph node using 42 cell type markers and identified 25 immune clusters. Principal component analysis (PCA) of cluster abundances within the tumor demonstrated that CARD11-PIK3R3 CAR T cell treated tumors segregated from CAR or untreated mice and were composed of distinct immune clusters. This difference is driven primarily by the abundance of a CARD11-PIK3R3 CAR T cell specific cluster and secondarily by two myeloid cell clusters (Fig. 3.3a).

We found that the mixed myeloid and CD11c-myeloid clusters were significantly enriched in CARD11-PIK3R3 CAR T cell treated animals, while CAR alone animals had significantly higher abundance of a monocyte and CD11b-myeloid cluster (Fig. 3.3b). The CD11c+ monocyte cluster dominated the overall immune abundance of CARD11-PIK3R3 CAR T cell treated tumors composing 60-75% of the immune compartment compared to 50% of CAR alone treated mice (Supplemental Fig. 3.3b). Both clusters that increased with CARD11-PIK3R3 CAR T treatment showed higher costimulatory markers CD80 and CD86 and higher expression of Fc receptors CD16/32, indicating a more inflammatory monocyte/macrophage population. Additionally, both increasing clusters have higher PD-L1, which is known to be induced by high levels of IFN-γ (Fig. 3.3b).

To investigate overall monocyte/macrophage abundances we manually gated CD11b+CD64+ immune cells and observed a total increase in the abundance of mono/macs with CARD11-PIK3R3 CAR T treatment (Fig. 3.3c). Manual gating also revealed distinct immune populations of CD11c+ monocytes, CD80/CD86 double positive fraction, and iNos+ Monocytes supporting our unbiased clustering observations (Fig. 3.3d). iNos+ monocytes were not only observed to increase in abundance but also by cell number per gram of tissue, indicating an absolute increase in this effector tumor monocyte as well as a relative increase (Fig. 3.3e). We evaluated the peripheral blood immune clustering composition of CARD11-PIK3R3 CAR treated animals and observed a significant shift in 11 clusters (Extended Datal Fig. 3.3a,b), indicating a broad reorganization of peripheral immune cells as compared to CAR alone treatment. One major immune cluster that increased with CARD11-PIK3R3 CAR treatment was a significant increase in circulating monocytes. Although the source of this expansion is unclear, they may be a contributing population to the observed increased infiltration in the tumor.

CARD11-PIK3R3 CAR treated animals were observed to have lower frequency of Tregs as compared to CAR treated animals (Fig. 3.3f). While total Treg/gram cell count was similar between the two treatment groups, the ratio of adoptively transferred effectors and endogenous effectors to Tregs was significantly higher in CARD11-PIK3R3 CAR mice as compared to CAR alone. Additionally, we observed an increase in endogenous CD8+ central memory and effector cells within CARD11-PIK3R3 CAR T cell treated tumors (Fig. 3.3g). In both the spleen and peripheral blood we noted that both CD4+ and CD8+ endogenous T cells were cycling at a higher rate in CARD11-PIK3R3 CAR T cell treated animals (Fig. 3.3h, Extended Data Fig. 3.3c). Cycling of endogenous immune cells were not observed in the tumor, indicating any increase in the endogenous immune T cell frequencies is likely due to increased infiltration rather than proliferation in the tumor (Extended Data Fig. 3.3b).

3.6. Scratching the Surface on Mechanism: The Role of IFN-γ

Tissue cytokine analysis of animals undergoing active CARD11-PIK3R3 CAR mediated tumor rejection revealed that IFN-γ was elevated in the tumor, spleen and blood (Fig. 3.4a). IFN-γ has known anti-tumor effects, directly inhibiting tumor proliferation, and indirectly driving polyclonal immune responses through increased antigen presentation [8,9]. IFN-γ also causes secretion of CXCL9 and CXCL10 from surrounding endothelial cells, fibroblasts and immune cells[3]. Interestingly these chemokines were upregulated in tissues of CARD11-PIK3R3 CAR treated animals (Fig. 3.2d).

We hypothesized that IFN-γ secreted by CARD11-PIK3R3 CAR T cells was shaping some of the endogenous immune response and playing a role in the dramatic tumor rejection observed in both hCD19-B16 as well as hALPPL2-40L tumor models. To test this, we engrafted wildtype and IFN-γRKO C57BL/6 mice with hCD19-B16 tumors and treated with CAR or CARD11-PIK3R3 CAR T cells 9 days later (here we used OT-I T cells for a controlled TCR to prevent toxicity) (Fig. 3.4b). Strikingly, in control T cell treated animals, we observed faster tumor growth in IFN-γRKO mice as compared to wildtype, suggesting that even without a productive CAR T cell response the endogenous immune system plays a role in delaying tumor growth. Interestingly, in IFN-γRKO mice, CARD11-PIK3R3 CAR T cells still had some impact on tumor growth, however the tumors grew substantially larger than those in wildtype mice before regressing briefly (Fig. 3.4c). CARD11-PIK3R3 CAR T cells initially controlled hCD19-B16F10 tumors in wildtype mice, however this tumor control was significantly reduced in IFN-γRKO mice, resulting in shorter overall survival (Fig. 3.4d). While this experiment is likely slightly confounded by the loss of hCD19-B16F10, resulting in tumor relapse in both IFN-γRKO and wildtype mice, we believe it demonstrates that IFN-γ is a key mediator of the CARD11-PIK3R3

CAR T cell anti-tumor response, and this response relies partially on engagement with the host immune system via IFN-γ sensitivity.

3.7. Building Multi-Modal Responses: CARD11-PIK3R3 and Payloads

CARD11-PIK3R3 induces highly effective and dramatic anti-tumor CAR T cell responses without the need for harsh pre-conditioning regimes. CARD11-PIK3R3 CAR T cell treatment results in impressive accumulation of both engineered and endogenous T cells within the TME, blood and spleen. CARD11-PIK3R3 CAR T cells secrete effector molecules like IFN-γ and IL-2, and the tumors and lymphoid organs of animals treated with CARD11-PIK3R3 CAR T cells have high levels of immune recruiting chemokines. When the host immune cells cannot respond to IFN-γ we see a decreased efficacy in CARD11-PIK3R3 CAR T cells, suggesting IFN-γ is a key mediator of anti-tumor response that relies partially on engagement with the host immune system. Finally, we observe that myeloid populations within the TME of CARD11-PIK3R3 CAR T cell treated mice are shifted towards a more inflammatory and activated state. Altogether, CARD11-PIK3R3 CAR treatment induces an effective anti-tumor response that suggests engagement and active influence over the TME and host immune system. However, in multiple syngeneic models, after a period of successful tumor regression, we commonly observe antigen negative tumor relapse. This suggests that epitope spread, the phenomenon in which the endogenous immune system becomes activated and produces tumor specific T cell responses to neoantigens, is not occurring in CARD11-PIK3R3 CAR T cell treated animals.

In most cases, syngeneic CAR T cell *in vivo* models require preconditioning for the expansion of the CAR therapy; however, this preconditioning step removes or greatly reduces

endogenous immune cells that would respond to and be influenced by CAR payloads. Therefore, a significant benefit of using CARD11-PIK3R3 CAR T cells for delivery of immune modulating payloads is the ability to treat animals without lymphodepletion. The following three vignettes describe additional payloads that we hypothesize could improve CARD11-PIK3R3 CAR T cell response to induce full tumor clearance, and resistance to antigen negative relapse.

PD-L1: Unleashing Endogenous CD8 T Cells

PD-L1 is an inhibitory ligand that is often upregulated on cancer cells, as well as tumor associated immune infiltrates such as macrophages [11,12]. When bound by its receptor PD-1, PD-L1 acts to dampen lymphocyte activation and has therefore been the target of checkpoint therapies which seek to reinvigorate endogenous immune cells by blocking this axis [13–16]. IFN-γ can play a protumor role, with chronic interferon signaling causing tumor cells and tumor associated immune cells to upregulate expression of PD-L1[11,17], leading to exhaustion of anti-tumor T cells. We observed an increase of inflammatory myeloid cells in the TME of microenvironment CARD11-PIK3R3 CAR T cell treated animals, though these myeloid cells also expressed the inhibitory ligand PD-L1 at high rates.

While we observed significant infiltration of antigen experienced (CD44high) endogenous CD8+ T cell populations in CARD11-PIK3R3 CAR treated tumors, it is unclear if these cells are potentiating an anti-tumor response. We also observe highly activated myeloid populations in CARD11-PIK3R3 CAR T cell treated tumors, we also found that PD-L1 expression was increased in these populations (Fig. 3.3b). We hypothesized that epitope spread may be hindered due to PD-L1 high levels, either preventing full activation of endogenous T cells during priming or resulting in inhibition or exhaustion of these cells.

To test this, we treated hALPPL2-40L tumor bearing animals with CAR or CARD11-PIK3R3 CAR T cells on day 13 post tumor inoculation. We then dosed animals three times with an αPD-L1 checkpoint inhibitor (B7-H1) via IP injection, focusing checkpoint delivery during the first week post adoptive T cell transfer, as we hypothesize this is a key window for immune response (Fig. 3.5a). While studies are ongoing, tumor growth curves of animals treated with CARD11-PIK3R3 CAR T cells and checkpoint are not different from animals treated with CARD11-PIK3R3 CAR T cells alone. These preliminary data may have a variety of explanations including but not limited to: 1) PD-L1 checkpoint therapy is not relevant or synergistic in this model, 2) PD-L1 checkpoint therapy and CAR T cell dosing requires further optimization. Future studies will continue to assess the effects and therapeutic efficacy of CARD11-PIK3R3 CAR T cells with PD-L1 checkpoint therapy.

FLT-3L: Expanding Antigen Presenting Cells

Migratory CD103+ DCs are rare antigen presenting cell population that collect tumor debris, travel to the tumor-draining lymph node and prime endogenous neoantigen CD8+ T cell responses[18,19]. FLT3-L is a key growth factor for these cells[20], and previous studies have demonstrated the CD103+ DC population can be expanded and partially matured through injection of FLT3-L[21]. Furthermore, engineered T cell therapies expressing FLT3-L have previously been demonstrated to induce expansion of intra-tumoral CD103+ DCs and epitope spread[10].

As previously mentioned, syngeneic CAR T cell *in vivo* models typically require lymphodepleting preconditioning; however, this can damage the endogenous immune cells that are the target of the CAR payloads. In fact, to achieve results with FLT3-L secreting CAR T cell

therapies, Lai et al [10] had to modify their lymphodepletion protocol to minimize this issue. A benefit of using CARD11-PIK3R3 CAR T cells for delivery of FLT3-L is the ability to treat animals without lymphodepletion. Midpoint assessment of hALPPL2-40L tumors treated with CARD11-PIK3R3 CAR T cells revealed a general upregulation of CD103+ expression within intra-tumoral myeloid compartments (Fig. 3.3b). We therefore hypothesized that CARD11-PIK3R3 CAR T cells secreting FLT3-L may induce epitope spread by expanding the dendritic cell compartment, preventing antigen negative relapse, while avoiding the need for preconditioning.

To test this, we constructed an hALPPL2-BBz CAR with a self-cleaving T2A sequence followed by soluble FLT3-L (CAR-FLT3L) (Fig. 3.6a). We transduced murine T cells to create the following groups: CAR, CAR-FLT3L, CARD11-PIK3R3 CAR and CARD11-PIK3R3 CAR-FLT3L. These cells were adoptively transferred to hALPPL2-40L tumor bearing mice, and tumor growth was assessed via caliper measurements 2x times per week. Seven days post adoptive transfer of T cells, we isolated tumor, spleen, blood, and tumor draining lymph nodes from a subset of animals. These tissues were assessed via CyTOF for cell abundance and phenotype. Additionally, serum was collected from tumor, spleen, and blood to determine the cytokine/chemokine profile (Fig. 3.6b). We observed that CARD11-PIK3R3 CAR-FLT3L group demonstrated superior tumor control to CARD11-PIK3R3 CAR treatment alone, indicating a beneficial relationship between CARD11-PIK3R3 and FLT3-L payload to drive increased tumor control (Fig. 3.6c). Further investigations of the immune changes driving this increased efficacy are ongoing.

IL27: A Pleiotropic Anti-Tumor Cytokine

IL-27 is a member of the IL-6 sub-family of type I cytokines, which also includes IL-6, IL-12, and IL-23. IL-27 receptor is expressed by a broad range of immune cells, including naive T cells, activated B cells, monocytes and activated dendritic cells. Originally discovered as the cytokine that induces CD4+ Th1 T cell differentiation through increased T-bet expression[22], IL-27 has both stimulatory and inhibitory roles. In CD8+ T cells, there is evidence that it promotes proliferation of a stem-like state and stimulates the production of IL-10 and IFN-γ[23–26]. IL-27 is noted to influence monocytes during DC differentiation, improving antigen presentation through upregulation of MHCII and enhanced antigen processing[27]. IL-27 secreting cancer cell lines are cleared in immunocompetent mice, inducing tumor specific CD8+ T cell responses that are protective after re-challenge[28,29].

Finally, there is evidence that IL-27 works synergistically with IL-2 for anti-tumor responses, which is highly relevant to CARD11-PIK3R3 CAR treatment which induces high levels of IL-2[30]. Altogether, IL-27 is a complex and pleiotropic cytokine but has clear anti-tumor effects. Here we believe that IL-27 could act in concert with CARD11-PIK3R3 CAR T cells, improving intra-tumoral DC antigen presentation to increase the likelihood of epitope spread and promoting proliferation of long-lived anti-tumor CD8 T cells, both of the host and adoptively transferred cells. To assess this, we constructed an hALPPL2 targeted CAR with a self-cleaving peptide sequence followed by IL-27 (Fig. 3.7a). We transduced murine T cells to create the following groups: CAR, CAR-IL27, CARD11-PIK3R3 CAR and CARD11-PIK3R3 CAR-IL27. These cells were adoptively transferred to hALPPL2-40L tumor bearing mice, and tumor growth was assessed via caliper measurements 2x times per week. Seven days post adoptive transfer

of T cells, we isolated tumor, spleen, blood, and tumor draining lymph nodes from a subset of animals. These tissues were assessed via CyTOF for cell abundance and phenotype (Fig. 3.7b). Additionally, serum was collected from tumor, spleen, and blood to determine the cytokine/chemokine profile.

Our preliminary tumor growth analysis demonstrated that the CARD11-PIK3R3 CAR-IL27 T cells had superior tumor control as compared to the CAR-IL27 alone or CARD11-PIK3R3 CAR groups (Fig. 3.7c). This suggests IL-27 is contributing a novel and potentially synergistic benefit to the CARD11-PIK3R3 CAR platform that is driving a new axis of anti-tumor immune response. Ongoing investigation of midpoint immune composition and cytokine and chemokine analysis will help elucidate key immune populations and mechanisms of tumor control that are elicited by the combination CARD11-PIK3R3 CAR-IL27 T cells.

3.8. Conclusion and Next Steps

CARD11-PIK3R3 improves CAR T cell therapy in multiple immunocompetent tumor models, and with multiple scFvs, suggesting that effects of CARD11-PIK3R3 are agnostic to tumor type and target. We discovered CARD11-PIK3R3 CAR T cells to have improved memory phenotype *in vivo*. These cells produce many inflammatory cytokines *in vitro* and cause significant changes to the cytokine and chemokine milieu of the TME and periphery, notably increasing expression of immune recruiting chemokines such as CXCL9 and CXCL10. Using high dimensional analysis, we found the TME of CARD11-PIK3R3 CAR treated animals was characterized by an increase in inflammatory myeloid populations. CARD11-PIK3R3 CAR treated animals ultimately succumb to antigen negative tumors, indicating that inclusion of

CARD11-PIK3R3 is insufficient for induction of epitope spread. Based on our findings here, we suggest three payloads or combinatorial therapies, PD1/PD-L1 checkpoint blockade, FLT3-L and IL-27, which we believe may work synergistically with CARD11-PIK3R3 to better endogenous immune system engagement and tumor rejection.

While results are still preliminary, we find that co-expression of FLT3-L or co-expression of IL-27 greatly improves CARD11-PIK3R3 CAR T cell response, resulting in nearly full tumor clearance. In future studies, CARD11-PIK3R3 CAR-FLT3L or CARD11-PIK3R3 CAR-IL-27 treated animals will be rechallenged with antigen negative tumor rechallenges and endogenous TCR sequencing will be performed and to determine the extent of epitope spread. Finally, we will seek to characterize the TME and periphery of these CARD11-PIK3R3 CAR + payload treated animals to better understand mechanisms of full tumor rejection.

3.9. Methods

Vector Construction

Murinized CARs were constructed using a CD8α signaling peptide (MALPVTALLLPLALLLHAARP) followed by the FLAG-tag (DYKDDDK) and scFv, which was either anti-CD19 (FMC63) or anti-ALPPL2 ($M25^{FYIA}$). This extracellular region was fused to a murine CD8a hinge/transmembrane domain, and murine 4-1BB and CD3z intracellular domains. CAR constructs, without additional payloads, contained a T2A self-cleaving peptide followed by enhanced green fluorescent protein (eGFP) to assess expression. All CARs were cloned into a retroviral MSCV vector. CARs with additional payloads were constructed by replacing the eGFP with murine FLT3-L or IL-27 sequences, and CAR expression was assessed by FLAG staining. To construct the CARD11-PIK3R3 payload, human CARD11-PIK3R3 followed by a self-cleaving T2A and mCherry sequence was cloned into the retroviral MSCV vector. For ectopic expression of human CD19 and human ALPPL2, coding sequences were cloned into the pHR′SIN:CSW vector under an EF1a constitutive promoter. For ALPPL2 a hemagglutinin (HA)–tag (YPYDVPDYA) was inserted 3′ of its predicted signaling peptide (MQGPWVLLLLGLRLQLSLG). All constructs were cloned via Infusion cloning (Clontech #ST0345) or Gibson assembly.

Cell Lines

The cancer cell lines used were K562 myelogenous leukemia cells (ATCC #CCL-243), B16-F10 melanoma cancer cells (ATCC #CRL-6475), 40L mesothelioma cancer cells (a gift from the Coussens Lab), KPCY-2838c3 (Kerafast # EUP013-FP) and KPCY-6499c4 (Kerafast # EUP015-FP) pancreatic cancer cells. Lentivirus was produced with Lenti-X 293ts (Clontech

#11131D). K562s, B16-F10, KPCY-2838c3 and KPCY-6499c4 were lentivirally transduced to stably express human CD19. CD19 levels were determined by flow cytometry (Biolegend, clone HIB19), and all cell lines were sorted for purified CD19 expression. 40Ls were lentivirally transduced to stably express human ALPPL2 with an HA tag. HA tag expression (Biolegend, clone 16B12) was used as a proxy for ALPPL2 expression levels during flow cytometry and sorting for a purified population. K562 cells were cultured in IMDM + 10% FBS with penicillin/streptomycin and sodium pyruvate. Lenti-X 293ts, B16-F10s, 40Ls and KPCY cell lines were cultured in DMEM + 10% FBS with penicillin/streptomycin and sodium pyruvate. All cell lines were routinely tested for mycoplasma contamination.

Retrovirus Production and Transduction of Murine T Cells

Pantropic VSV-G pseudotyped retrovirus was produced via transfection of Lenti-X 293T cells (Clontech #11131D) with a MSCV transgene expression vector and the viral packaging plasmid pCL-Eco (Addgene #12371) using Fugene (Promega #E2311). CD4, CD8 or CD3+ T cells were isolated from the spleens of C57BL/6, C57BL/6-Tg(TcraTcrb)1100Mjb/J, B6.SJL-*Ptprc*^{a} *Pepc*^{b}/BoyJ, or B6J.129(Cg)-Igs2tm1.1(CAG-cas9*)Mmw/J mice using Mojo Sort Negative Selection kits (Biolegend # 480033,# 480035 or #480031). Mouse T cells were activated for 24 hours using anti-CD3/anti-CD28 Mouse T-Activator Dynabeads (Invitrogen #11453D), and cultured in RPMI + 10% FBS with HEPES, b-mercaptoethanol, NEAA, sodium pyruvate penicillin/streptomycin, and 100U/mL recombinant IL-2. Retroviral supernatants were added to T cells in Retronectin (Takara) coated plates and spinduction was performed for 1 hour at 2000xg at 30°C. For experiments requiring TCR knockout, T cells were harvested from CAS9 mice and AAV containing TCRb targeting guides was added at 3e5 MOI post spinfection. After

24 hours, Dynabeads were removed and T cells were resuspended and cultured in fresh media containing 100 U/mL IL-2 until adoptive transfer or *in vitro* assay. Transduction efficiency was determined by flow cytometry prior to adoptive transfer.

In vitro Luminex Assay

Engineered murine T cells were co-cultured with antigen positive target cells at a ratio of 1:1, T cells were plated based on their CAR+ percentage. 24 hours post co-culture, cells were pelleted, and supernatants were collected and sent to Eve Technologies for Luminex assessment of 32 chemokines and cytokines.

In vivo Assays

C57BL/6 or B6.SJL-*Ptprc*^{a} *Pepc*^{b}/BoyJ male mice ages 7-12 weeks were dosed subcutaneously with tumor cells. Murine T cells were manufactured as described above, and CAR+ mouse T cells were adoptively transferred via retro-orbital injection, no preconditioning was performed on recipient mice before T cell transfer. Tumor volume was measured 2-3x weekly, using the following equation: (length x width^{2})/2. Mice were euthanized when tumors reached 2000mm^{3} or measured 20mm in any direction or those with progressively ulcerating tumors. Tumors below 50mm^3 or above 150mm^3 were excluded for tumor growth curves in hALPPL2-40L groups. αPD-L1 checkpoint therapy was dosed via I.P. injection at 100ug/100ul PBS.

40L In vivo Assay Midpoint Assessment

A subset of mice was euthanized at 7 days post T cell transfer, and blood, spleen, tumor and tumor draining lymph nodes were harvested for Luminex and CyTOF analysis. Blood was collected via cardiac puncture and allowed to clot at room temperature for 30-60 minutes, after which serum was isolated by centrifuging clotted blood at 2000xg for 10 minutes at room temperature. Blood serum was diluted 1:1 with PBS and stored at -80C before shipment to Eve Technologies. Tissue serum was collected by gently mashing tissues in a standard volume of PBS to create tissue homogenate. Tissue homogenate was centrifuged at 500xg for 5 minutes at room temperature, the pelleted tissue was further processed to isolate single cells for CyTOF analysis and resulting supernatant was transferred to new tube and centrifuged at 2000xg for 10 minutes to pellet any remaining debris. Tissue homogenate serum was collected, diluted 1:1 with PBS and stored at -80C before shipment to Eve Technologies. Tissue homogenates were processed to single cell suspension and a small aliquot was stained with murine CD45 and live/dead DRAQ7 before being run on flow to count total hematopoietic cell number from each tissue.

CyTOF Cisplatin and Fixation

Single cell suspensions were stained with Cisplatin (diluted 1:2000) for 1 minute on ice. Cells were immediately quenched with PBS with EDTA plus BSA, washed and transferred to a cluster tube. Cells were then fixed with 1.6% PFA for 10 minutes, and washed 3 times with PBS supplemented with BSA. Fixed cell pellets were stored at -80C until ready for barcoding and staining.

CyTOF Barcoding and Staining

When ready to barcode and stain, cell pellets were thawed at room temperature for 20 minutes, washed and subsequently resuspended in PBS with 0.02% saponin. 20-plex Pd barcodes were resuspended in PBS with 0.02% saponin and immediately added to cluster tubes, staining for 15 minutes at room temperature while shaking. Barcoded samples were washed 3 times, then combined to one 15mL conical tube for staining. Combined pellets were resuspended with 5ul of FC block for 5 minutes, followed by the addition of the extracellular stain and incubation at room temperature for 30 minutes while shaking. Cells were then washed twice, and permeabilized with 1mL of ice cold MeOH for 10 minutes. Samples were washed three times, and incubated with the intracellular stain for 30 minutes at room temperature while shaking. Cells were washed twice more, before being resuspended in PBS with 4% PFA and intercalator (diluted 1:5000) and stored at 4C until run of CyTOF. Just before CyTOF run, cells were washed 3 times, then resuspended in Cell Acquisition Solution (Maxpar® Cell Acquisition Solution Plus for CyTOF® XT) with EQ four Calibration beads (Standard Biotools 201078) for downstream normalization.

CyTOF Analysis

FSC files were normalized and debarcoded using the Premessa pipeline (https://github.com/ParkerICI/premessa) and uploaded to Cell Engine for manual gating of immune populations. Hematopoietic cells (CD45+) were exported as FCS files and run through the CytoNorm normalization pipeline (https://github.com/saeyslab/CytoNorm) to allow for intra-barcode plate comparisons. A normalization control composed of cells from tumor, blood and spleen samples of a control C57BL/6 mouse was included in each barcode plate to allow

for normalization. Normalized, debarcoded, hematopoietic cell FCS files were then run through the CATALYST pipeline (https://rdrr.io/bioc/CATALYST/) for unbiased clustering, high dimensional visualization, protein expression heatmaps, and statistical analysis of differential cluster abundance. Manual gating of major immune cell populations was performed as described in Allen et. al 2020. Absolute cell counts were back calculated based on frequencies calculated from CyTOF and total CD45+ cell counts acquired from each tissue using flow cytometry during midpoint takedown processing. Statistically significant differences in population frequencies and absolute cell counts or counts/g of tissue were calculated with a two way T test.

3.10. Figures

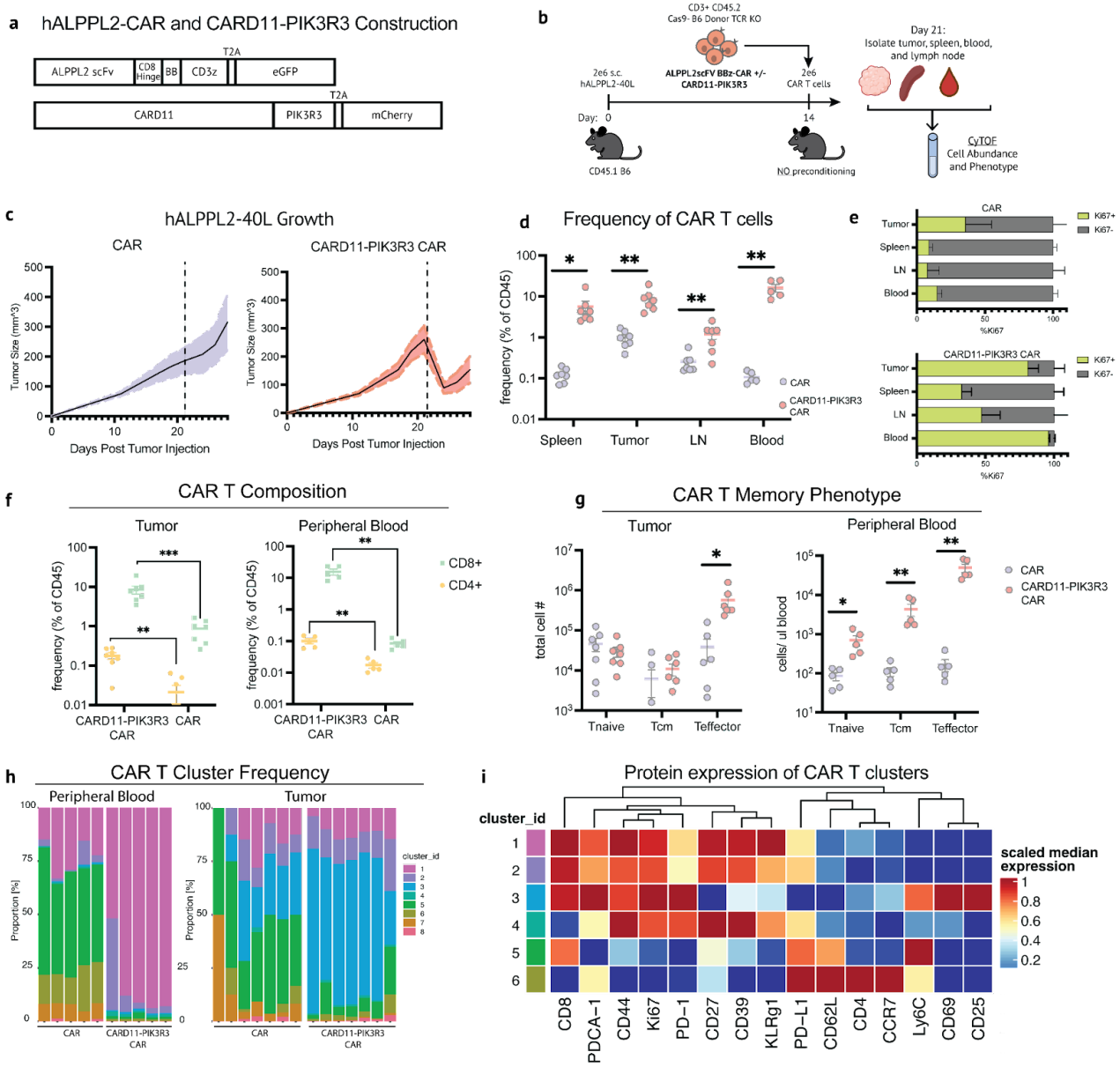

Figure 3.1 CARD11-PIK3R3 T Cells Demonstrate Greater Expansion and Increased numbers of T Cell Memory Phenotype in periphery

(a) Schematic of hALPPL2-CAR and CARD11-PIK3R3 construct design. **(b)** Schematic depicting hALPPL2-40L *in vivo* experiment timeline. **(c)** hALPPL2-40L tumor growth curves of CAR and CARD11-PIK3R3 CAR treated mice. **(d)** Frequency of manually gated CD45.2+ CAR T cells, as percent of CD45+ cells. P values determined by unpaired t-test. **(e)** Frequency of Ki67 positive cells, as percent of all CAR T cells. (Figure legend continued on the next page.)

(Figure legend continued from the previous page.) **(f)** CD4+ and CD8+ CAR T cell frequency, as percent of CD45+ cells. P values determined by unpaired t-test. **(g)** T cell subset phenotypes of CAR T cells determined by effector/effector memory (CD44+, CD61L-), Naïve (CD44-, CD62L+), and T central memory (CD44+, CD62L+), as measured by cell number per gram of tumor (left) and cells/uL in the blood (right). P values determined by unpaired t-test. **(h)** Stacked bar plots of relative cluster abundance of CD45.2+ CAR T clusters using FlowSom unbiased clustering. **(i)** Heatmap of protein expression of 2 increasing and 2 decreasing CAR T specific clusters with CARD11-PIK3R3 treatment.

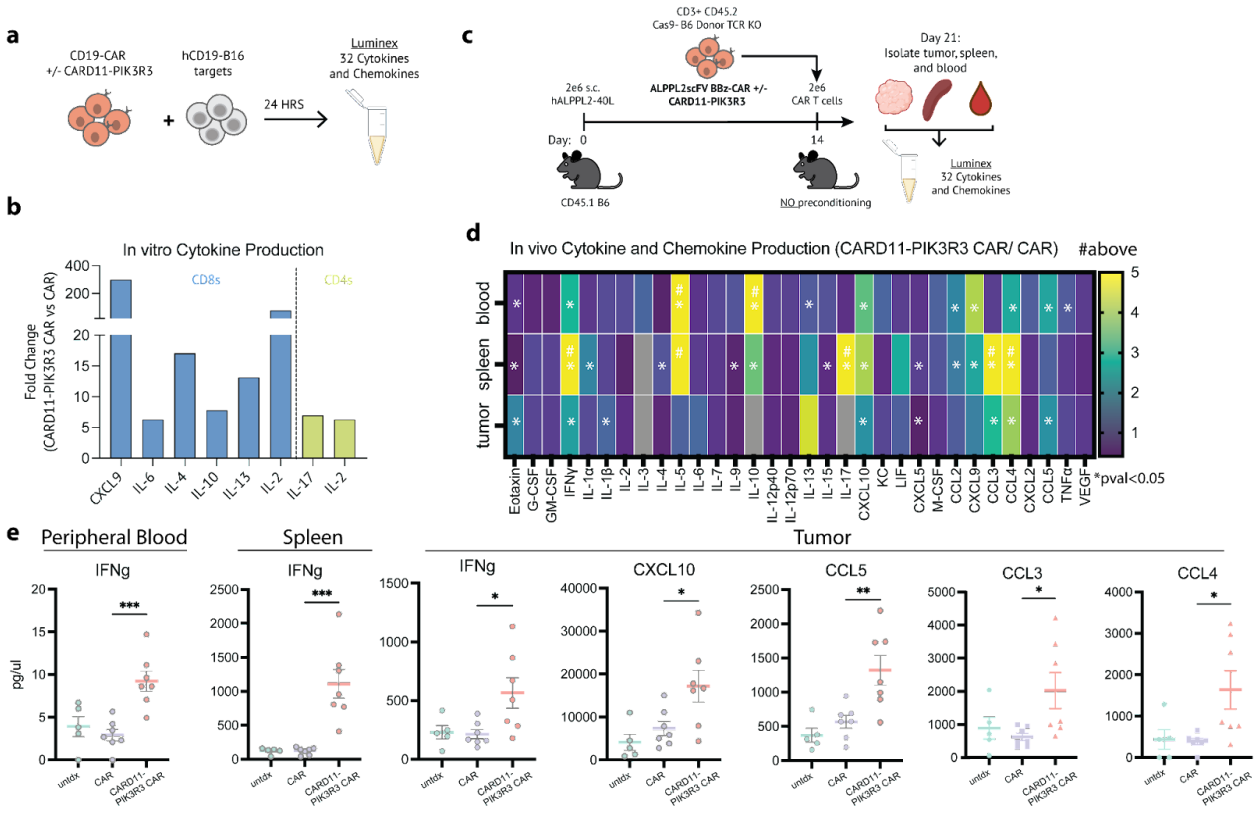

Figure 3.2 CARD11-PIK3R3 CAR T cells secrete higher levels of effector cytokines and chemokines *in vitro* and induce changes to mediator milieu *in vivo*

(a,c) Schematic depicting supernatant collection from *in vitro* co-culture assay (a) or serum collection from *in vivo* tissues (c). **(b)** Selected *in vitro* cytokines and chemokines, values depicted as fold change of CARD11-PIK3R3 CAR vs CAR. **(d)** heat map of fold change of median values of cytokines or chemokines expresses *in vivo* from CARD11-PIK3R3 CAR vs CAR treated mice. P values determined by unpaired t-test and coloring determined by median fold change of CARD11-PIK3R3 vs CAR. **(e)** Selected *in vivo* cytokines and chemokines from peripheral blood, spleen or tumor of mice treated with untransduced, CAR, or CARD11-PIK3R3 CAR T cells.

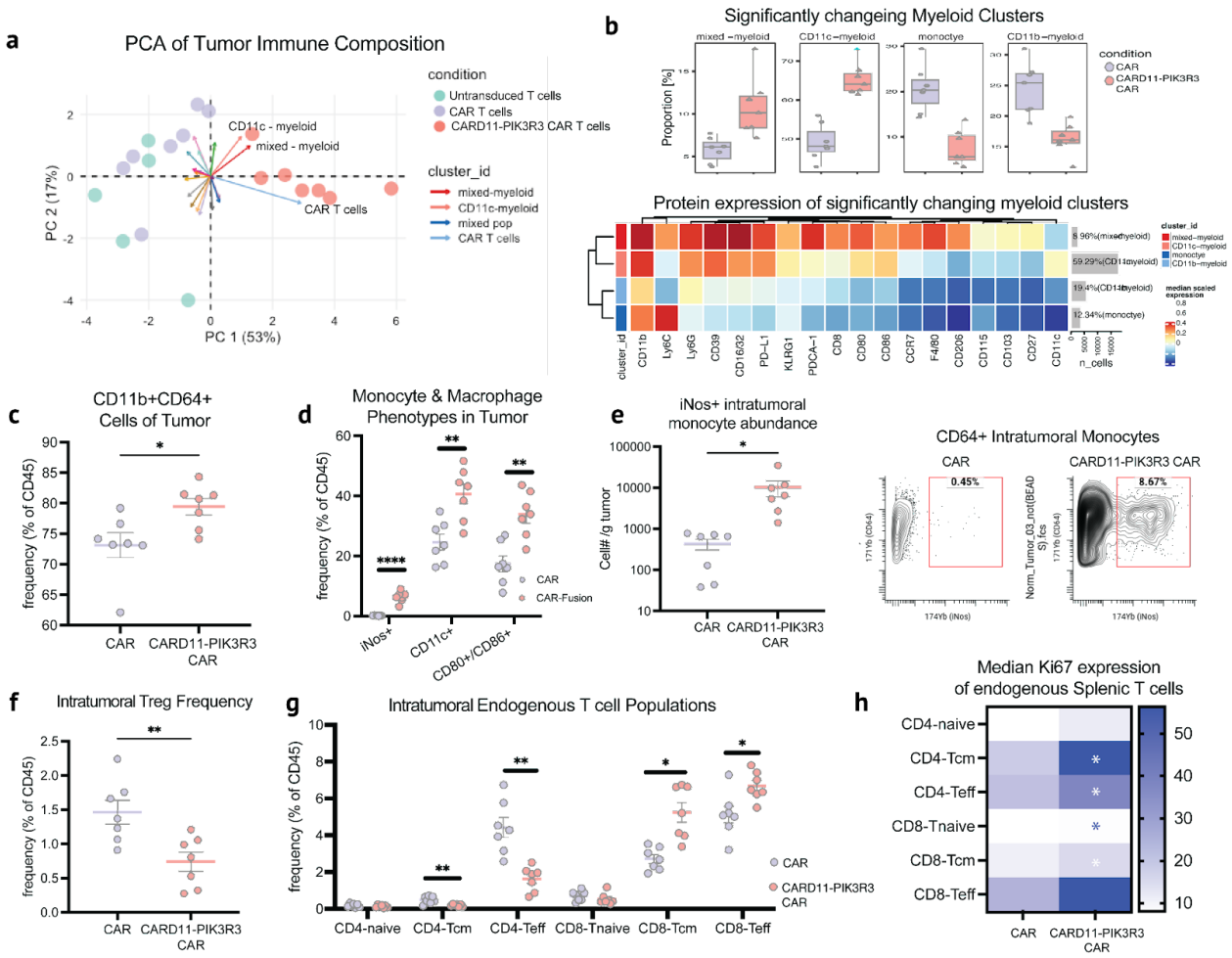

Figure 3.3 CARD11-PIK3R3 CAR T cells remodel the tumor microenvironment by increasing inflammatory myeloid compartment, decreasing regulatory T cells, and increasing cycling of endogenous local and peripheral T cells.

(a-b) FlowSOM cluster abundance analysis of 25 immune clusters across tumor, spleen, lymph node and tumor. PCA plot of cluster abundances within tumor (a). Four significantly changing myeloid clusters and relative abundance in CARD11-PIK3R3 CAR vs CAR groups (b, top) and heatmap of characteristic protein expression depicted in clusters (b, bottom). **(c-d,f)** Manual gating of CD11b+CD64+ (c) or iNOS+, CD11c+, CD80+/CD86+ (d), or Treg (f) populations, depicted as percent of total CD45+ cells. **(e)** Number of iNOS+ monocytes per gram of tumor (left) and representative flow plots (right). **(g)** T cell phenotype of intratumoral endogenous T cells, depicted as percent of CD45+ cells. **(h)** Median Ki67 of endogenous T cells isolated from the spleen. P values determined by unpaired t-test and coloring determined by median Ki67 expression.

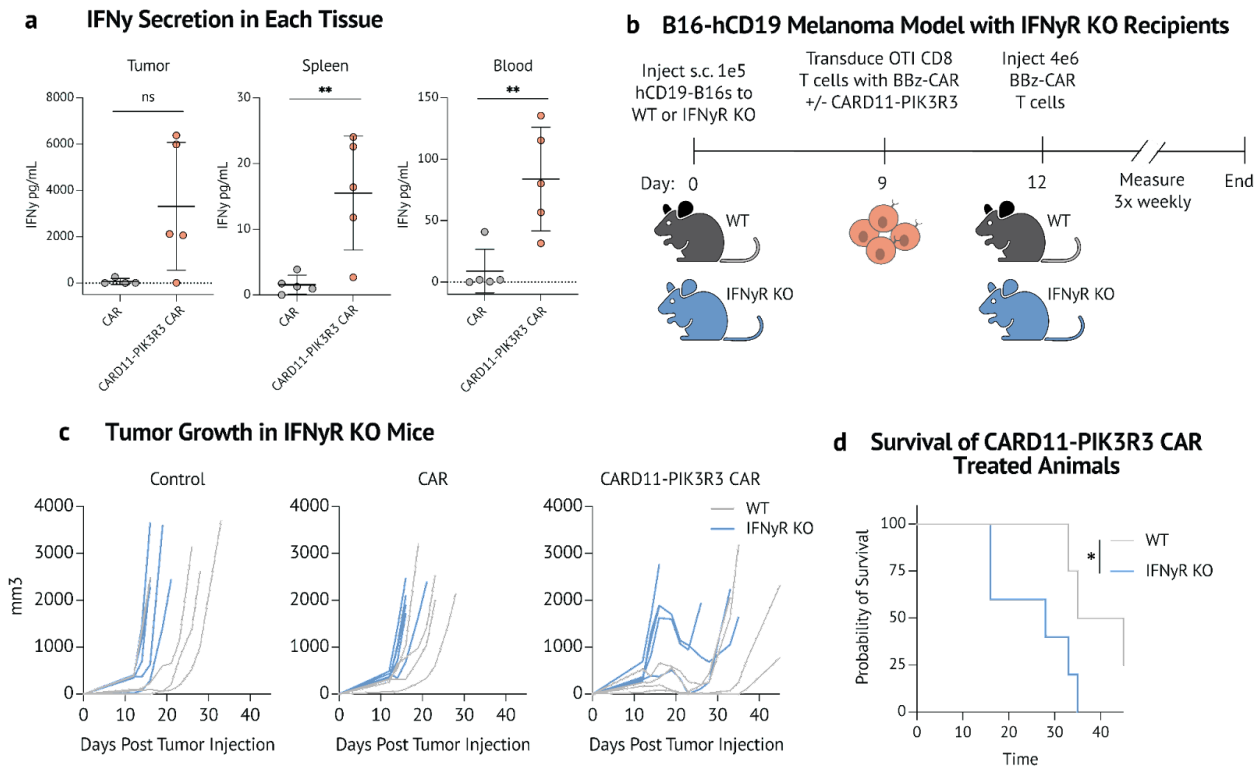

Figure 3.4 The Role of IFN-γ in CARD11-PIK3R3 CAR Anti-tumor Response

(a) IFN-γ serum levels of tumor, spleen and blood collected from hCD19-B16F10 tumor bearing animals treated with CAR or CARD11-PIK3R3 CAR T cells 5 days post T cell injection. **(b)** Schematic depicting control or CAR +/- CARD11-PIK3R3 treatment of hCD19-B16F10 tumor bearing animals of either wildtype (C57BL/6) or IFN-γRKO background. **(c-d)** hCD19-B16F10 tumor growth curves (c) and survival (d) of CAR and CARD11-PIK3R3 CAR treated mice.

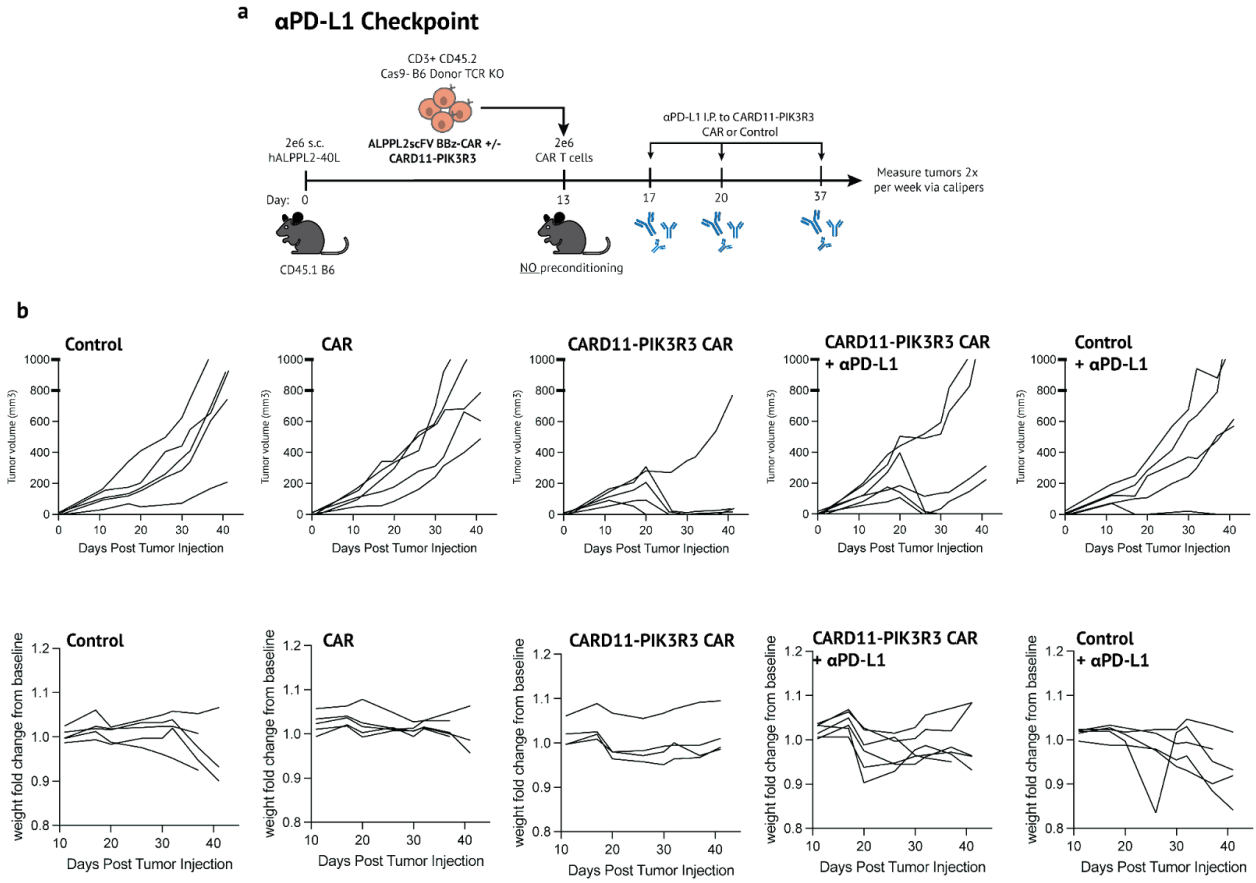

Figure 3.5 CARD11-PIK3R3 CAR + aPD-L1 Checkpoint Therapy

(a) Schematic depicting experimental timeline for hALPPL2-40L with aPD-L1 checkpoint *in vivo* experimental timeline. **(b)** hALPPL2-40L tumor growth curves (top) and animal weight change (bottom).

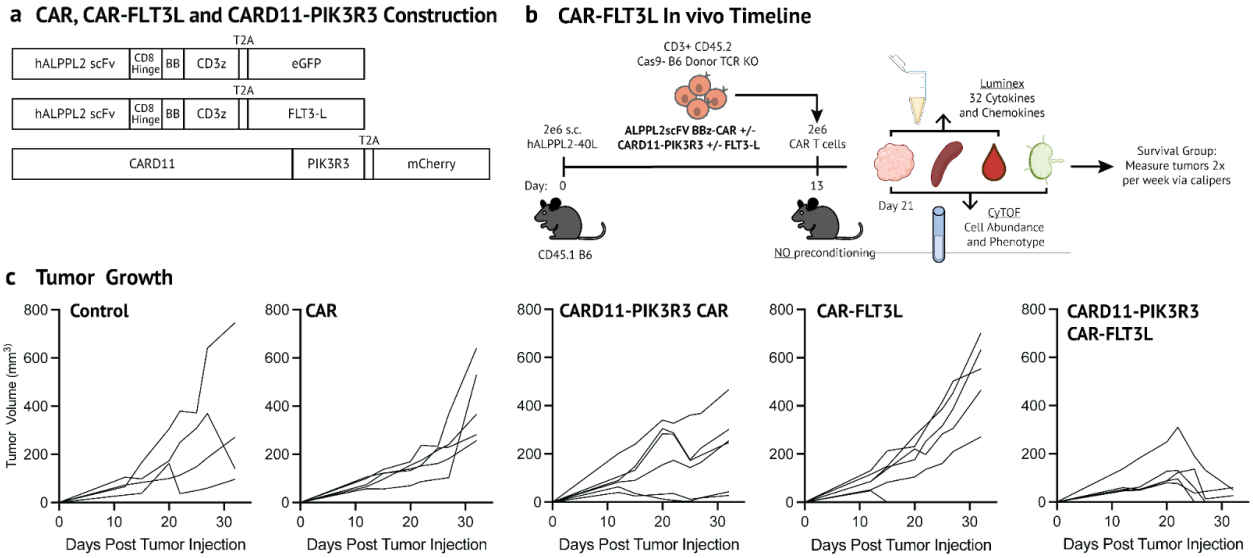

Figure 3.6 CARD11-PIK3R3 CAR with FLT3-L Payload

(a) Schematic of hALPPL2-CAR with and without FLT3-L payload, and CARD11-PIK3R3 construct design. **(b)** Schematic depicting experimental timeline for hALPPL2-40L *in vivo* with CAR mediated FLT3-L secretion. **(c)** hALPPL2-40L tumor growth curves.

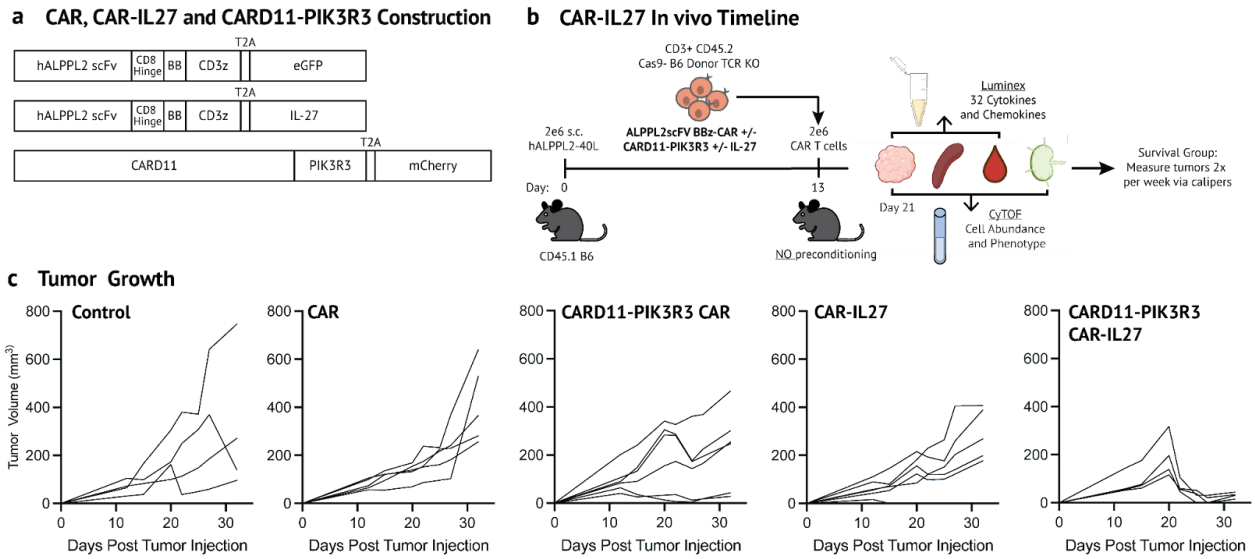

Figure 3.7 CARD11-PIK3R3 CAR with IL-27 Payload

(a) Schematic of hALPPL2-CAR with and without IL-27 payload, and CARD11-PIK3R3 construct design. **(b)** Schematic depicting experimental timeline for hALPPL2-40L *in vivo* with CAR mediated IL-27 secretion. **(c)** hALPPL2-40L tumor growth curves.

3.11. Extended Data Figures

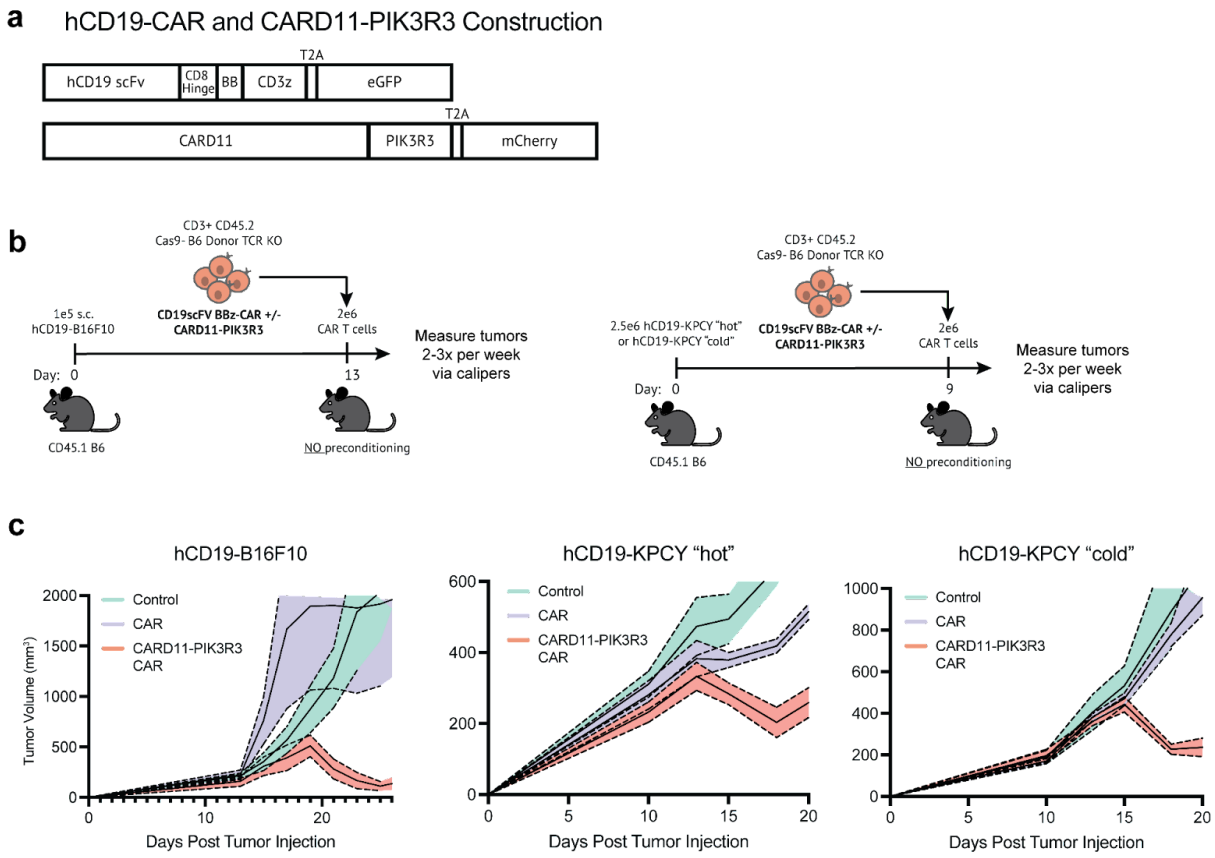

Extended Data Figure 3.1 CARD11-PIK3R3 CAR T Cells are Effective in Multiple Immunocompetent Tumor Models.

(a) Schematic of hCD19-CAR and CARD11-PIK3R3 construct design. **(b)** Schematic depicting hCD19-B16F10 (left) or hCD19-KPCY (right) *in vivo* experimental timeline. **(c)** hCD19-B16F10 (left), hCD19-KPCY "hot" (middle) or hCD19-KPCY "cold" (right) tumor growth curves.

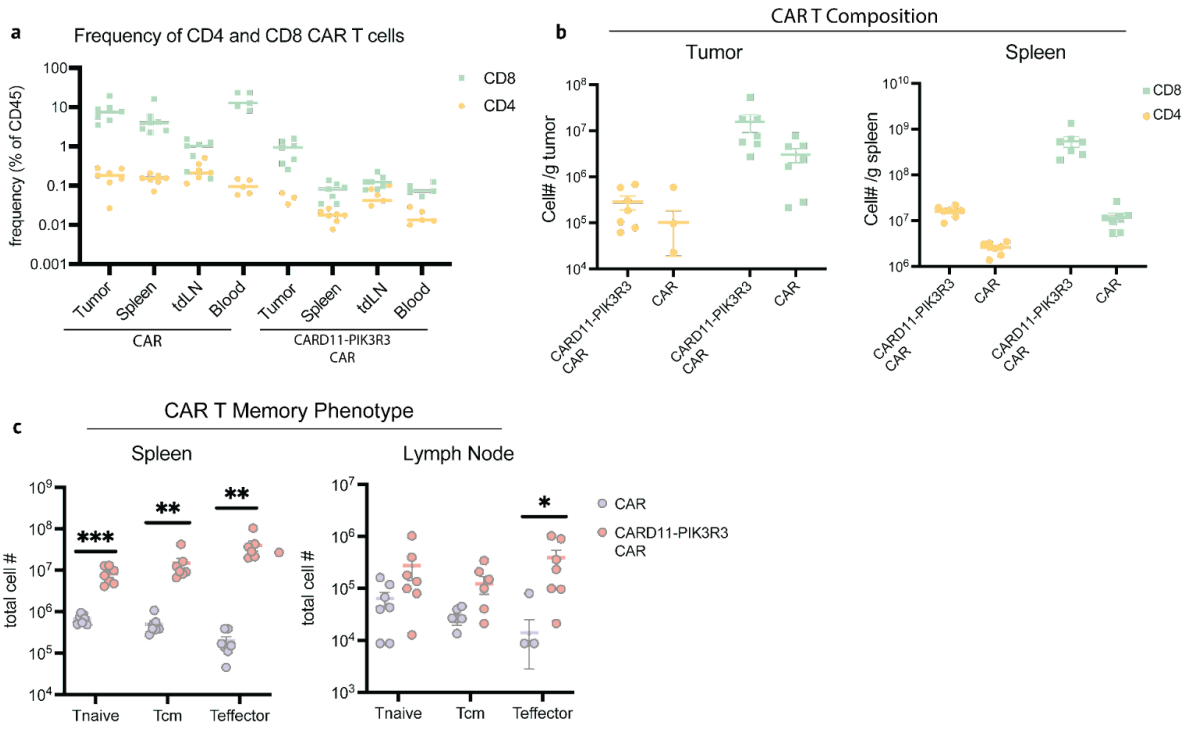

Extended Data Figure 3.2 CARD11-PIK3R3 CAR T Cell Phenotype and Composition

(a-b) CD4+ and CD8+ CAR T cell populations represented as a percent of CD45+ cells (a) or number per gram of tissue (b). **(c)** T cell subset phenotypes of CAR T cells determined by effector/effector memory (CD44+, CD61L-), Naïve (CD44-, CD62L+), and T central memory (CD44+, CD62L+), as measured by cell number per gram of tumor. P values determined by unpaired t-test.

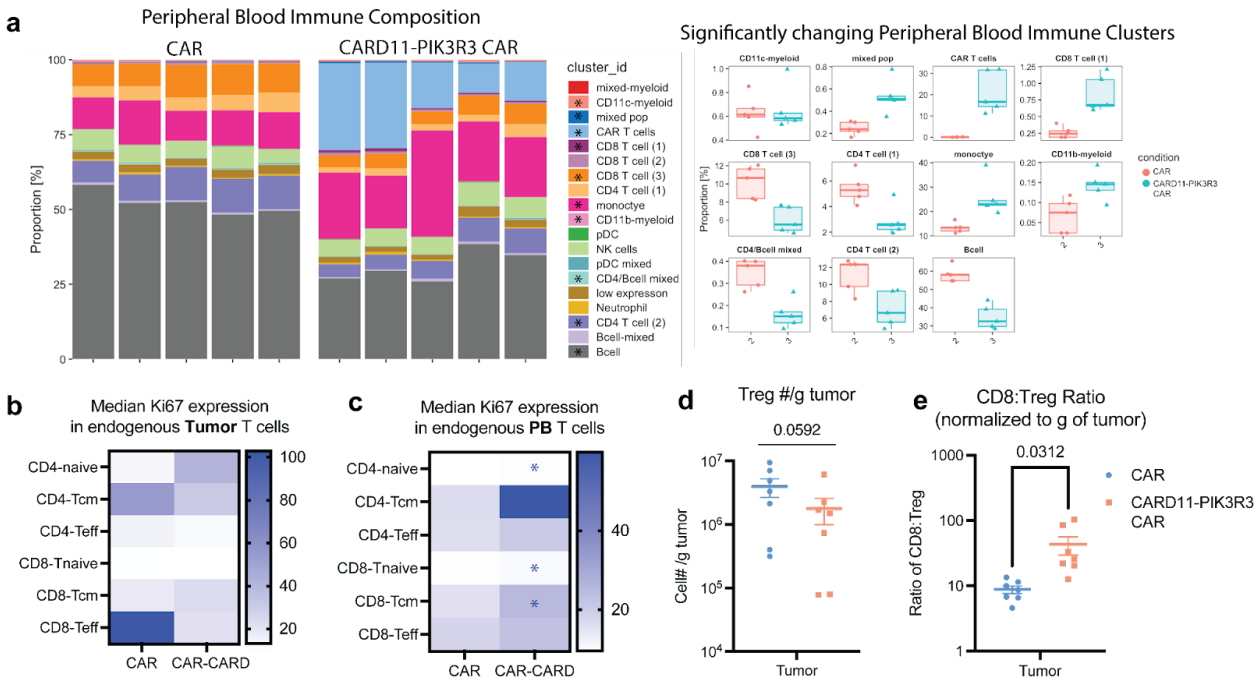

Extended Data Figure 3.3 Endogenous Immune Cell Phenotype and Composition

(a) Stacked bar plots of relative cluster abundance of CD45+ immune clusters of the blood using FlowSom unbiased clustering (left). Relative abundance of eleven immune clusters in CARD11-PIK3R3 CAR vs CAR groups (right). **(b-c)** Median Ki67 of endogenous T cells isolated from the tumor (b) and peripheral blood (c). P values determined by unpaired t-test and coloring determined by median Ki67 expression. **(d-e)** Number of Tregs (d) or the ratio comparing the number of CD8+ T cells to Tregs (e) normalized per gram of tissue within CAR and CARD11-PIK3R3 CAR treated tumors. P values determined by unpaired t-test.

3.12. References

1. Gooden, M. J. M., de Bock, G. H., Leffers, N., Daemen, T. & Nijman, H. W. The prognostic influence of tumour-infiltrating lymphocytes in cancer: a systematic review with meta-analysis. Br. J. Cancer 105, 93–103 (2011).
2. Julie Garcia, Jay Daniels, Yujin Lee, Iowis Zhu Kathleen Cheng, Qing Liu, Daniel Goodman, Cassandra Burnett, Calvin Law, Chloe Thienpont, Josef Alavi, Camillia Azimi, Garrett Montgomery, Kole T. Roybal, Jaehyuk Choi. Naturally occurring mutations in human T cell lymphomas enhance engineered T cell therapies. Nature. In Review.
3. Tokunaga, R. et al. CXCL9, CXCL10, CXCL11/CXCR3 axis for immune activation - A target for novel cancer therapy. Cancer Treat. Rev. 63, 40–47 (2018).
4. Schaller, T. H., Batich, K. A., Suryadevara, C. M., Desai, R. & Sampson, J. H. Chemokines as adjuvants for immunotherapy: implications for immune activation with CCL3. Expert Rev. Clin. Immunol. 13, 1049–1060 (2017).
5. Spranger, S., Bao, R. & Gajewski, T. F. Melanoma-intrinsic β-catenin signalling prevents anti-tumour immunity. Nature 523, 231–235 (2015).
6. Jin, J. et al. CCL2: An Important Mediator Between Tumor Cells and Host Cells in Tumor Microenvironment. Front. Oncol. 11, 722916 (2021).
7. Van Gassen, S. et al. FlowSOM: Using self-organizing maps for visualization and interpretation of cytometry data. Cytometry A 87, 636–645 (2015).
8. Früh, K. & Yang, Y. Antigen presentation by MHC class I and its regulation by interferon gamma. Curr. Opin. Immunol. 11, 76–81 (1999).
9. Steimle, V., Siegrist, C. A., Mottet, A., Lisowska-Grospierre, B. & Mach, B. Regulation of MHC class II expression by interferon-gamma mediated by the transactivator gene CIITA. Science 265, 106–109 (1994).

10. Lai, J. et al. Adoptive cellular therapy with T cells expressing the dendritic cell growth factor Flt3L drives epitope spreading and antitumor immunity. Nat. Immunol. 21, 914–926 (2020).
11. Liu, Y. et al. Immune Cell PD-L1 Colocalizes with Macrophages and Is Associated with Outcome in PD-1 Pathway Blockade Therapy. Clin. Cancer Res. 26, 970–977 (2020).
12. Zou, W. & Chen, L. Inhibitory B7-family molecules in the tumour microenvironment. Nat. Rev. Immunol. 8, 467–477 (2008).
13. Freeman, G. J. et al. Engagement of the PD-1 immunoinhibitory receptor by a novel B7 family member leads to negative regulation of lymphocyte activation. J. Exp. Med. 192, 1027–1034 (2000).
14. Topalian, S. L. et al. Safety, activity, and immune correlates of anti-PD-1 antibody in cancer. N. Engl. J. Med. 366, 2443–2454 (2012).
15. Topalian, S. L. et al. Survival, durable tumor remission, and long-term safety in patients with advanced melanoma receiving nivolumab. J. Clin. Oncol. 32, 1020–1030 (2014).
16. Chamoto, K., Yaguchi, T., Tajima, M. & Honjo, T. Insights from a 30-year journey: function, regulation and therapeutic modulation of PD1. Nat. Rev. Immunol. (2023) doi:10.1038/s41577-023-00867-9.
17. Spranger, S. et al. Up-regulation of PD-L1, IDO, and T(regs) in the melanoma tumor microenvironment is driven by CD8(+) T cells. Sci. Transl. Med. 5, 200ra116 (2013).
18. Broz, M. L. et al. Dissecting the tumor myeloid compartment reveals rare activating antigen-presenting cells critical for T cell immunity. Cancer Cell 26, 638–652 (2014).
19. Roberts, E. W. et al. Critical Role for CD103(+)/CD141(+) Dendritic Cells Bearing CCR7 for Tumor Antigen Trafficking and Priming of T Cell Immunity in Melanoma. Cancer Cell 30, 324–336 (2016).

20. Wilson, K. R., Villadangos, J. A. & Mintern, J. D. Dendritic cell Flt3 - regulation, roles and repercussions for immunotherapy. Immunol. Cell Biol. 99, 962–971 (2021).
21. Salmon, H. et al. Expansion and Activation of CD103(+) Dendritic Cell Progenitors at the Tumor Site Enhances Tumor Responses to Therapeutic PD-L1 and BRAF Inhibition. Immunity 44, 924–938 (2016).
22. Pflanz, S. et al. IL-27, a heterodimeric cytokine composed of EBI3 and p28 protein, induces proliferation of naive CD4+ T cells. Immunity 16, 779–790 (2002).
23. Huang, Z. et al. IL-27 promotes the expansion of self-renewing CD8+ T cells in persistent viral infection. J. Exp. Med. 216, 1791–1808 (2019).
24. Stumhofer, J. S. et al. Interleukins 27 and 6 induce STAT3-mediated T cell production of interleukin 10. Nat. Immunol. 8, 1363–1371 (2007).
25. Mayer, K. D. et al. Cutting edge: T-bet and IL-27R are critical for in vivo IFN-gamma production by CD8 T cells during infection. J. Immunol. 180, 693–697 (2008).
26. Liu, Z. et al. IL-27 enhances the survival of tumor antigen-specific CD8+ T cells and programs them into IL-10-producing, memory precursor-like effector cells. Eur. J. Immunol. 43, 468–479 (2013).
27. Jung, J.-Y., Roberts, L. L. & Robinson, C. M. The presence of interleukin-27 during monocyte-derived dendritic cell differentiation promotes improved antigen processing and stimulation of T cells. Immunology 144, 649–660 (2015).
28. Hisada, M. et al. Potent antitumor activity of interleukin-27. Cancer Res. 64, 1152–1156 (2004).
29. Salcedo, R. et al. IL-27 mediates complete regression of orthotopic primary and metastatic murine neuroblastoma tumors: role for CD8+ T cells. J. Immunol. 173, 7170–7182 (2004).

30. Salcedo, R. et al. Immunologic and therapeutic synergy of IL-27 and IL-2: enhancement of T cell sensitization, tumor-specific CTL reactivity and complete regression of disseminated neuroblastoma metastases in the liver and bone marrow. J. Immunol. 182, 4328–4338 (2009).

Chapter 4

Engineering Modular Multi-modal Receptors for Enhanced Cancer Cell Therapies

Material from this chapter comes from the following work:

Garcia J.*, Foisey M.*, Hyrenius-Wittsten A., Liu R., Zhu I., Roybal K. T. Engineering modular multi-modal receptors for enhanced cancer cell therapies. (2023). Manuscript in Preparation.

*These authors contributed equally to this work.

4.1. Abstract

CAR T cell therapies, while highly effective in leukemias, have struggled to make impact in solid tumors where hostile tumor microenvironments result in poor infiltration, proliferation, inhibition of function and loss of CAR T cell persistence. Previously developed synthetic Notch (synNotch) and synthetic intramembrane proteolysis receptors (SNIPRs) allow for control and customization of therapeutic immune cells. SNIPR T cells can deliver user-defined cell intrinsic or extrinsic payloads, such as transcription factors, cytokines, and antibodies in an antigen specific, spatially controlled manner. While these receptor circuits could be used to address the many challenges of complex tumors, these receptors lack the ability to initiate proliferative and cytotoxic programs like CARs or TCRs, limiting their ability to expand, deliver payload and kill. Therefore, successful and persistent engineered T cells require both the ability to recognize, activate and kill tumor cells, as well as the ability to produce payloads to counteract a wide range of challenges encountered in solid tumor microenvironments.

Here, we have engineered a novel ‘Hybrid’ SNIPR CAR receptor, called HYBRID-Rs, whose architecture incorporates signaling domains (e.g. co-stimulation, CD3z, etc.) that can initiate activation of T cells concomitant with custom transcriptional regulation typical of a synNotch receptor. These HYBRID-Rs are functional and represent a new class of synthetic receptors that activate short timescale signaling and long term custom transcriptional responses in a single receptor architecture. In particular, we have utilized HYBRID-Rs to control the expression of the recently discovered CARD11-PIK3R3 protein.

4.2. Introduction

CAR T cell therapies redirect a patient's own T cells towards their cancer, acting in an antigen specific manner to eliminate cancer cells while ignoring healthy non-cancerous tissue. These therapies present promising avenues for treatment of refractory solid and hematological cancers, and in fact multiple CD19 targeted CAR T cell therapies have been approved for treatment of refractory B cell leukemias and lymphomas[1,2]. While these therapies initially show promising results, a large proportion of these patients eventually undergo relapse in part due to antigen loss[3]. Beyond antigen loss, CAR T cell therapies commonly fail due to their inability to persist, proliferate and perform effector function long term[4]. Often, in solid tumors, the tumor microenvironment is immunosuppressive, secreting inhibitory factors such as TGFb, and expressing inhibitory ligands such as PD-L1, all leading to an ineffective CAR T cell response. Additionally, neoplasms often recruit supportive tissue and immune cells to establish and maintain a pro-tumor environment[5]. Overall, CAR T cell therapies are very promising, but are limited in their capacity to overcome the complex, and diverse set of challenges that different cancer types present (Fig. 4.1). To address these challenges, CAR T cell therapies need advanced engineered functions such as the ability to secrete cytokines or express potent modifiers that induce long-term persistence and proliferation, or produce transcription factors that help maintain effector function, secrete enzymes or antibodies that can counteract immunosuppressive environments or express secondary CARs to attack heterogeneous tumors.

Previously developed synNotch receptor circuits allow for cells to sense user-defined extracellular inputs (e.g. tumor or tissue-related antigens) and drive the expression of therapeutic gene programs, such as secretion of a cytokine or expression of a CAR (Fig. 4.1)[6–8]. Recently, the Roybal lab have designed simple receptors that only include an scFv, a hinge domain from CD8, the y-secretase cleavable Notch TMD, and the highly positively charged

STS. These synthetic intramembrane proteolysis receptors (SNIPRs) are compact and more highly expressed in primary T cells[9]. Additionally, these receptors have minimal basal activity while exhibiting enhanced transcriptional induction as compared to the original synNotch designs. SNIPRs, while effective at induction of user defined payload transcription, do not stimulate signaling that can quickly initiate cellular processes such as metabolic reprogramming, proliferation, growth factor production, or cytotoxicity like CARs or TCRs. Here, we sought to develop a single receptor architecture that could elicit both fast timescale signaling through kinase cascades and long term transcriptional activity similar to that of a SNIPR (Fig. 4.1). We demonstrate the need to optimize intracellular signaling domains to achieve highest transcriptional output while inducing cytotoxic capabilities. We show that these receptors can be built with multiple different costimulatory domains and adapted for use with a variety of antigen targeting scFvs. Finally, we have paired these receptors with the recently discovered onco-fusion potency enhancer, CARD11-PIK3R3, resulting in improved anti-tumor efficacy with a hypothesized more favorable safety profile.

4.3. HYBRID-Rs: Short-term Proximal Signaling with Long-Term Genetic Circuitry

Previously published synNotch receptors induce differing levels of transcriptional activation, indicating that the notch proteolytic cleavage event is tunable, based on receptor design[9]. This data suggests that a portion of the synthetic notch receptors, when bound by antigen, do not result in cleavage of the intracellular tail and instead remain bound at the cell membrane. In theory, this pool of receptors that remain uncleaved at the plasma membrane should be able to signal while the fraction of receptors that undergo full cleavage can drive expression of the custom gene circuit. To develop HYBRID-Rs, we first sought to determine if

and how costimulatory and ITAM containing proximal signaling domains could be included in the intracellular tail of SNIPR. We constructed 6 CD19 targeted HYBRID-Rs, modulating the placement of each of the three internal signaling regions (4-1BB costimulatory domain, CD3z ITAM containing domain, Gal4-VP64 transcription factor) (Fig. 4.2a). Intracellular domains were separated by 4x GS linkers. We found that all six configurations of these receptors could be successfully expressed by primary human T cells (Extended Data Fig. 4.1a).

We dually transduced primary human T cells with each receptor and the Gal4-VP64 response element driving a blue fluorescent protein (BFP) reporter, and sorted for a purified double positive population. Transduced T cells were then co-cultured at a 1:1 ratio with K562 cells with or without CD19 ligand expression. Forty-eight hours later we assessed co-cultures via flow for the expression of BFP and the activation marker CD69. HYBRID-Rs displayed a range of activity, somewhat dictated by which intracellular domain was closest to the transmembrane domain (TMD) (Fig. 4.2b). HYBRID-Rs with the 4-1BB costimulatory domain placed closest to the TMD displayed high circuit induction with CD19-K562s, but were leaky, turning on the circuit in the presence of CD19 negative K562s. Meanwhile, HYBRID-Rs with CD3z closest to the TMD were less leaky, but also exhibited lower circuit induction with CD19-K562s. Finally, the circuits with best antigen positive induction and lowest leak were those with the Gal4-VP64 transcription factor (TF) positioned nearest to the TMD. All variations of the HYBRID-Rs expressed CD69 upon stimulation with CD19-K562s, indicating that the proximal signaling domains were inducing T cell activation (Fig. 4.2c). Interestingly, the HYBRID-R with the greatest leak (BB-CD3z-TF) also expressed CD69 at a high rate when compared to a second generation BB-CD3z CAR, indicating that though there is significant cleavage and translocation of the internal signaling domains for transcription, there is still sufficient proximal signaling for activation.

Initially, we sought to further characterize a top candidate, the TF-BB-CD3z design, as this had the best signal to noise while also maintaining internal signaling domain configuration most similar to that of a second-generation CAR. We found that when stained with cell trace far red (CTFR) and co-cultured with CD19-K562s, the HYBRID-R (TF-BB-CD3z) T cells proliferate similarly to BB-CD3z CAR T cells (Fig. 4.2d). These receptors also performed similarly to the CAR in an Incucyte killing assay, indicating that the proximal signaling domains are functioning sufficiently to induce T cell activation and cytotoxicity programs (Fig. 4.2e). However, we noted that when activated with antigen positive targets, HYBRID-R configurations produced less IL-2 as compared to CAR, indicating that proximal signaling in HYBRID-Rs may not be as robust as that induced by a CAR (Fig. 4.2f).

To further challenge these receptors, we sought to determine if the HYBRID-R with the TF-BB-CD3z configuration could control tumor growth *in vivo*. We constructed a BCMA targeted HYBRID-R (TF-BB-CD3z) to use in comparison to a BCMA targeted BB-CD3z second generation CAR that we have previously found to be successful in controlling BCMA expressing K562 tumors (BCMA-K562). While the BCMA HYBRID-R exhibited slightly less circuit induction, we found that it was still a clean circuit that induced T cell activation (Extended Data Fig. 4.1b). However, when dosed to BCMA-K562 tumor bearing animals we found the HYBRID-R (TF-BB-CD3z) T cells could not control K562 tumor growth while 4/5 animals dosed with CAR T cells fully cleared their tumors (Supplemental Fig. 4.1c).

4.4. Optimization of HYBRID-R Proximal Signaling

This poor *in vivo* efficacy in combination with the lack of IL-2 secretion suggested HYBRID-Rs were inducing suboptimal T cell activation. We found that the HYBRID-R with the best cytokine secretion was the BB-CD3z-TF configuration. We therefore sought to optimize the BB-CD3z-TF configuration, with the aim of reducing the circuit leak while maintaining T cell activation. We hypothesized that the amino acids closest to the cell membrane of 4-1BB might be inducing noise. We therefore designed two truncated versions of the BB-CD3z-TF HYBRID-Rs; the first which removed only the juxtamembrane domain, a basic rich string of residues that anchors the receptor within the cell membrane, of 4-1BB (ΔN6BB-CD3z-TF). The design second was further truncated, removing all amino acids from the N-terminus until just before the first TRAF binding site (ΔN17BB-CD3z-TF) (Fig. 4.3a). NF-kB transcriptional activity is one of the primary outputs of 4-1BB signaling[10]. Therefore, to quantify T cell activation of truncated HYBRID-Rs with a more direct output for 4-1BB signaling activity, we used an NF-kB signaling jurkat reporter cell line, which expresses mCherry upon NF-kB activity. We transduced this line with the HYBRID-Rs as well as first and second-generation CARs, then co-cultured with CD19-K562s for 24 hours before assessing NF-kB induction via flow (Fig. 4.3b). As expected, a first generation CD3z CAR induced little NF-kB signaling as compared to second generation BB-CD3z CAR. The leaky BB-CD3z-TF HYBRID-R also induced high NF-kB signaling, while the TF-BB-CD3z HYBRID-R had considerably less signaling, suggesting that the distance of 4-1BB from the cell membrane may be important for signaling output. We found that both the ΔN6BB-CD3z-TF and ΔN17BB-CD3z-TF HYBRID-Rs had increased NF-kB as compared to the TF-BB-CD3z HYBRID-R. In primary T cells co-transduced with the truncated HYBRID-Rs and the BFP reporter, we found that while the ΔN6 truncation significantly reduced antigen negative circuit induction, the ΔN17 exhibited very little circuit leak. Through simple truncations we were

able to boost the proximal signaling of the HYBRID-R, while fully ameliorating issues of basal transcriptional circuit activity (Fig. 4.3b).

We next sought to test the anti-tumor efficacy of this optimized HYBRID-R, using M28 tumors, which are a xenograft model of mesothelioma that naturally express the human tumor specific antigen ALPPL2[11,12]. We constructed an ALPPL2 targeted HYBRID-R ΔN17BB-CD3z-TF, then transduced primary CD3+ T cells with this receptor and the BFP reporter. As we observed with the BCMA HYBRID-R ΔN17BB-CD3z-TF, the ALPPL2 targeted receptor circuit exhibited slightly less transcriptional output however we found that it was still a clean circuit that induced T cell activation (Extended Data Fig. 4.2b). We adoptively transferred 4 x 10^6 control, CAR or HYRBID-R T cells to M28 tumor bearing mice 7 days post tumor implantation. Both CAR and HYBRID-R T cells controlled tumor growth over approximately 35 days, while control T cells did not. This data set demonstrates that ΔN17BB-CD3z-TF HYBRID-Rs can perform CAR-like anti-tumor function while maintaining antigen specific transcriptional genetic circuit control.

4.5. HYBRID-Rs with CD28 Costimulatory Domains

CD28 is another costimulatory domain commonly used in second-generation CAR T cells. CD28 CARs are generally thought to lack some of the persistence of 4-1BB CARs, however they also induce faster target killing *in vitro* and more rapid tumor clearance *in vivo* as compared to 4-1BB CARs [13–15]. CD28 costimulatory domain CARs have found success in the clinic, including several products approved for commercial clinical use by the FDA. Therefore, we sought to expand the modalities of HYBRID-Rs by designing receptors with CD28

costimulation. Similar to the 4-1BB designs, we began by constructing 6 CD19 targeted CD28 containing HYBRID-Rs, each with a different orientation of the three intracellular domains, separated by GS linkers (Extended Data Fig. 4.3a). We transduced these receptors to primary human T cells along with the BFP reporter and co-cultured them with antigen positive or negative targets. All 6 HYBRID-Rs induced T cell activation, as measured by CD69 expression, in response to co-culture with antigen positive targets (Extended Data Fig. 4.3b). Similar to the 4-1BB receptor suite, we noticed a variety of transcriptional signaling outputs (Extended Data Fig. 4.3b), however in general CD28 receptors exhibited a higher amount of antigen negative circuit induction, or leak. The receptors with CD28 positioned closest to the membrane induced high circuit induction, regardless of antigen state, producing receptors that were “always on”. While those with CD3z first were less productive circuits, though with less noise. Finally, unlike the 4-1BB receptors, we found that even the TF first receptors were quite leaky, though they exhibited higher circuit induction in the presence of CD19-K562s.

While the CD3z-TF-CD28 HYBRID-R demonstrated lower circuit induction, it was the cleanest circuitry overall, and we therefore decided to further characterize its activity (Fig. 4.4a). *In vitro* CD3z-TF-CD28 HYBRID-R T cells proliferated and induced target killing similar to CD28-CD3z CARs (Fig. 4.4b,c). When assessed in the xenograft leukemia model of Nalm6, we found that both CD28-CD3z CAR and CD3z-TF-CD28 HYBRID-R T cells controlled tumor burden, while control T cells did not (Fig. 4.4d,e,f). This data set suggested that CD28 HYBRID-Rs are functional *in vivo*, however circuit induction was limited in the best design.

We therefore sought to optimize the CD28 containing HYBRID-Rs, following a similar methodology as with the 4-1BB receptors. Some of the best circuit induction was observed in receptors with CD28 proximal to the cell membrane, however similar to 4-1BB, these were highly leaky circuits. In the original 6 designs we observed that some of the leak was improved

when CD28 was moved farther from the cell membrane, we therefore sought to determine if the presence or length of a flexible GS linker could affect circuit induction. In primary human T cells, we found that both the removal (no GS linker) or extension (8x GS) of the GS linker between the TMD and CD28 intracellular domain caused greater circuit leak (Extended Data Fig. 4.3c).

We next turned to a truncation approach. CD28 has 3 main signaling motifs (Extended Data Fig. 4.3c), YMNM which recruits PI3K and Grb2, PRRP which binds ITK, and PYAP which can bind both Grb2 and Lck [16]. In CD28-CD3z CAR T cells, previous studies have demonstrated that the PYAP signaling motif is sufficient to induce long term, anti-tumor activity [17]. We hypothesized that truncation of CD28 may reduce circuit leak, and therefore developed a CD28-CD3z-TF with 21 amino acid truncation from the N terminus of CD28, which preserves the PYAP region. In primary human T cells, we found this truncated CD28 HYBRID-R exhibited high antigen specific circuit induction with low leak (Extended Data Fig. 4.3c,d). Further *in vitro* and *in vivo* experimentation is required to fully characterize the CAR and circuit capacities of this optimized receptor. Altogether, this data set again proves that costimulatory and ITAM containing domains can be included in SNIPR architectures to induce T cell activation, however costimulatory domain specific optimization likely needs to occur to achieve the best circuit induction while maintaining T cell activation programs.

4.6. Benchmarking to TCR Response Elements

Other groups have developed methods for antigen or T cell activation gated expression of genetic payloads. One such example is the use of TCR response elements (REs), in which a genetic cassette of choice can be placed downstream of a transcriptional promoter that is

activated during T cell activation, such as NFAT. NFAT response elements were initially developed to induce fluorescent protein expression upon T cell activation, allowing for detection and tracking of activated T cells [18]. Further iterations have employed this NFAT promoter to deliver cytokines, such as IL-12, under T cell activating conditions [19]. Here, we sought to compare the HYBRID-R circuits with the established NFAT TCR RE (Fig. 4.5a). We constructed an NFAT-BFP reporter, stringing together four 30bp tandem repeats of the IL-2 promoter NFAT binding region followed by a YB TATA upstream of our fluorescent reporter, BFP (Fig. 4.5a)[20]. We dually transduced primary human T cells with a CD19 targeted BB-CD3z CAR and the NFAT reporter, and sorted for a purified double positive population. We manufactured CD19 targeted HYBRID-R (ΔN17BB-CD3z-TF) T cells with the BFP reporter as previously described. CAR + NFAT RE and HYBRID-R T cells did not exhibit BFP expression when cultured alone, indicating that both circuits have minimal leak in unstimulated conditions (Fig. 4.5b). When stimulated with CD19-K562s, HYBRID-R circuits are capable of inducing greater expression of the transcriptional circuit as compared to NFAT REs. Additionally, HYBRID-Rs are CAR antigen specific, triggering only when the CAR is present, while the NFAT RE is turned on by both CAR and TCR (Dynabead) stimulation (Fig. 4.5b). Overall, HYBRID-Rs are a more potent and orthogonal receptor circuit as compared to standard TCR REs.

4.7. Combining HYBRID-Rs with Payloads

Currently, CAR therapies struggle in solid tumor settings to achieve significant anti-tumor potency and long-term persistence. As a result, these expensive and high-risk therapies have seen failure time and again in the clinic. Recently, our group discovered a potent modifier of engineered T cells, the onco-fusion CARD11-PIK3R3. CARD11-PIK3R3, when co-expressed in

CAR or TCR therapies, induces secretion of potent effector molecules and cytokines, such as IL-2, enhances target killing even in the absence of exogenous IL-2, and induces dramatic tumor control in both xenograft and immunocompetent syngeneic tumor models. Most impressively, we have found that inclusion of CARD11-PIK3R3 alleviates the requirement for lymphodepleting regimens in syngeneic models of solid tumors. Previous data has demonstrated that CARD11-PIK3R3 CAR therapies are well tolerated *in vivo* long term[21]. However, when expressed in TCR replete primary human T cells and dosed to NSG mice, CARD11-PIK3R3 CAR T cells induced accelerated graft-versus-host disease (GVHD), a common finding in xenograft settings if the TCR is not knocked out[22]. Only in settings of TCR knockout was CARD11-PIK3R3 CAR therapy well tolerated. Furthermore, this finding was expanded to syngeneic settings, where GVHD is not typically an issue as donor T cells are derived from genetically identical recipients. Here, we believe auto-reactive TCRs present within the polyclonal T cell population were energized by CARD11-PIK3R3, resulting in lethal toxicity. This finding was again ameliorated upon murine TCR knockout.

To avoid TCR mediated toxicity and the requirement for TCR depletion, we sought to use HYBRID-R circuits for antigen controlled expression of CARD11-PIK3R3. We constructed a Gal4-VP64 response element driving CARD11-PIK3R3 with a self cleaving T2A sequence followed by a BFP reporter (CARD11-PIK3R3 T2A BFP RE). We co-expressed the CARD11-PIK3R3 T2A BFP RE with the HYBRID-R (ΔN17BB-CD3z-TF) in primary human T cells and sorted for a purified double positive population (Fig. 4.6a). When co-cultured with CD19-K562s, both the HYBRID-R driving BFP alone, and the circuit driving the CARD11-PIK3R3 T2A BFP RE exhibit high expression of BFP (Fig. 4.6b). The BFP MFI shift is less dramatic in the CARD11-PIK3R3 T2A BFP RE circuit, likely due to the size of CARD11-PIK3R3 which is transcribed first upstream of BFP. Additionally, we found that the

HYBRID-R (ΔN17BB-CD3z-TF) driving CARD11-PIK3R3 T2A BFP RE T cells secrete more IL-2 than the CAR or HYBRID-R alone, a phenotype typical of CARD11-PIK3R3 expression (Fig. 4.6c). This data set indicates that HYBRID-R circuit control of CARD11-PIK3R3 can induce known CARD11-PIK3R3 phenotypes in an antigen specific manner.

Finally, we sought to assess the anti-tumor efficacy of HYBRID-R circuits driving CARD11-PIK3R3 expression in an immunotherapy refractory solid tumor model of melanoma. To achieve this, we expressed human CD19 on the murine melanoma cell line, B16-F10. We transduced C57BL/6 murine T cells with a CD19 targeted murinized BB-CD3z CAR, with and without co-expression of CARD11-PIK3R3. Additionally, we manufactured HYBRID-R (ΔN17BB-CD3z-TF) T cells with a BFP RE, or HYBRID-R (ΔN17BB-CD3z-TF) with the driving CARD11-PIK3R3 T2A BFP RE. Of note, none of the HYBRID-R or CARD11-PIK3R3 sequences were murinized. We inoculated C57BL/6 mice with 1 x 10^5 hCD19-B16 tumor cells, then adoptively transferred 4 x 10^6 receptor positive cells 12 days later and assessed tumor volume 3x weekly via caliper measurements (Fig. 4.6d). While control, CAR and HYBRID-R T cells had very little anti-tumor effect, both CARD11-PIK3R3 CAR and HYBRID-R driving CARD11-PIK3R3 could initially control tumors. CARD11-PIK3R3 CAR and HYBRID-R driving CARD11-PIK3R3 T cell treated animals ultimately began relapsing, likely due to hCD19 antigen loss, which has previously been established as a mechanism of tumor escape in this model (Fig. 4.6e). Further work will be required to demonstrate the full safety profile and efficacy of HYBRID-R driving CARD11-PIK3R3 circuits. This proof-of-concept data indicates that potent anti-tumor efficacy of CARD11-PIK3R3 engineered T cells can be achieved through induction with HYBRID-R circuits.

4.8. Conclusion

CAR T cell therapies have made remarkable strides in the treatment of refractory leukemias but have repeatedly failed to achieve significant anti-tumor efficacy in solid tumors. In part, CAR T cell therapies alone are likely unable to achieve the persistence, potency, and efficacy required to have impact in highly immunosuppressive and refractory solid tumors. Instead, additional payloads such as cytokines, enzymes, genetic deletions or amplifications, and potency enhancers are being paired with CAR therapies to boost overall efficacy. However, some payloads are toxic, such as IL-12, and require strict tumor specific secretion, while others such as CARD11-PIK3R3 are well tolerated but require labor intensive TCR deletion for enhanced safety.

Previously developed synthetic Notch (synNotch) and SNIPR receptors allow for control of such payloads in therapeutic immune cells, however these receptors cannot initiate cytotoxicity like CARs or TCRs. Using SNIPR circuits requires the additional expression of a CAR or TCR, which can be challenging due to size constraints of lentiviral cargo as well as the need for additional antigen targeting. Here, we have designed HYBRID-Rs, a single receptor architecture that induces simultaneous T cell activation and orthogonal user defined transcriptional activity, providing researchers with the ability to redirect patient T cells against cancerous cells while simultaneously delivering payloads to counteract challenges encountered in cancers. We have paired these receptors with payloads such as CARD11-PIK3R3, and found they induce sufficient CAR activity and antigen restricted payload expression, resulting in improved anti-tumor efficacy with a hypothesized more favorable safety profile.

4.9. Methods

Vector Construction

Intracellular domains of HYBRID-Rs containing the appropriate costimulatory domain, CD3zeta domain, Gal4VP64 and GSlinkers were synthesized by Twist. Hybrid CARs were built by fusing the CD19 scFv [71] to the corresponding receptor scaffold and intracellular tail. All receptors contain an n-terminal CD8α signal peptide (MALPVTALLLPLALLLHAARP) for membrane targeting and a flag-tag (DYKDDDDK) for easy determination of surface expression with α-flag PE (Biolegend 637310). The receptors were cloned into a modified pHR'SIN:CSW vector containing a PGK promoter for all primary T cell experiments. Select hybrid CARs were cloned to a MSCV vector for retroviral transduction of murine T cells, these receptors were not murinized. Murinized CARs were constructed using a human CD8α signaling peptide (MALPVTALLLPLALLLHAARP) followed by the FLAG-tag (DYKDDDK) and scFv, which was anti-CD19 (FMC63). This extracellular region was fused to a murine CD8a hinge/transmembrane domain, and murine 4-1BB and CD3z intracellular domains. Murine CAR constructs contained a T2A self-cleaving peptide followed by enhanced green fluorescent protein (eGFP) to assess expression. Murine CARs were cloned into a retroviral MSCV vector. To construct the CARD11-PIK3R3 payload for murine transduction, human CARD11-PIK3R3 followed by a self-cleaving T2A and mCherry sequence was cloned into the retroviral MSCV vector. For ectopic expression of human CD19, coding sequences were cloned into the pHR′SIN:CSW vector containing an EF1a promoter. All constructs were cloned via Infusion cloning (Clontech #ST0345) or Gibson assembly.

Cell Lines

The cancer cell lines used were K562 myelogenous leukemia cells (ATCC #CCL-243), B16-F10 melanoma cancer cells (ATCC #CRL-6475) and A549 lung epithelial carcinoma cells (ATCC #CCL-18). K562s, A549s and B16-F10s were lentivirally transduced to stably express human CD19. CD19 levels were determined by flow cytometry (Biolegend, clone HIB19). All cell lines were sorted for purified CD19 expression. A549s were additionally transduced to express the nuclear stain mKate2. Lenti-X 293ts were used for virus production (Clontech #11131D). K562 cells were cultured in IMDM + 10% FBS with penicillin/streptomycin and sodium pyruvate. Lenti-X 293t, B16-F10 and A549 cell lines were cultured in DMEM + 10% FBS with penicillin/streptomycin and sodium pyruvate. All cell lines were routinely tested for mycoplasma contamination.

Primary Human T cell Isolation and Culture

Primary CD3+, CD4+ and CD8+ T cells were isolated from anonymous donor blood after apheresis by negative selection (STEMCELL Technologies #15062 & 15063). Blood was obtained from Blood Centers of the Pacific (San Francisco, CA) as approved by the University Institutional Review Board. T cells were cryopreserved in RPMI-1640 (UCSF cell culture core) with 20% human AB serum (Valley Biomedical Inc., #HP1022) and 10% DMSO. After thawing, T cells were cultured in human T cell medium consisting of X-VIVO 15 (Lonza #04-418Q), 5% Human AB serum and 10 mM neutralized N-acetyl L-Cysteine (Sigma-Aldrich #A9165) supplemented with 30 units/mL IL-2 (NCI BRB Preclinical Repository) for all experiments unless otherwise noted. *In vivo* experiments were completed with bulk CD3+ cells isolated in a similar manner.

Lentivirus Production and Transduction of Human T cells

Pantropic VSV-G pseudotyped lentivirus was produced via transfection of Lenti-X 293T cells (Clontech #11131D) with a pHR'SIN:CSW transgene expression vector and the viral packaging plasmids pCMVdR8.91 and pMD2.G using Mirus TransIT-Lenti (Mirus #MIR 6606). Primary T cells were thawed the same day, and after 24 hours in culture, were stimulated with Human T-Activator CD3/CD28 Dynabeads (Life Technologies #11131D) at a 1:3 cell:bead ratio. At 48 hours, viral supernatant was harvested, and the primary T cells were exposed to the virus for 24 hours. In some cases, previously prepared and frozen concentrated virus was used in place of fresh. At day 5 post T cell stimulation, the Dynabeads were removed, T cells were sorted, and expanded until day 10-14 when they were rested and could be used *in vitro* or *in vivo* assays. T cells were sorted for assays with a Beckton Dickinson (BD) FACS ARIA II.

Retrovirus Production and Transduction of Murine T Cells

Pantropic VSV-G pseudotyped retrovirus was produced via transfection of Lenti-X 293T cells (Clontech #11131D) with a MSCV transgene expression vector and the viral packaging plasmid pCL-Eco using Fugene (Promega #E2311). CD4, CD8 or CD3+ T cells were isolated from the spleens of C57BL/6 mice using Mojo Sort Negative Selection kits (Biolegend # 480033,# 480035 or #480031). Mouse T cells were activated for 24 hours using anti-CD3/anti-CD28 Mouse T-Activator Dynabeads (Invitrogen #11453D), and cultured in RPMI + 10% FBS with HEPES, b-mercaptoethanol, NEAA, sodium pyruvate penicillin/streptomycin, and 100U/mL recombinant IL-2. Retroviral supernatants were added to T cells in Retronectin (Takara) coated plates and spinduction was performed for 1 hour at 2000 rpm at 30°C. Following transduction, T cells were resuspended and cultured in fresh media containing 100

U/mL IL-2 until adoptive transfer or *in vitro* assay. Transduction efficiency was determined by flow cytometry prior to adoptive transfer.

Primary Human In vitro Assays

Transduced primary human T cells were co-cultured with target cells at the indicated effector to target ratios and co-culture time courses. For cytokine assays, cells were co-cultured in media lacking exogenous IL-2, supernatants were collected 24-48 hours after start, frozen at -80C, and thawed later for assessment via ELISA (Invitrogen #BMS221INST). For proliferation assays, transduced T cells were first stained with Cell Trace Far Red (Invitrogen # C34572) according to manufacturer protocol before co-culture with targets. For killing assay, transduced T cells were co-cultured on the adherent CD19, mkate2+ expressing A549 cell line and images were captured and analyzed using incucyte.

Murine In vitro Assays

Engineered murine T cells were co-cultured with antigen positive target cells at a ratio of 1:1, T cells were plated based on their CAR+ percentage. For ELISA, cells were pelleted 24 hours post co-culture, supernatants were collected and frozen at -80C then thawed later for assessment via ELISA (Invitrogen #BMS601).

Flow Cytometry

For all in vitro human and murine T cell assays, cells were washed with PBS 2% FBS twice, stained with surface staining markers at room temperature for 20 minutes, washed twice, and resuspended in PBS 2% FBS with DRAQ7 (diluted 1:1000) before analysis on a BD FACSymphony X-50 Flow Cytometer.

Xenograft In vivo Assays

NOD.Cg-Prkdc^{scid} Il2rg^{tm1Wjl}/SzJ (NSG) mice were dosed tumor cells via subcutaneous injection (solid tumor) or tail vein injection (Nalm6). Mice with similar sized tumor burden were randomized to receive treatments of CAR T cells. Engineered or control T cells were dosed via retro-orbital injection. Subcutaneous tumors were measured with digital calipers twice weekly, and tumor volume was calculated using the following formulas: (length x width^2)/2. Mice were euthanized when tumors reached 2000mm^3 or measured 20mm in any direction or those with progressively ulcerating tumors. For Nalm6 leukemic model, tumors were measured twice weekly using Xenogen In-Vivo Imaging System (IVIS), death was defined hind limb loss, poor body score, or loss of 15% of more of body weight, whichever occurred first. Animal drinking water was supplemented with Clavomox to prevent bacterial infections.

Syngeneic In vivo Assays

C57BL/6 or B6.SJL-*Ptprc^a Pepc^b*/BoyJ male mice ages 8-12 weeks were dosed subcutaneously or intravenously with tumor cells. Murine T cells were manufactured as

described above, and CAR+ mouse T cells were adoptively transferred via retro-orbital injection to mice, no preconditioning was performed on recipient mice before T cell transfer. Tumor volume was measured 2x weekly, using the following equation: (length x width^2)/2. Mice were euthanized when tumors reached 2000mm^3 or measured 20mm in any direction, or with progressively ulcerating tumors.

4.10. Figures

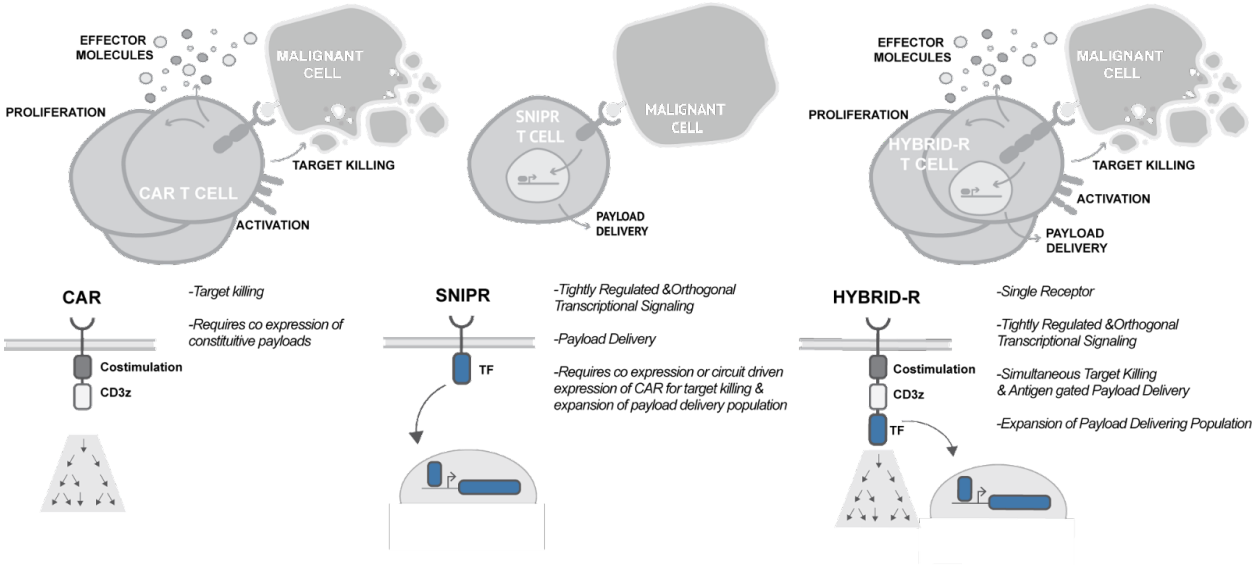

Figure 4.1 CAR, SNIPR and HYBRID-R Design and Functionality

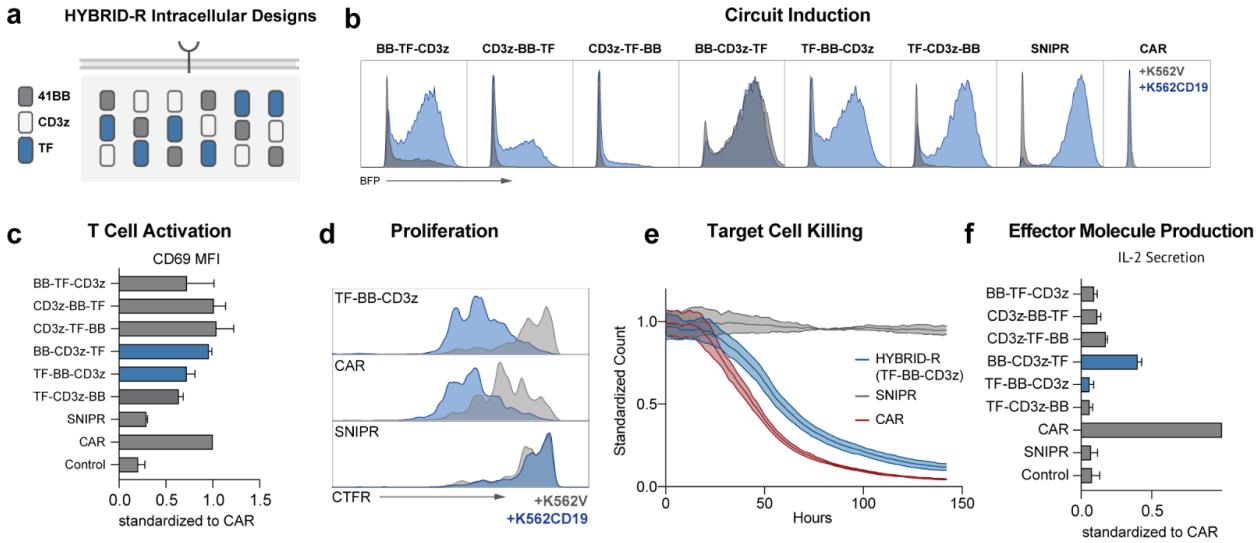

Figure 4.2 HYBRID-Rs Combine Short-term Proximal Signaling with Long-Term Genetic Circuitry.

(a) Schematic of 4-1BB, CD3z and GAL4-VP64 (TF) orientation in 6 HYBRID-R designs. **(b-c,f)** Histograms depicting BFP RE circuit induction (b), CD69 MFI standardized to CAR (c), and IL-2 secretion (f) of HYBRID-R with BFP RE circuits after 48 hours of co-culture with K562s. **(d)** Proliferation as assessed via CTFR dilution peaks of engineered T cells measured after co-culture with K562s. **(e)** Target cell counts collected via Incucyte and standardized to SNIPR.

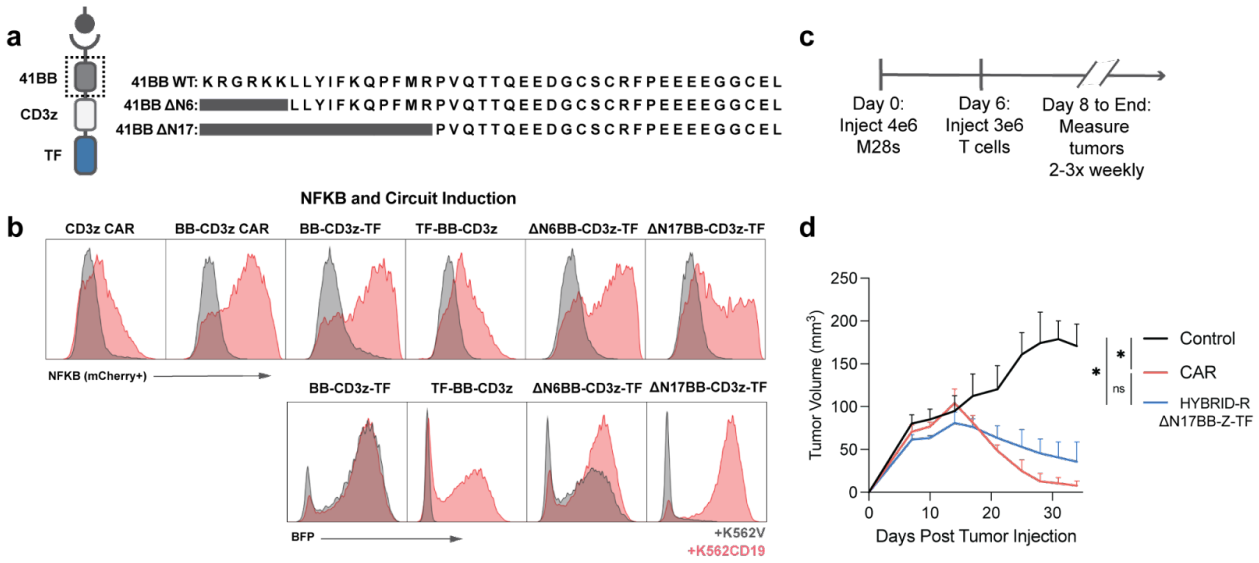

Figure 4.3 Optimization of HYBRID-R Proximal Signaling

(a) Schematic depicting amino acid sequence of wildtype and truncated 4-1BB intracellular domain. **(b)** NFKB reporter activity (top) and BFP RE circuit induction (bottom) of HYBRID-Rs and controls. **(c)** Schematic depicting M28 *in vivo* experiment timeline. **(d)** Tumor growth curves. P values determined by one-way ANOVA followed by Tukey's multiple comparisons test.

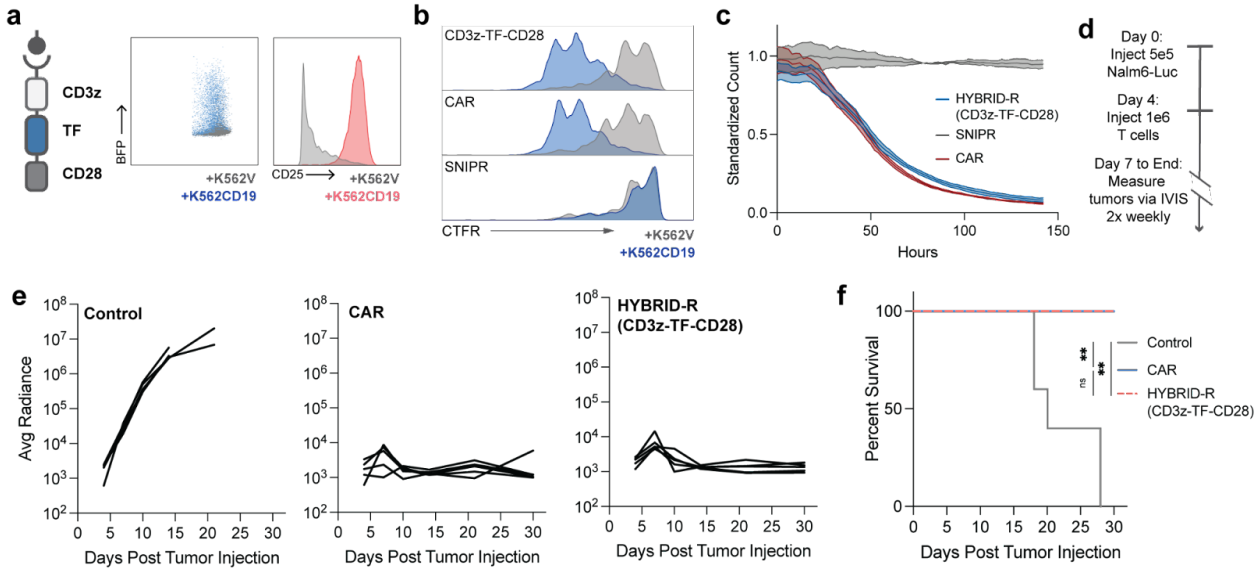

Figure 4.4 HYBRID-Rs with CD28 Costimulatory Domains.

(a) Schematic of HYBRID-R with CD3z-TF-CD28 intracellular tail (left) and BFP RE circuit induction and CD25 activation marker expression of HYBRID-R (CD3z-TF-CD28) (right). **(d)** Proliferation as assessed via CTFR dilution peaks of engineered T cells measured after co-culture with K562s. **(c)** Target cell counts collected via Incucyte and standardized to SNIPR. **(d)** Schematic depicting Nalm6 *in vivo* experiment timeline. **(e-f)** Radiance (e) and survival analysis **(f)** of Nalm6-Luc-GFP tumor bearing animals. Radiance measured via IVIS and used as a proxy for tumor burden.

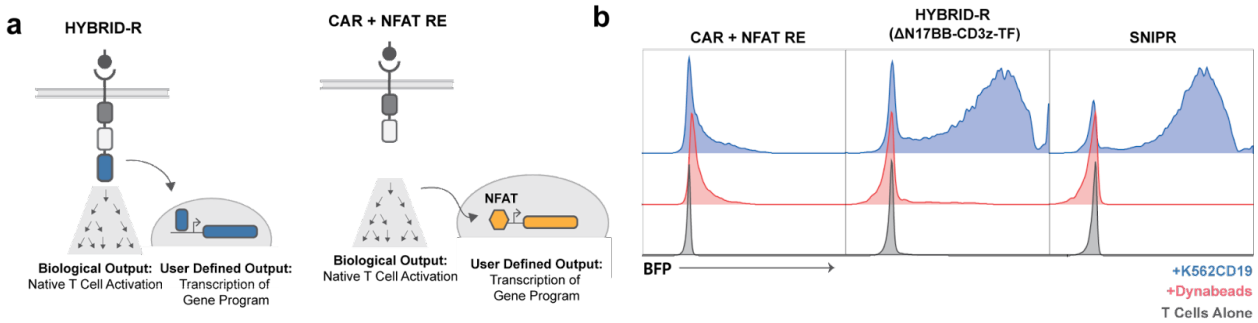

Figure 4.5 Benchmarking TCR REs to HYBRID-Rs

(a) Schematic of HYBRID-R and NFAT RE circuits. **(b)** BFP RE circuit induction at rest (T cells alone), with TCR stimulation (Dynabeads) and CAR stimulation (K562-CD19s).

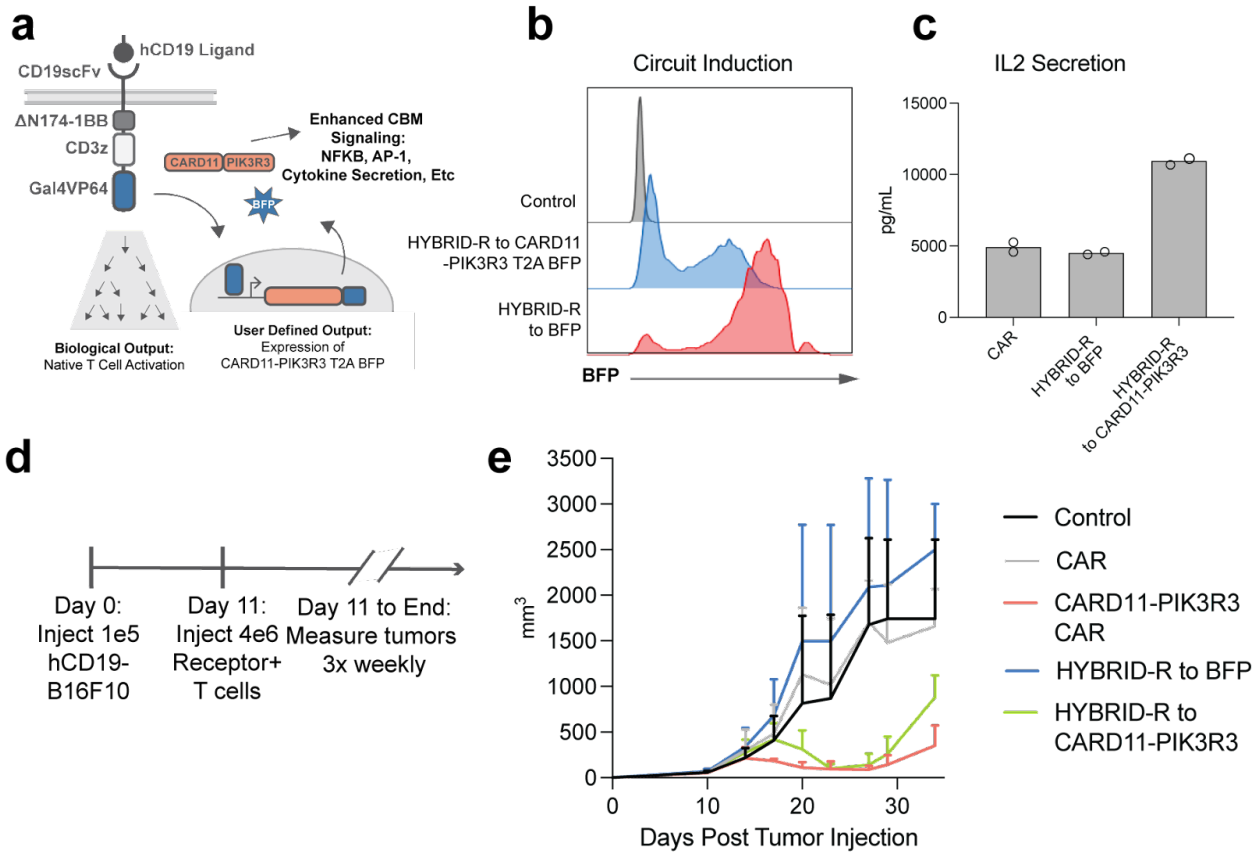

Figure 4.6 Combining HYBRID-Rs with Payloads

(a) Schematic of HYBRID-R with CARD11-PIK3R3 T2A BFP circuit. **(b-c)** BFP RE circuit induction (b) and IL-2 secretion (c) 48 hours after co-culture with K562 targets. **(d)** Schematic depicting hCD19-B16 *in vivo* experiment timeline. **(e)** Tumor growth curves. P values determined by one-way ANOVA followed by Tukey's multiple comparisons test.

4.11. Extended Data Figures

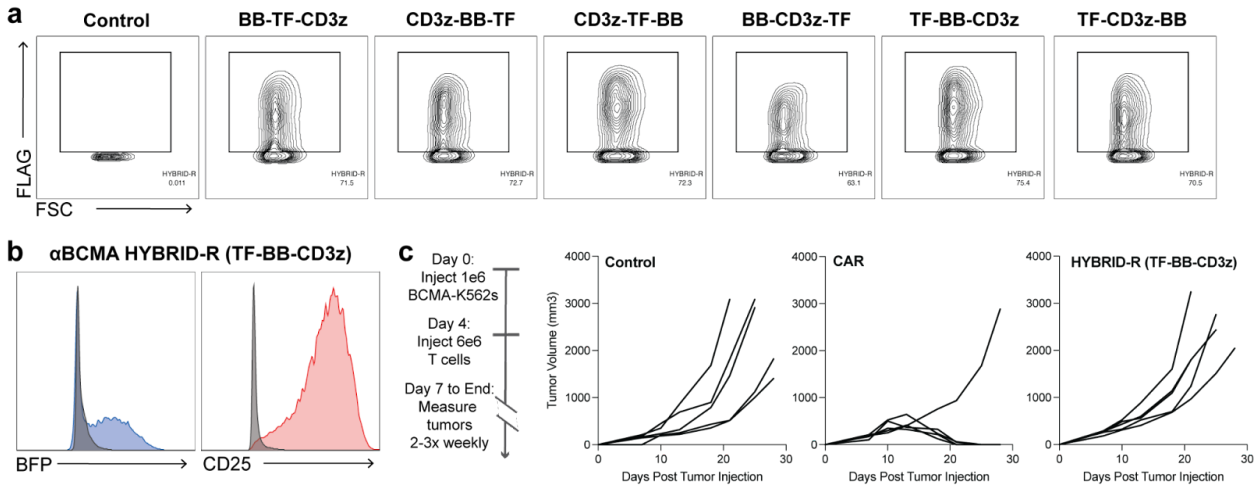

Extended Data Figure 4.1 Proof-of-Concept HYBRID-Rs Express in Primary Human T Cells but Lack Anti-tumor Efficacy

(a) Flow plots indicating expression of CD19 targeted HYBRID-Rs (FLAG) in primary human T cells. **(b)** BFP RE circuit induction and CD25 activation marker expression of BCMA targeted HYBRID-R (TF-BB-CD3z). **(c)** Schematic depicting K562 *in vivo* experiment timeline. (**d)** Tumor growth curves.

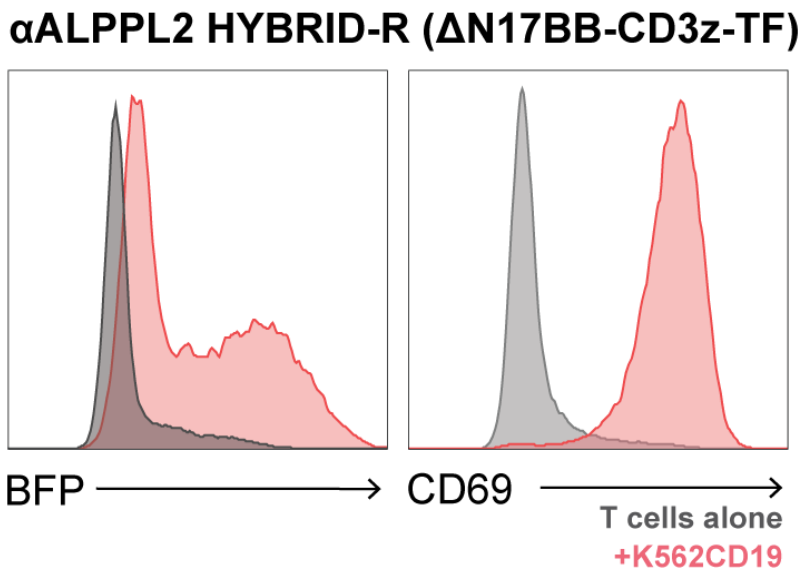

Extended Data Figure 4.2 An Optimized ALPPL2 Targeted HYBRID-R

BFP RE circuit induction and CD25 activation marker expression of ALPPL2 targeted HYBRID-R (DN14BB-CD3z-TF).

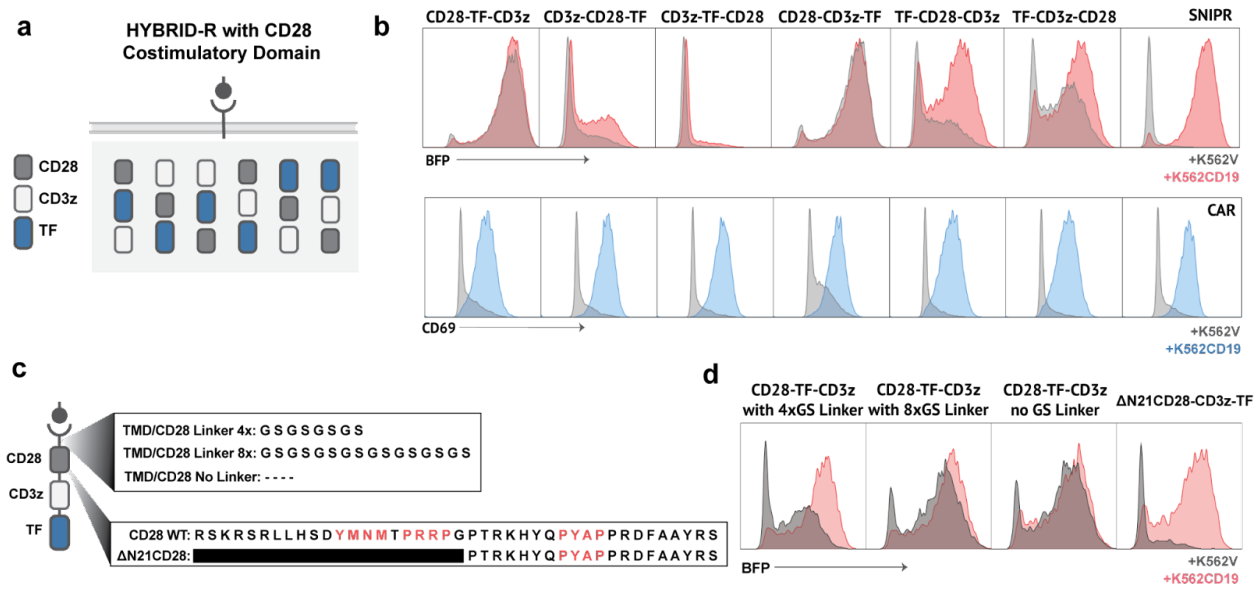

Extended Data Figure 4.3 Optimization of CD28 HYBRID-Rs

(a) Schematic of CD28, CD3z and GAL4-VP64 (TF) orientation in 6 HYBRID-R designs. **(b)** Histograms depicting BFP RE circuit induction (top) and CD69 expression (bottom) HYBRID-Rs after 48 hours of co-culture with K562s. **(c)** Schematic depicting amino acid sequence linker sequence between TMD and CD28, and the sequence of wildtype and truncated CD28 intracellular signaling domain. **(d)** Histograms depicting BFP RE circuit induction of CD28 HYBRID-R variants.

4.12. References

1. Maude, S. L. et al. Tisagenlecleucel in Children and Young Adults with B-Cell Lymphoblastic Leukemia. N. Engl. J. Med. 378, 439–448 (2018).
2. Neelapu, S. S. et al. Axicabtagene Ciloleucel CAR T-Cell Therapy in Refractory Large B-Cell Lymphoma. N. Engl. J. Med. 377, 2531–2544 (2017).
3. Majzner, R. G. & Mackall, C. L. Tumor Antigen Escape from CAR T-cell Therapy. Cancer Discov. 8, 1219–1226 (2018).
4. Srivastava, S. & Riddell, S. R. Chimeric Antigen Receptor T Cell Therapy: Challenges to Bench-to-Bedside Efficacy. The Journal of Immunology 200, 459–468 (2018).
5. Liu, T., Zhou, L., Li, D., Andl, T. & Zhang, Y. Cancer-associated fibroblasts build and secure the tumor microenvironment. Frontiers in Cell and Developmental Biology vol. 7 Preprint at https://doi.org/10.3389/fcell.2019.00060 (2019).
6. Morsut, L. et al. Engineering Customized Cell Sensing and Response Behaviors Using Synthetic Notch Receptors. Cell 164, 780–791 (2016).
7. Roybal, K. T. et al. Engineering T Cells with Customized Therapeutic Response Programs Using Synthetic Notch Receptors. Cell 167, 419–432.e16 (2016).
8. Roybal, K. T. et al. Precision Tumor Recognition by T Cells With Combinatorial Antigen-Sensing Circuits. Cell 164, 770–779 (2016).
9. Zhu, I. et al. Modular design of synthetic receptors for programmed gene regulation in cell therapies. Cell 185, 1431–1443.e16 (2022).
10. Zapata, J. M. et al. CD137 (4-1BB) Signalosome: Complexity Is a Matter of TRAFs. Front. Immunol. 9, 2618 (2018).
11. Su, Y. et al. ALPPL2 Is a Highly Specific and Targetable Tumor Cell Surface Antigen. Cancer Res. 80, 4552–4564 (2020).

12. An, F. et al. Targeted drug delivery to mesothelioma cells using functionally selected internalizing human single-chain antibodies. Mol. Cancer Ther. 7, 569–578 (2008).
13. Hamieh, M. et al. CAR T cell trogocytosis and cooperative killing regulate tumour antigen escape. Nature doi:10.1038/s41586-019-1054-1.
14. Zhao, Z. et al. Structural Design of Engineered Costimulation Determines Tumor Rejection Kinetics and Persistence of CAR T Cells. Cancer Cell 28, 415–428 (2015).
15. Sadelain, M., Rivière, I. & Riddell, S. Therapeutic T cell engineering. Nature 545, 423–431 (2017).
16. Boomer, J. S. & Green, J. M. An enigmatic tail of CD28 signaling. Cold Spring Harb. Perspect. Biol. 2, a002436 (2010).
17. Boucher, J. C. et al. CD28 Costimulatory Domain-Targeted Mutations Enhance Chimeric Antigen Receptor T-cell Function. Cancer Immunol Res 9, 62–74 (2021).
18. Hooijberg, E., Bakker, A. Q., Ruizendaal, J. J. & Spits, H. NFAT-controlled expression of GFP permits visualization and isolation of antigen-stimulated primary human T cells. Blood 96, 459–466 (2000).
19. Zhang, L. et al. Improving adoptive T cell therapy by targeting and controlling IL-12 expression to the tumor environment. Mol. Ther. 19, 751–759 (2011).
20. Jutz, S. et al. Assessment of costimulation and coinhibition in a triple parameter T cell reporter line: Simultaneous measurement of NF-κB, NFAT and AP-1. J. Immunol. Methods 430, 10–20 (2016).
21. Julie Garcia, Jay Daniels, Yujin Lee, Iowis Zhu Kathleen Cheng, Qing Liu, Daniel Goodman, Cassandra Burnett, Calvin Law, Chloe Thienpont, Josef Alavi, Camillia Azimi, Garrett Montgomery, Kole T. Roybal, Jaehyuk Choi. Naturally occurring mutations in human T cell lymphomas enhance engineered T cell therapies. Nature. In Review.

22. King, M. A. et al. Human peripheral blood leucocyte non-obese diabetic-severe combined immunodeficiency interleukin-2 receptor gamma chain gene mouse model of xenogeneic graft-versus-host-like disease and the role of host major histocompatibility complex. Clin. Exp. Immunol. 157, 104 (2009).

Publishing Agreement

It is the policy of the University to encourage open access and broad distribution of all theses, dissertations, and manuscripts. The Graduate Division will facilitate the distribution of UCSF theses, dissertations, and manuscripts to the UCSF Library for open access and distribution. UCSF will make such theses, dissertations, and manuscripts accessible to the public and will take reasonable steps to preserve these works in perpetuity.

I hereby grant the non-exclusive, perpetual right to The Regents of the University of California to reproduce, publicly display, distribute, preserve, and publish copies of my thesis, dissertation, or manuscript in any form or media, now existing or later derived, including access online for teaching, research, and public service purposes.

DocuSigned by:
Julie Garcia
D433C9294A2549B...
Author Signature

8/24/2023
Date